SAINT-PETERSBURG UNIVERSITY

VOLKOV GRIGORY ALEKSANDROVICH

INCUBATION CHARACTERISTICS OF CRITICAL STATES OF CONDENSSED MATTER

SCIENTIFIC SPECIALTY

1.1.8. SOLID MECHANICS

DISSERTATION FOR THE DEGREE OF

DOCTOR OF PHYSICAL AND MATHEMATICAL SCIENCES

TRANSLATION FROM RUSSIAN

SCIENTIFIC ADVISER

CORRESPONDING MEMBER OF
THE RUSSIAN ACADEMY OF SCIENCES,
DOCTOR OF PHYSICAL AND
MATHEMATICAL SCIENCES, PROFESSOR

PETROV YURI VIKTOROVICH

SAINT-PETERSBURG 2024

Content

Introduction

Problems related to determining the conditions for transient processes in continuous media, such as fracture or change in the aggregate state, are among the most common and important problems in fracture mechanics. For equilibrium processes, in the case of a slow change in external conditions, there are traditional theoretical approaches and calculation methods that allow finding the critical values of the problem parameters that determine the fracture process. However, when a continuous medium is subjected to an impact of the shock type, some phenomena are observed that do not fit into the framework of traditional equilibrium approaches. Thus, the development of new methods that allow predicting the threshold characteristics of an external high-speed impact that will initiate transient processes is an important fundamental task of continuum mechanics.

One of the most practically important problems of this kind is the problem of predicting the failure of brittle continuous medium under high-speed impact action. For example, brittle materials such as concrete, cement or various types of rocks are widely used in construction. At the same time, the designed structures can be subjected not only to static but also to dynamic effects such as explosions, earthquakes, vibrations and various impact loads. Therefore, the strength of materials under intense dynamic loading remains one of the most important problems of modern scientific and engineering practice. Experimental studies show that strength characteristics depend on the loading history [1, 2, 3, 4]. For example, an increase in the deformation rate of a material leads to an increase in the stress level at the moment of failure [5, 6, 7, 8, 9, 10, 11, 12]. This phenomenon in fracture mechanics is usually called the strain rate sensitivity of dynamic strength.

Not many analytical and experimental approaches have been developed to describe this feature of the dynamic fracture. In the first works, researchers tried to determine the dependence of strength on the strain rate in the form of a certain power dependence [13, 14]. However, this method implicitly assumes that this type of dependence is a property of the material, and its coefficients are the strength parameters for the material under study. Therefore, with this approach, it is impossible to predict the conditions of material fracture under an arbitrary external load, and therefore, it cannot be accepted as a general solution to such problems. At the same time, F. Tuler and B. Butcher proposed one of the first phenomenological approaches that takes into account the duration and amplitude of the load pulse. Tuler-Butcher criterion contains two material constants, the values of which they estimated by fitting of the theoretical curve to the experimental data [15]. The main disadvantage of the Tuler-Butcher (TB) criterion is the lack of even an imaginary experimental scheme that allows measuring the values of the model parameters. At the same time, D. Grady and J. Lipkin managed, using the TB criterion for the case of rigid loading with a constant strain rate, to establish that the dynamic strength of aluminum is proportional to the cube root of the strain rate [13].

The FIB model, which was developed within the framework of a special standard for determining the dynamic strength of concrete, can be attributed to purely approximating methods. This model can be considered as a bilinear approximation of the static and dynamic branches of the strength-rate sensitivity curve of the material in semi-logarithmic coordinates. Thus, it can be assumed that this method of predicting dynamic strength is, for the most part, a purely engineering approach that does not take into account the features of the fracture. However, there are studies showing that the strength characteristics of modern high-strength concrete cannot be described within the FIB criterion. In this regard,

various researchers offer their own modifications of the dynamic strength criterion by analogy with FIB, for example, J. Tedesco and K. Ross [16], Grote et al. [17], K. Li and H. Meng [18, 19], Zhou and Hao [20], Hao Y. and Hao H. [21, 22, 23], and others [24, 25, 26].

Such modified criteria are also, roughly speaking, a simple approximation of the experimentally observed strength-strain-rate curve. Usually, when determining the strength properties for a particular material, a small adjustment of the coefficients is still required in criteria of this kind, which makes the criterion unique for the material under consideration.

It is also worth noting a number of methods for studying the problem of dynamic strength of brittle materials, which are based on the analysis of the microstructure of the material. To predict failure on the macro level, existing microdefects in the material are considered, their growth and subsequent propagation as a result of impact loading are analyzed [27, 28, 29, 30]. Such approaches are widely used in numerical modeling of failure of brittle and quasi-brittle materials subjected to high rate deformation. However, their use for predicting the dynamic strength of real materials is difficult, since this requires determining the values of a large number of structural parameters of the medium, such as the dimensions and spatial distribution of initial defects. Another difficulty is that such microstructural models simulate a complex physical process, such as failure at both micro and macro levels. All these circumstances significantly complicate their use in real engineering practice in analytical and even numerical modeling.

It is worth mentioning separately the model developed by D. Kimberly, B. Paliwal and K. Ramesh, who proposed a semi-analytical scheme for calculating the dynamic strength of brittle materials taking into account the initial distribution of defects [31, 32]. Their later numerical analysis, which predicted the ultimate stress

level for arbitrary combinations of possible values of the problem parameters, made it possible to identify a certain universal normalization relationship describing the rate dependence of strength for a wide range of brittle solids. Later, this approach was applied by A. Tonge and K. Ramesh [30] in developing a model describing the interactions of defects at different scale levels during high strain rate brittle fracture of a material. However, the values of such microparameters as the average defect density and pore size cannot be measured using standard equipment in a conventional mechanical laboratory. This circumstance significantly complicates the application of this approach in engineering practice for real materials. Similar methods for predicting failure include the approach based on the DFH (Denoual, Forquin and Hild) model, which was developed to describe the physical processes occurring during dynamic fragmentation of brittle anisotropic media [33, 34]. It was shown how this method can be used to model dynamic split tests of ceramic materials under impact compression [35]. However, as with all microstructural models, the practical application of this approach is difficult due to the presence of microstructural parameters such as the effective volume, crack velocity coefficient or shape parameter, the values of which cannot be measured in independent tests. Dynamic split tests under impact compression can also be modeled using the PRM (Pontiroli, Rouquand and Mazars) model [36, 37], which is based on the description of defect growth in the material, which allows it to distinguish between the effects of tensile and compressive loading during static tests. The use of this model in the case of high strain rate loading is carried out by introducing a certain dynamic coefficient calculated using an empirical formula, in which the exponential growth of the critical stress level with the strain rate is assumed as a material property [38]. In numerical schemes, the Johnson-Holmquist (JH) [39, 40, 41, 42] or Sandia GeoModel [43, 44] models are usually used, which also contain a relatively large number of parameters describing the system's response to various types of external influences. The values of the model

parameters are determined by comparing the simulation results with experimentally measured values.

An analysis of the previously listed methods related to the prediction of the dynamic strength of materials allows us to conditionally divide them into two groups. The first group includes approaches in which the strain rate dependence of strength is simply approximated by, for example, a power or exponential dependence, and is perceived as a property of the material. In a sense, such approaches are a generalization of traditional static methods for predicting strength, since they imply instantaneous fracture of the medium upon reaching a certain critical stress level. A common drawback of such methods is that the type of the approximating function for a specific material is not known a priori, which in turn makes it difficult to determine the values of its coefficients.

The second group of methods is based on modeling fracture at the microstructural level. Such models are usually quite difficult to apply in practice, since in addition to their overall complexity, it is necessary to know a priori the values of the material structure parameters, the measurement of which is in itself a rather complex scientific task. However, it is worth noting that in some cases, such as, for example, with the Paliwol-Ramesh model, based on microstructural analysis, it is possible to determine the values of the material macro parameters that determine its strength strain rate dependence. However, in addition to the fact that the values of these macro parameters are difficult to calculate, the strain rate dependence calculated for these obtained values may poorly correspond to the data of real dynamic tests. This circumstance forces us to make various corrections to the resulting model, due to which it, losing its universality, becomes more like an approximating dependence.

Taking into account the above, the following disadvantages can be noted for most of the listed approaches:

1. Dynamic strength models based on the approximation principle are not universal. This requires conducting a separate study to determine the values of its strength parameters for each type of high strain rate impact.
2. The overall complexity of most of the listed approaches based on microstructural analysis significantly complicates their application in wide engineering practice.

Explanation of the features of dynamic strength requires fundamentally new approaches that take into account the characteristic features of high strain rate processes. One of such approaches was proposed by Yu. V. Petrov and A. A. Utkin in 1987, in which they proposed to consider the fracture of a material as a process developing in time, rather than occurring instantly, including both slow and high-strain rate processes. In this regard, they introduced the concept of incubation time as a certain characteristic time of the process, which is a parameter of the dynamic strength of a continuous medium on the macro level [45, 46, 47]. Later, this approach was successfully used in a number of problems of dynamic fracture [48, 49, 50, 51, 52]. Thus, supplementing the traditional parameter, quasi-static strength σ_c, by a second parameter, the incubation time τ, made it possible to explain and predict various phenomena due to transient processes at high strain rate loading. It later turned out that the idea underlying the incubation time criterion allows one to describe not only the strain rate dependence of strength, but also to solve many related problems, for example, those related to assessing the energy efficiency of fracture under impact or constructing diagrams of inelastic deformation under high strain rate loading.

Thus, to solve specific problems using the incubation time criterion, it is necessary to be able to determine the value of τ for the material under study using some, if possible, standardized algorithm.

Basically, the dynamic strength properties of materials are experimentally manifested as a strain rate or time dependence of strength. One of the most common types of testing is the Hopkinson split-bar experiment, which allows realizing high-speed compression or tension of a sample with the ability of directly measuring the impact pulse passing through the sample [53, 54, 55]. The result of such tests is usually the dependence of the stress level at the moment of failure on the loading rate, presented as a limited set of experimental points [56, 57]. At the same time, the overall complexity of conducting dynamic tests usually does not provide for a large number of experimental points. It is this set of points, from which the incubation time value is to be estimated. It is also worth noting that when registering high-speed processes, it is impossible to exclude the presence of random and systematic errors in the measured values

In slow static tests, the number of samples and the permissible level of error in the measured values are determined by standards and other regulatory documents. At the same time, for dynamic high strain rate tests, there is no clear unified understanding of the required number of samples to be tested for a reliable assessment of the ultimate stress level at a certain loading rate. This becomes especially important when solving applied problems that require knowing the level of reliability of estimations of the parameter values, which are used directly in calculations. Therefore, simple selection of model parameter values that provide good agreement between the calculated curves and experimental data may not be sufficient.

Thus, the problem of an assessment of model parameters is also a fundamental task not only for the development of methods on the basis of the incubation time criterion, but also for most of the other mentioned models of dynamic fracture of continuous media.

The relevance of the topic is due to the need of developing new standardized methods for testing materials under high strain rate loading conditions, the results of which will be used to evaluate a set of values of defining parameters that make it possible to predict critical conditions for the occurrence of fracture for arbitrary dynamic impact.

The goal of the work is to develop methods that allow studying various effects that arise in various transient processes in continuous media under high strain rate impact effects.

To achieve the goal of the work, the following tasks are solved:

1. Development of methods for processing dynamic test data, allowing to estimate the values of the incubation time parameter, which determines the time sensitivity of a continuous medium to the loading rate. Mathematical justification of the proposed method, as well as a study of its applicability in problems related to high strain rate and shock-pulse fracture of continuous media.

2. Study of the influence of equilibrium parameters of a continuous medium, namely temperature and external hydrostatic pressure, on the values of model strength characteristics. Identification of the corresponding dependencies for incubation time and critical stress, as well as substantiation of the proposed models on the problems related to acoustic and pulse cavitation of liquids.

3. Conducting a study of the characteristics of the energy capacity of dynamic fracture; finding optimal modes of impact destructive action on a continuous medium during contact interaction, with the aim of substantiating the practical significance of the developed methods based on the concept of incubation time.

4. Development of methods for processing dynamic test data that allow for the assessment of optimal values of strength model parameters, namely not only the incubation time, but also the critical stress that determines the stability of the medium directly to the stress level of the loading. Verification and testing of the proposed method on the example of processing dynamic test data for brittle materials.

5. Establishing a relationship with the parameters of other phenomenological approaches that predict critical conditions for the fracture of continuous media under high-speed impacts, identifying a new mechanical interpretation of the basic parameters of the incubation time criterion.

Novelty

In this paper, studied are the effects that arise in non-stationary transient processes under high-intensity extreme impacts, characterized by regularities that are modeled on the basis of a structural-temporal approach based on the concept of incubation time. The effects under study do not have a satisfactory explanation based on traditional approaches, most of which are direct extrapolation of quasi-static approaches assuming the presence of threshold characteristics in continuous media.

Particular attention is paid to the problem associated with a new method for assessing the values of key material parameters, since it is the possibility of accurate assessment that allows finding new patterns of fracture of continuous media under high strain rate impact loading.

1) A novel method has been developed for assessing the values of incubation time based on data from dynamic tests under high strain rate and shock-pulse loading in the form of a confidence interval with a given level of confidence probability.

2) A model of the onset of phase transformations of continuous media as a result of the action of a nonequilibrium mechanical load is constructed. Using the example of the phase transition of a liquid into a gaseous state, it is shown for the first time how the acoustic nonequilibrium effect affects the conditions of phase equilibrium. The "corrected" curves of the "liquid-vapor" phase equilibrium for water located in the zone of action of a subthreshold ultrasonic wave are calculated.

3) For the first time, the energy intensity of dynamic fracture during contact interaction of a rigid particle with an elastic half-space was investigated depending on the shape of the contacting surfaces. It has been investigated how the presence of a supersonic stage of interaction affects the existence of optimal loading modes. A method for taking the supersonic stage into account was proposed.

4) A method for processing high strain rate test data has been developed, allowing for simultaneous assessment of two strength parameters: incubation time and critical stress.

5) For the first time, an analytical approach was developed that makes it possible to identify the rate dependence of the fracture mode in brittle two-component materials, based only on the results of a comparative analysis of the rate dependence of the material strength and static test data, without any studies of the structure of the fractured samples.

6) A new analytical approach has been developed that allows revealing the rate dependence of plastic deformation mechanisms in metals. The efficiency of the proposed approach has been verified by comparing the results obtained for alloys with coarse-grained and ultrafine-grained structures.

7) Based on the developed methods, a new interpretation of the parameters of the incubation time criterion has been given.

The theoretical and practical significance of the conducted research consists in the development of methods based on the concept of incubation time in problems of predicting critical conditions for the occurrence of transient processes under non-equilibrium loading. The standardized methodology for assessing the value of incubation time for a specific material developed within the framework of the work based on the results of processing the experimentally observed strain rate dependence of dynamic strength will contribute to a wider implementation of the methods of the structural-time approach in scientific and engineering practice. Also, the assessment of incubation time in the form of a confidence interval allows for a more objective comparison of the strength properties of various materials.

The developed analytical models, allowing to estimate the energy consumptions of dynamic fracture, helped to identify the optimal values of the loading parameters corresponding to the most energy-efficient fracture effect. These models can be useful in solving various practical problems, for which it is important to counteract fracture of any structural elements, or, on the contrary, to destroy materials that require mechanical processing.

A new method that allows one to reveal the strain rate dependence of the fracture modes of two-component brittle materials or processes of inelastic deformation of metals is not only of great scientific interest, but also has great practical significance, for example, in the creation and development of new heterogeneous materials that are planned to be used in structures experiencing high strain rate impacts during operation.

The reliability of the obtained results in the field of fracture mechanics is due to the use of ideas underlying the incubation time criterion, which has proven

itself well over the past 30 years in solving many problems related to predicting critical characteristics of transient processes in completely different areas of mechanics and physics. The randomized method of sign-perturbed sums used in the work to estimate the values of model parameters has also been tested. Over the past ten years, many works devoted to the method have been published in international rating publications. Also, the results of studies confirming the mathematical correctness of the method of sign-perturbed sums have been repeatedly reported at international congresses held under the auspices of IEEE.

Structure and volume of the dissertation

The dissertation consists of an introduction, 5 chapters, a conclusion, 41 figures, 7 tables, a bibliography of 188 titles and a list of the author's publications for the defense consisting of 31 titles. The length of the dissertation is 188 pages.

The first chapter presents the main ideas of application of the incubation time criterion for modeling the train rate dependence of strength, and also presents a method for estimating the value of the incubation time, based on the randomized method of sign-perturbed sums. A detailed analysis of the main idea of the method is carried out, and a theorem on the fulfillment of the conditions of applicability of the method for the problem under study and the limitations of the obtained estimate is proved. The efficiency of the proposed method is shown using experimental data for various materials as an example. Interval estimation of the value of the incubation time allows drawing additional conclusions about the strength properties of the material, which may not be obvious from a point estimate.

The second chapter is devoted to the study of the influence of the equilibrium parameters of the state of a continuous medium, namely temperature and external hydrostatic pressure, on the values of the model strength parameters. Temperature dependences for the incubation time and critical stress are proposed.

The performance of the proposed models is tested on the example of application to problems related to acoustic and pulsed cavitation of liquids. It is also shown how the developed methods can be used to find the changed conditions of phase equilibrium of a continuous medium located in the area of action of a background acoustic ultrasonic field.

In the third chapter, the results of the study of the features of the energy intensity of dynamic fracture are presented with the goal to substantiate the practical significance of the developed methods based on the concept of incubation time. The existence of optimal modes of impact destructive action on a continuous medium during contact interaction is shown. The influence of the supersonic phase of interaction of contacting surfaces on the optimal (from the point of view of energy consumption) values of the parameters of the fracture problem is considered.

The fourth chapter presents a new method for processing dynamic test data, which allows for the optimal evaluation together of the values of two model strength parameters, namely: the incubation time and the critical stress, which determines the stability of the medium relative to the stress level of the loading. The proposed method is tested on the example of processing dynamic test data for brittle materials. It is shown how the new method can be used to determine that failure in brittle two-component media under slow and high strain rate loading occurs differently.

The fifth chapter is devoted to a new mechanical interpretation of the parameters of the incubation time criterion. A consistent comparison of the developed methods with models of other authors is carried out, and a relationship with the parameters of other phenomenological approaches predicting the critical conditions of fracture of condensed media under high-speed impact-pulse loading is established.

Methodology and research methods

The solutions to the problems presented in the work were obtained by consistent use of the ideas of the structural-temporal approach, built on the concept of incubation time. This approach has proven to be efficient in solving various problems in completely different areas of mechanics and physics, which are related to the study of the conditions for transient processes in continuous media as a result of high-speed impact.

When developing models, differential and integral-differential equations are formulated and then solved by analytical and numerical methods. Randomized methods are used to determine the values of model parameters, since, because of the specifics of the problem, traditional statistical methods do not allow for a mathematically sound assessment. The calculated dependences are compared with the results of experiments, for which a detailed analysis of the experiment schemes is carried out.

Data from high strain rate tests obtained within the framework of proven experimental methods is used to test the applicability of the approaches developed in this work. In most cases, the results of tests using the Kolsky method [55] are used within the generally accepted experimental scheme with split Hopkinson bars [53, 54, 55]. In these tests, the sample is loaded in such a way, that the sample is in a state of quasi-static equilibrium, which allows for almost direct measurement of the time profile of stresses in the sample. The main result of tests on split bars is the dependence of the critical stress level in the material on the straining rate, the values of which usually vary in the range of about $10^2 - 10^3\ 1/s$. Based on the results of data processing within the framework of the developed methods, the values of the strength parameters, incubation time and critical stress are determined, for which the theoretical time and rate dependences of strength are then calculated. In some cases, for additional verification, the calculated curves are

compared with the data obtained in other experimental setups, for example, on a free-falling load test setup, where a lower straining rate is about $10^1\ 1/s$ [58, 59, 60]. For comparison with the results in the range of higher straining rates about $10^3\ 1/s$, the data obtained in the experimental setup for spall fracture are used, in which the specimen is loaded due to the reflection of the shock wave from the free surface of the specimen [61, 62, 63, 64, 65, 66, 67, 68].

The proposed data processing method takes into account the specifics of dynamic tests, which are usually characterized by a small number of experimental observations, as well as the presence of random noise during measurements. The most significant limitation that does not allow the use of generally accepted static methods is the small number of experimental points, therefore, to obtain a mathematically sound estimate of the values of the dynamic strength parameters, the randomized method of sign-perturbed sums (SPS) was chosen. In the original formulation, this method was proposed to estimate the values of the parameters of a linear dynamic system with a small number of test observations and weak assumptions on almost arbitrary random noise [69, 70, 71]. The result of this randomized algorithm is a confidence region containing the true value of the target parameter with a given level of confidence. In this work, the validity of this method for nonlinear model functions that describe experimentally observed dependences in the problems under consideration is proved.

Approbation of the work

The results of the dissertation were presented and discussed at the following international and Russian scientific conferences, seminars and congresses:

XXIV St. Petersburg Readings on Strength Problems (St. Petersburg 2024);

XXIII Winter School on Continuous Media Mechanics (Perm 2023);

XIII All-Russian Congress on Theoretical and Applied Mechanics (St. Petersburg, 2023);

International summer school conference “Advanced problems in materials” (St.-Petersburg, 2022);

The 7th International Conference on Crack Paths (Online 2021);

International online conference Digitalization of industrial thermal processes and units (online 2020);

1st Virtual European Conference on Fracture (Online 2020);

XLVIII International summer school conference “Advanced problems in materials” (St.-Petersburg 2020);

XLVII International Summer School-Conference “Advanced Problems in Mechanics” (Saint-Petersburg 2019);

XXXIV International Conference on Interaction of Intense Energy Fluxes with Matter (Elbrus 2019);

International Summer School-Conference “Advanced Problems in Mechanics” (Saint-Petersburg 2018);

22nd European Conference on Fracture - ECF22 (Belgrad 2018);

IEEE 56th Annual Conference on Decision and Control, CDC 2017, (Melbourne 2017);

12th International Conference on the Mechanical Behavior of Materials, (Karlsruhe 2015);

XI All-Russian Congress on Fundamental Problems of Theoretical and Applied Mechanics (Kazan 2015);

II All-Russian scientific and practical conference “Geomechanical and geotechnological problems of efficient development of solid mineral deposits in the northern and north-eastern regions of Russia” (Yakutsk 2013);

13th International Conference on Fracture (Beijing 2013);

8th European Solid Mechanics Conference (Graz 2012);

19th European Conference on Fracture (Kazan 2012);

Conference-seminar “Current trends in continuum mechanics” (St. Petersburg 2012);

St. Petersburg Scientific Council on Combustion and Explosion as part of the United Scientific Council on Materials Science, Mechanics and Strength at the St. Petersburg Scientific Center of the Russian Academy of Sciences (St. Petersburg 2022).

Support

The candidate's scientific research was carried out with the support of 5 grants under the personal supervision of the author, including 1 grant from the Russian Science Foundation (20-79-10078), 1 grant from the Russian Foundation for Basic Research (20-31-70053) and 3 grants from the President of the Russian Federation for young candidates of science (MK-5890.2013.1, MK-7596.2015.1, MK-6312.2018.1).

A significant part of the research was carried out with the support of a grant from the Ministry of Science and Higher Education of the Russian Federation (megagrant No. 075-15-2022-1114) and a grant from the Russian Science Foundation (22-11-00091).

Acknowledgements

The author is grateful to Yuri Viktorovich Petrov for many years of fruitful scientific communication, for help and support in writing this work, and for the opportunity to take part in the development of ideas of the structural-temporal approach and solving related problems. I also express my gratitude to Oleg Nikolaevich Granichin for a deep discussion and assessment of new methods of applying randomized algorithms in traditional problems of fracture mechanics.

Publications

On the topic of the dissertation, 52 articles have been published in international journals, 44 of which are included in the Scopus and Web of Science databases.

Personal contribution of the author

In obtaining most of the results presented in the dissertation, the ideas of the structural-temporal approach formulated by the scientific consultant of the work, Professor of St. Petersburg State University, Corresponding Member of the Russian Academy of Sciences, Doctor of Physical and Mathematical Sciences Yu.V. Petrov, who at the initial stage set the problems that were relevant for solution, were used. The author of the work took direct part in solving the problems set.

Specifically, the author did the following:

1. developed a method for finding a confidence interval with a given level of confidence probability for assessing the incubation time based on high strain rate testing data under impact-pulse loading;
2. developed a model of phase transformations of continuous media under the action of a nonequilibrium mechanical load; calculated the curves of the phase

equilibrium "liquid-vapor" for water located in the region of a subthreshold ultrasonic wave;

3. found the dependence of the energy spent on the fracture of an elastic medium upon impact of a solid particle on the duration of the resulting impact; studied the influence of the supersonic stage of interaction on the existence of optimal loading modes and proposed a method for taking this stage into account;
4. developed a method for processing high strain rate test data, allowing for the assessment together of two strength parameters: incubation time and critical stress;
5. developed an analytical model that allows identifying the strain rate dependence of the fracture mechanism of brittle two-component materials;
6. elaborated an analytical approach that allows identifying the strain rate dependence of the mechanisms of plastic deformation of metals;
7. proposed a new interpretation of the parameters of the incubation time criterion.

On the whole, a concept for studying strength under high strain rate impacts is proposed, correct methods for processing experimental results are indicated, and algorithms for determining the values of the parameters of the fracture criterion are developed.

Publication of key results

Scopus and Web of Science

1. Lukashov, R., Volkov, G. An analytical approach to deduce loading rate-sensitivity of fracture mode of concrete and mortar (2024) International Journal of Impact Engineering, 187, 104915.
2. Zhao, S., Petrov, Y.V., Zhang, Y., Volkov, G.A., Xu, Z., Huang, F. Modeling of the thermal softening of metals under impact loads and their

temperature–time correspondence (2024) International Journal of Engineering Science, 194, 103969.

3. Evstifeev, A.D., Volkov, G.A. A Variational Approach to the Determination of the Dynamic Strength of a Material (2023) Technical Physics, 68 (2), pp. 139-143.
4. Granichin, N.O., Volkov, G.A., Gruzdkov, A.A., Petrov, Y.V. Instability of the Water Phase Diagram under Short Pulse Loading (2023) Mechanics of Solids, 58 (5), pp. 1599-1605.
5. Zhao, S., Petrov, Y.V., Volkov, G.A. The modified relaxation plasticity model and the non-monotonic stress–strain diagram (2023) International Journal of Mechanical Sciences, 240, 107919.
6. Volkov, G.A., Petrov, Y.V. On the Analysis of Two Theoretical Approaches to Predict the Material Strength under Dynamic Loading (2022) Mechanics of Solids, 57 (8), pp. 1958-1963.
7. Zhao, S., Petrov, Y.V., Volkov, G.A. Modeling the Nonmonotonic Behavior Flow Curves under Dynamic Loads (2022) Physical Mesomechanics, 25 (3), pp. 221-226.
8. Volkov, G., Smirnov, I. A probabilistic approach to evaluate dynamic and static strength of quasi-brittle materials through high-rate testing (2022) International Journal of Mechanical Sciences, 216, 106960.
9. Smirnov, I.V., Mikhailova, N.V., Yakupov, B.A., Volkov, G.A. Analysis of Dependences of Threshold Parameters for Acoustic Cavitation Onset in a Liquid on an Ultrasonic Frequency, Hydrostatic Pressure, and Temperature (2022) Technical Physics, 67 (2), pp. 161-170.
10. Volkov, G.A., Gruzdkov, A.A., Petrov, Y.V. A Randomized Approach to Estimate Acoustic Strength of Water (2022) Advanced Structured Materials, 164, pp. 633-640.

11. Volkov, G., Logachev, A., Granichin, N., Zhao, Y.-P., Zhang, Y., Petrov, Y. The influence of background ultrasonic field on the strength of adhesive zones under dynamic impact loads (2021) Materials, 14 (12), 3188.
12. Khlopkov, E.A., Dmitrievskiy, A.A., Pomytkin, S.P., Lyubomudrov, S.A., Makarova, T.A., Volkov, G.A., Turzakov, A.S., Vyunenko, Y.N. Influence of the Mechanical Load on the Operating Temperature of Ring-Shaped Bundle Force Elements (2021) Russian Engineering Research, 41 (2), pp. 162-165.
13. Granichin, N., Volkov, G., Petrov, Y., Volkova, M. Randomized approach to determine dynamic strength of ice (2021) Cybernetics and Physics, 10 (3), pp. 122-126.
14. Petrov, Y., Logachev, A., Granichin, N., Volkov, G. Adhesive Joint Fracture Under Combined Pulsed and Vibrational Loading (2020) Structural Integrity, 16, pp. 100-105.
15. Granichin, N.O., Volkov, G.A., Petrov, Y.V. Delamination of the Planar Adhesion Zone under Combined Dynamic Actions (2020) Technical Physics, 65 (1), pp. 68-72.
16. Mikhailova, N., Onawumi, P.Y., Volkov, G., Smirnov, I., Broseghini, M., Roy, A., Petrov, Y., Silberschmidt, V.V. Ultrasonically assisted drilling in marble (2019) Journal of Sound and Vibration, 460, 114880.
17. Atroshenko, S.A., Chevrychkina, A.A., Evstifeev, A.D., Volkov, G.A. Destruction of ABS Polymer in the Glass State under Dynamic Stressing (2019) Physics of the Solid State, 61 (11), pp. 2075-2082.
18. Chernyavskaya, N.V., Volkov, G.A., Khlopkov, E.A. Possibilities of Ultrasonic Initiation of the Operation of TiNi Alloy Ring-Shaped Force Elements (2019) Russian Metallurgy (Metally), 2019 (10), pp. 1015-1017.

19. Evstifeev, A.D., Volkov, G.A., Chevrychkina, A.A., Petrov, Y.V. Strength Performance of 1230 Aluminum Alloy under Tension in the Quasi-Static and Dynamic Ranges of Loading Parameters (2019) Technical Physics, 64 (5), pp. 620-624.
20. Evstifeev, A.D., Volkov, G.A., Chevrychkina, A.A., Petrov, Y.V. Dynamic Strength Characteristics of Materials: Influence of the Specimen Size on Strain Rate (2019) Technical Physics, 64 (4), pp. 523-526.
21. Mikhailova, N.V., Volkov, G.A., Petrov, Y.V., Smirnov, I.V., Onawumi, P., Roy, A., Silberschmidt, V. Relations between Parameters of Fracture Processes on Different Scale Levels (2018) Doklady Physics, 63 (11), pp. 459-461.
22. V'yunenko, Y.N., Volkov, G.A., Khlopkov, E.A. Temperature Factor to Control Deformation–Power Behavior of Ring-Shaped Bundle Force TiNi Elements (2018) Technical Physics, 63 (8), pp. 1167-1170.
23. Chevrychkina, A.A., Evstifeev, A.D., Volkov, G.A. Analysis of the Strength Characteristics of Acrylonitrile–Butadiene–Styrene Plastic under Dynamic Loading (2018) Technical Physics, 63 (3), pp. 381-384.
24. Gorbushin, N.A., Granichin, N.O., Logachev, A.N., Petrov, Y.V., Volkov, G.A. Destruction of the adhesion zone by combined pulsed-vibrational impacts (2018) Materials Physics and Mechanics, 36 (1), pp. 114-120.
25. Volkova, M.V., Granichin, O.N., Volkov, G.A., Petrov, Y.V. On the Possibility of Using the Method of Sign-Perturbed Sums for the Processing of Dynamic Test Data (2018) Vestnik St. Petersburg University: Mathematics, 51 (1), pp. 23-30.
26. Gorbushin, N., Vitucci, G., Volkov, G., Mishuris, G. Influence of fracture criteria on dynamic fracture propagation in a discrete chain (2018) International Journal of Fracture, 209 (1-2), pp. 131-142.

27. Volkova, M.V., Granichin, O.N., Petrov, Y.V., Volkov, G.A. Dynamic fracture tests data analysis based on the randomized approach (2017) Advances in Systems Science and Applications, 17 (3), pp. 34-41.
28. Mikhailova, N.V., Volkov, G.A., Meshcheryakov, Y.I., Petrov, Y.V., Utkin, A.A. Failure-delay effect in destruction of steel samples under spalling conditions (2017) Technical Physics, 62 (4), pp. 547-552.
29. Volkov, G.A., Petrov, Y.V., Utkin, A.A. On some principal features of data processing of spall fracture tests (2017) Physics of the Solid State, 59 (2), pp. 310-315.
30. Petrov, Y.V., Smirnov, I.V., Volkov, G.A., Abramian, A.K., Bragov, A.M., Verichev, S.N. Dynamic failure of dry and fully saturated limestone samples based on incubation time concept (2017) Journal of Rock Mechanics and Geotechnical Engineering, 9 (1), pp. 125-134.
31. Peck, D., Volkov, G., Mishuris, G., Petrov, Y. Resolution of the threshold fracture energy paradox for solid particle erosion (2016) Philosophical Magazine, 96 (36), pp. 3775-3789.
32. Volkov, G.A., Petrov, Y.V., Gruzdkov, A.A. Acoustic strength of water and effect of ultrasound on the liquid-vapor phase diagram (2015) Technical Physics, 60 (5), pp. 753-756.
33. Volkov, G.A., Petrov, Y.V., Gruzdkov, A.A. Liquid-vapor phase equilibrium conditions in an ultrasonic field (2015) Doklady Physics, 60 (5), pp. 229-231.
34. Gorbushin, N.A., Volkov, G.A., Petrov, Y.V. Simulation of the behavior of the cutting force during ultrasonic rotary machining of materials using structure-time fracture mechanics (2014) Technical Physics, 59 (6), pp. 852-856.

35. Gorbushin, N.A., Volkov, G.A., Petrov, Y.V. On the effect of the geometrical shape of a particle on threshold energy in erosion damage (2013) Technical Physics, 58 (3), pp. 388-392.
36. Volkov, G.A., Gorbushin, N.A., Petrov, Y.V. On the dependence of the threshold energy of small erodent particles on their geometry in erosion fracture (2012) Mechanics of Solids, 47 (5), pp. 491-497.
37. Bratov, V., Petrov, Y., Volkov, G. Existence of optimal energy saving parameters for different industrial processes (2011) Applied Mechanics and Materials, 82, pp. 208-213.
38. Petrov, Y., Bratov, V., Volkov, G., Dolmatov, E. Incubation time based fracture mechanics and optimization of energy input in the fracture process of rocks (2011) Advances in Rock Dynamics and Applications, pp. 163-184.
39. Volkov, G.A., Bratov, V.A., Gruzdkov, A.A., Babitsky, V.I., Petrov, Y.V., Silberschmidt, V.V. Energy-based analysis of ultrasonically assisted turning
40. (2011) Shock and Vibration, 18 (1-2), pp. 333-341.
41. Volkov, G.A., Silberschmidt, V.V., Babitskii, V.I., Gruzdkov, A.A., Bratov, V.A., Petrov, Y.V. Energy aspects of ultrasonic intensification of treatment of metals (2010) Doklady Physics, 55 (4), pp. 184-185.
42. Volkov, G.A., Gruzdkov, A.A., Petrov, Y.V. Cavitation resistance of cryogenic liquids: Incubation time criterion (2009) Technical Physics, 54 (11), pp. 1708-1710.
43. Volkov, G.A., Silberschmidt, V.V., Mitrofanov, A.V., Gruzdkov, A.A., Bratov, V.A., Petrov, Y.V. Minimization of fracture-pulse energy under contact interaction (2009) Doklady Physics, 54 (7), pp. 322-324.
44. Volkov, G.A., Gruzdkov, A.A., Petrov, Y.V. The incubation time criterion and the acoustic strength of sea water (2007) Acoustical Physics, 53 (2), pp. 119-122.

Other publications

45. Volkov, G.A., Bratov, V.A., Borodin, E.N., Evstifeev, A.D., Mikhailova, N.V. Numerical simulations of impact Taylor tests (2020) Journal of Physics: Conference Series, 1556 (1), 012059.
46. Evstifeev, A.D., Volkov, G.A. Effect of Mg on dynamic properties of Al-Mg alloys (2020) Procedia Structural Integrity, 28, pp. 2261-2266.
47. Mikhailova, N., Smirnov, I., Volkov, G. Modelling of pressure-temperature conditions for cavitation initiation in different liquids (2019) Vibroengineering Procedia, 27, pp. 121-125.
48. Khlopkov, E.A., Zhurbenko, P.N., Tikhomirov, A.A., Volkov, G.A., Zatulsky, G.Z., Vyunenko, Yu.N. The influence of the temperature conversion rate on the deformation processes of the shape memory effect and transformation plasticity (2019) IOP Conference Series: Materials Science and Engineering, 656 (1), 012024
49. Volkov, G., Borodin, E., Bratov, V. Numerical simulations of Taylor anvil-on-rod impact tests using classical and new approaches (2017) Procedia Structural Integrity, 6, pp. 330-335.
50. Chevrychkina, A.A., Volkov, G.A., Estifeev, A.D. An experimental investigation of the strength characteristics of ABS plastic under dynamic loads (2017) Procedia Structural Integrity, 6, pp. 283-285.
51. Khlopkov, E., Volkov, G., Vyunenko, Y. Specific features of the behavior of TiNi force elements in thermocycling (2017) Materials Today: Proceedings, 4 (3), pp. 4879-4883.
52. Volkova, M., Volkov, G., Granichin, O., Petrov, Y. Sign-perturbed sums approach for data treatment of dynamic fracture tests (2017) 2017 IEEE 56th Annual Conference on Decision and Control, CDC 2017, 2018-January, pp. 1652-1656.

53. Volkov, G., Petrov, Y.V., Gorbushin, N. Threshold fracture energy for differently shaped particles impacting Halfspace (erosion-type fracture) (2013) 13th International Conference on Fracture 2013, ICF 2013, 4, pp. 2667-2671.

54. Volkov, G.A., Dolmatov, E.N., Petrov, Y.V. Optimization of energy input in the fracture process of rocks (2012) 19th European Conference on Fracture: Fracture Mechanics for Durability, Reliability and Safety, ECF 2012.

Main results

- Analytical model for predicting the dependence of the acoustic cavitation threshold on the frequency of the ultrasonic wave and the pulse cavitation threshold on the duration of the loading action [49, 72] (personal contribution is at least 80%)
- Modified model predicting cavitation threshold for variations in temperature and background liquid pressure [73] (personal contribution is at least 80%).
- - Method for calculating the phase equilibrium conditions of continuous media under the influence of high-rate background actions [74, 75] (personal contribution is at least 90%)
- Methods to account for the effect of the ultrasonic background field on adhesive strength [76, 77, 78, 79] (personal contribution is at least 70%)
- - Investigation of the energy input required to initiate the dynamic threshold fracture pulse from the impact contact interaction of a solid body with an elastic medium [80] (personal contribution is at least 80%)
- Threshold energy as a function of fracture pulse duration for different impactor shapes: discovery of energy-optimal impact modes [81, 82] (personal contribution at least 80%)

- Explanation of the paradoxical change in the character of the threshold energy dependence on the pulse duration, resulting from a smooth change in the geometry of the impactor surface. Consideration of the supersonic phase of the contact interaction [83] (personal contribution at least 70%)
- - Model of ultrasonically assited cutting and drilling of materials, construction of the dependence of the cutting force on the material feed rate [84, 85, 86, 87, 50] (personal contribution is at least 80%)
- - A new method for estimating incubation time values to provide a mathematically proven result by processing a limited dataset of high-rate tests with weak constraints on random measurement noise [88, 89, 90, 91, 91, 92, 93, 94, 95, 96, 97] (personal contribution of at least 80%)
- An analytical model that reveals the rate sensitivity of the fracture mode in two-component materials, i.e., the change in fracture mechanism with increasing impact velocity. New interpretation of the critical stress parameter [98] (personal contribution at least 95%)
- A new interpretation of the incubation time as a parameter that, unlike most other approaches, allows setting a non-uniform normalization for the loading rate [99] (personal contribution is at least 90%)
- An analytical model to reveal the rate sensitivity of the plastic deformation process. New interpretation of the dimensionless parameter α [100] (personal contribution is at least 95%)

Statements for the defense

1) A new method for estimating the values of the dynamic strength parameter of materials – the incubation time – in the form of a confidence interval determined by processing a limited set of high strain rate test data.

2) An analytical model that allows calculating the frequency dependence of the acoustic cavitation threshold.
3) An analytical model that allows predicting the conditions for the occurrence of phase transformations in continuous liquid media under the influence of non-equilibrium mechanical load.
4) Method of calculating “corrected” curves of “liquid-vapor” phase equilibrium for liquid media located in the zone of action of a sub-threshold ultrasonic wave.
5) Method for assessing the energy capacity of dynamic fracture during contact interaction of a rigid particle with an elastic half-space depending on the shape of the contacting surfaces.
6) A new method for combined assessing the values of two strength parameters – the incubation time and critical stress – by processing a limited set of experimental data obtained only under high strain rate shock-pulse loading.
7) An analytical model that allows identifying the rate dependence of the fracture mode in brittle two-component materials based on the results of a comparative analysis of the experimentally obtained strain rate dependence of the material strength and static test data, without additional studies of the structure of the fractured samples.
8) An analytical model that allows revealing the strain rate sensitivity of plastic deformation mechanisms in metals.
9) New mechanical interpretation of the parameters included in the incubation time criterion – the critical stress σ_c and the dimensionless parameter α.

Chapter 1 Strain rate aspects of continuous media fracture

To solve various problems using models formulated within the framework of the structural-temporal approach, it is necessary to know the value of the incubation time parameter. For its reasonable estimation, it is necessary to have standard methods for analysis of high strain rate test data. This chapter describes the proposed methodology for processing test data obtained in the form of strain rate or time dependence of strength.

The results presented in Chapter 1 have been published in the following papers [88, 89, 90, 91, 97].

1.1 Method of sign-perturbed sums for estimating material strength parameters within the framework of the structural-time approach

The expression for the most common form of the incubation time criterion, that is, the condition for the onset of destruction, can be written as follows:

$$\frac{1}{\tau}\int_{t-\tau}^{t} sign\big(\sigma(\xi)\big)\left(\frac{|\sigma(\xi)|}{\sigma_c}\right)^{\alpha} d\xi \le 1, \qquad (1.1)$$

where $\sigma(t)$ is the time profile of stress, while the incubation time τ, critical stress σ_c and dimensionless positive parameter α are the macroscopic material parameters. Note that in the general case, the loading effect $\sigma(t)$ can take both positive and negative values, therefore, to correctly take into account the influence of compressive stresses with fractional or even values of α, it is necessary to have a multiplier $sign\big(\sigma(\xi)\big)$.

According to the criterion, failure occurs at the time instant $t = t_*$, at which the expression (1.1) first becomes an equality. In other words, the failure time t_* can be defined as follows:

$$t_* = \min\left\{t > 0 \middle| \frac{1}{\tau}\int_{t-\tau}^{t} sign\big(\sigma(\xi)\big)\left(\frac{|\sigma(\xi)|}{\sigma_c}\right)^{\alpha} d\xi = 1\right\}, \qquad (1.2)$$

The physical nature of the parameter τ is related to the dynamics of relaxation microstructural processes at lower scale levels, which precede the manifestation of fracture at the macro level – the obvious failure of the sample, which is recorded in the experiment. In brittle solids, such processes can be associated with the origin of microcracks, their growth with subsequent coalescence, i.e. their merging into one larger one.

It is natural to assume that the rate of all these preparation processes will depend not only on the stress level, but also on how quickly it changes under the applied load. Thus, one can consider that the incubation time characterizes the sensitivity of the material to some average loading rate determined by the time profile of the loading effect.

The basic idea of the structural-temporal approach is based on the fact that any transition processes, such as macro failure, do not occur instantly, and their initiation and subsequent development require a certain amount of time. Thus, within the framework of the approach, the parameter τ can be considered as a primary measure of dynamic strength, which characterizes the strain rate sensitivity of the material, thereby determining the degree of influence of the loading rate on the ultimate stress level at this strain rate value.

The second parameter of criterion (1.2) σ_c in most cases can be interpreted as the static strength of the material σ_s, that is, as the ultimate stress level under slow loading with a low stress growth rate. However, further use of the criterion

showed [98] that in some cases, when the rate sensitivity of the material failure mode occurs, the value of σ_c may differ from experimentally measured in a static test σ_s. Therefore, in the general case, the parameter σ_c is more correctly referred to just as the critical stress, although in most cases, when the material failure mechanism does not depend on the impact rate, it can be taken as the static strength parameter, that is, $\sigma_c = \sigma_s$. It is worth noting that, like the incubation time τ, the parameter σ_c also affects the maximum stress level under high-speed loading.

The experience of the criterion application in problems of predicting failure shows, that for most brittle materials the value of the parameter α can be taken equal to one. However, in some cases, for an accurate description of the experimentally observed strain rate dependence of the material strength, it is necessary to use other values of this parameter. It is worth noting that the choice of values of parameter α different from unity turned out to be most popular when solving problems, in which the strain rate dependences of the dynamic yield strength are studied. It is a little more difficult to determine the mechanical meaning of the parameter α than the other parameters of the criterion τ and σ_c. Formally it can be interpreted as the sensitivity of the material to the amplitude of the loading pulse.

1.2 Loading at a constant strain rate

In most dynamic tests, macro fracture of the sample occurs at the stage of growth of stress and strain. This is usually due to the fact that in the tests a post-threshold loading is realized, i.e. it obviously leads to fracture. Since the fracture of brittle and quasi-brittle materials occurs faster due to the growth and propagation

of microcracks than due to the development of various processes associated with inelastic deformation, the loading law up to the moment of fracture can be approximated by a linear function. Thus, the time profile of the load can be written as follows:

$$\sigma(t) = H(t)E\dot{\varepsilon}t = H(t)\dot{\sigma}t, \tag{1.3}$$

where $\dot{\varepsilon}$ и $\dot{\sigma}$ are the strain and stress rates, E is the Young's modulus, and $H(t)$ – the Heaviside function. After substituting the expression for linear loading (1.3) into equation (1.2) and subsequent integration one obtains the following equation for the time instant of fracture t_*:

$$H(t_*)\left(\frac{t_*}{\tau}\right)^{\alpha+1} - H(t_* - \tau)\left(\frac{t_*}{\tau} - 1\right)^{\alpha+1} = k, \tag{1.4}$$

where $k = \frac{2\sigma_c}{E\dot{\varepsilon}\tau}$ is the dimensionless parameter that depends on the strength properties of the material and the loading rate. The first multiplier $H(t_*)$ is always equal to unity, since the time instant t_* cannot be negative by definition. Therefore, it is necessary to consider only two possible cases when the failure time instant is less than the incubation time, $t_* < \tau$, and, conversely, $t_* \geq \tau$. From equation (1.4) it follows that the condition $t_* < \tau$ is equivalent to $k < 1$. And recollecting the expression for the parameter k, one can obtain the following inequality:

$$k = \frac{2\sigma_c}{E\dot{\varepsilon}\tau} < 1 \Leftrightarrow \dot{\varepsilon} > \frac{2\sigma_c}{E\tau} = \dot{\varepsilon}_c,$$

where $\dot{\varepsilon}_c$ is a constant with the dimension of the strain rate, which value is determined by the strength material parameters τ и σ_c, as well as its Young's modulus E. Thus, within the framework of structural-temporal approach, the strength parameters determine a certain critical strain rate, comparison with which allows us to conclude whether the loading is high strain rate or low strain rate.

As a result, equation (1.4) with respect to the failure time instant t_* can be rewritten as follows:

$$\begin{cases} \left(\frac{t_*}{\tau}\right)^{\alpha+1} = k, & k < 1, \\ \left(\frac{t_*}{\tau}\right)^{\alpha+1} - \left(\frac{t_*}{\tau} - 1\right)^{\alpha+1} = k, & k \geq 1. \end{cases} \tag{1.5}$$

It is worth noting that the first equation has an analytical solution for arbitrary α, while the second one in general can be solved only by numerical methods.

As mentioned earlier, for brittle materials in most cases one can take $\alpha = 1$ and write the analytical solution for equation (1.5) in the following form:

$$\frac{t_*}{\tau} = \begin{cases} \sqrt{k}, & k < 1, \\ \frac{k+1}{2}, & k \geq 1, \end{cases}$$

or

$$t_* = \begin{cases} \sqrt{\frac{2\sigma_c \tau}{E\dot{\varepsilon}}}, & \dot{\varepsilon} > \frac{2\sigma_c}{E\tau}, \\ \frac{2\sigma_c + E\dot{\varepsilon}\tau}{2E\dot{\varepsilon}}, & \dot{\varepsilon} \leq \frac{2\sigma_c}{E\tau}. \end{cases} \tag{1.6}$$

By substituting the fracture time into the relationship describing the loading effect (1.3), we can obtain an analytical function describing the stress level at the time instant of fracture for an arbitrary strain rate:

$$\sigma_*(\dot{\varepsilon}) = \varphi_{\tau,\sigma_c}(\dot{\varepsilon}) = \begin{cases} \sigma_c + \frac{E\dot{\varepsilon}\tau}{2}, & \dot{\varepsilon} \leq \frac{2\sigma_c}{E\tau}, \\ \sqrt{2\sigma_c \tau E\dot{\varepsilon}}, & \dot{\varepsilon} > \frac{2\sigma_c}{E\tau}. \end{cases} \tag{1.7}$$

By analogy with the traditional concept of strength, the stress level at the moment of fracture is called the dynamic strength of the material, so it can be affirmed that the function $\varphi_{\tau,\sigma_c}(\dot{\varepsilon})$ describes the strain rate dependence of the

material strength. Often used is the ratio of dynamic strength to its static value denoted as DIF (dynamic increase factor). Figure 1.1 shows the strength-strain rate curve in dimensionless coordinates.

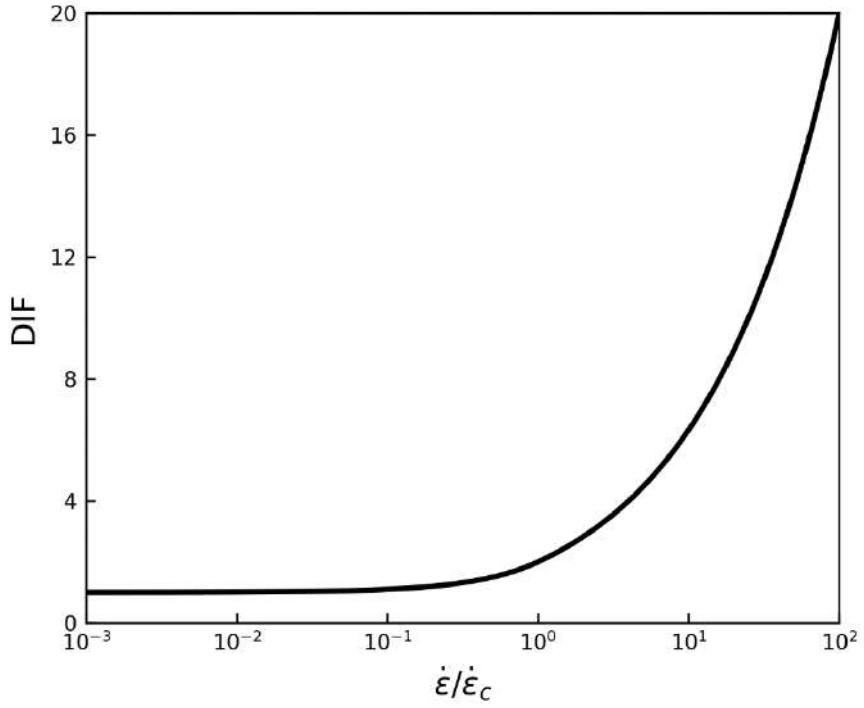

Figure 1.1. DIF strain rate curve in dimensionless coordinates calculated within the framework of the structural-temporal approach.

It should be noted that expression (1.7) predicts the strength of the material in both the dynamic and static cases within the framework of unique analytical two-parameter model. Moreover, knowledge of the values of the strength criterion parameters for a specific material allows estimating the critical amplitudes for the threshold load with a given time profile. Therefore, the assessment of the values of the strength parameters of the material τ and σ_c is a very important task, the reliable solution of which will contribute to a wider dissemination of the structural-temporal approach in practice.

Methods for assessing material parameters

Critical stress value σ_c can be determined in independent static tests by standard methods. As a result of statistical processing of the measured values, it is possible to obtain an estimate of σ_c, as the static strength of the material, with a certain degree of accuracy. Special attention in the tests should be paid to determining the process of sample failure, namely, what size of the fracture zone and/or what amount of damage is recorded in the experiment as the fact of failure. This is necessary to be sure that in high-rate tests the critical stress level is measured for exactly the same process of material failure as in slow loading. Not complying with this rule can lead to ambiguous situations, which will be partially analyzed further.

While the value of the parameter σ_c can be estimated from static tests, for the incubation time of fracture τ there are no implemented experimental methods for directly measuring its value. Earlier in [37] an experimental method for determining the incubation time of fracture in the form of an imaginary experiment was proposed, however, according to this scheme, no real empirical data have been yet obtained. Therefore, the only existing method is an implicit assessment of the incubation time by finding the maximum match between the theoretical curve and the dynamic test data. The form of the analytical curve, which is given by function $\varphi_{\tau,\sigma_c}(\dot{\varepsilon})$ from equation (1.7), depends on the parameters τ and σ_c. If we assume that the value of σ_c is known and is determined by the static strength of the sample, then the optimal value for τ can be found, for example, by the least squares method (LSM), which minimizes the sum of the absolute values of the discrepancies between the theoretically predicted and experimentally observed values of the tensile strength. The main disadvantage of this method is that it allows one to

determine only a certain value of the incubation time and does not provide any mathematically sound assessment of the reliability of the result.

Application of the method of sign-perturbed sums for estimating the values of material parameters that determine its strength according to the incubation time criterion

The main limitations for correct statistical analysis are usually a small number of experimental observations, as well as an unknown distribution of random noise. Therefore, to find the optimal value of the incubation time, the method of sign-perturbed sums or SPS-method (Sign Perturbed Sums) was proposed [69, 71]. This method is based on a randomized algorithm for analyzing a small number of process parameter measurements with relatively weak restrictions on the random noise. The only limitation is the assumption that the distribution of random noise is symmetrical relative to the zero value. With the SPS method, the result of the process parameter evaluation is a confidence interval containing the true value of the sought parameter, with a predetermined probability level. Initially, this method was formulated by its authors to estimate the parameters of a linear multidimensional function, and they proved that the set obtained in the framework of the method of sign-perturbed sums in *n*-dimensional space will contain the true values of the parameters with a pre-selected level of reliability, and this set will also be star-convex, that is, a set that has a point called the center, and all other points lie on rays emanating from the center. However, in the case of fracture problems, the function $\varphi_{\tau,\sigma_c}(\dot{\varepsilon})$ is nonlinear, therefore, in this work before using the SPS method, it will be proved that the result obtained within the framework of the method is justified, that is, the resulting set will be limited and will contain the true value of the parameter τ with a given probability.

One-dimensional case: estimation of the value of only the incubation time. The main idea of the sign-perturbed sums method

The results of dynamic tests usually are presented as a set of dynamic tensile strength values measured experimentally for different strain rate values:

$$\sigma_{*i} = \sigma_{*i}(\dot{\varepsilon}_i), \qquad i = 1 \dots N,$$

where N is the number of tests, which usually does not exceed 10, because of the overall complexity and labor intensity of the dynamic experiments. For further analysis, it is convenient to present the experimentally measured values σ_{*i} of the dynamic strength as the results of the following observation model:

$$\sigma_{*i} = \varphi(\tau_*, \dot{\varepsilon}_i) + v_i, \qquad i = 1 \dots N, \tag{1.8}$$

where v_i are random measurement noise values with an unknown distribution symmetric with respect to zero, and τ_* is the true value of the incubation time parameter. In other words, in relation (1.8) it is assumed that the results of real measurements differ from the values of the stress level at the moment of failure predicted by the structural-temporal approach only by the amount of random noise. It is also worth noting that in the case under consideration the SPS method provides an estimate for only one scalar parameter τ, therefore the confidence set T takes the form of a limited interval.

The observation model for the problem of fracture mechanics can be interpreted in the following form, more familiar to control theory. The observed value σ_* is the system's response to the external control factor $\dot{\varepsilon}$ and determines the current state of the dynamic system operating according to a certain rule determined by the function $\varphi(\tau, \dot{\varepsilon}_i)$. In the problem under consideration, it is required to estimate, based on the set of responses $\{\sigma_{*i}\}_{i=1}^{N}$ to various external

influences $\{\dot{\varepsilon}_i\}_{i=1}^{N}$, the internal parameter of the system τ, which has a constant value and determines the properties of the system.

As noted earlier, the simplest way to estimate the value of the incubation time τ is the least squares method, which minimizes the sum of the squares of the residuals of the observed and theoretically predicted values:

$$\sum_{i=1}^{N}\left(\sigma_{*i}-\varphi(\tau,\dot{\varepsilon}_i)\right)^2 \to \min_{\tau}. \tag{1.9}$$

Despite the fact that the method of least squares does not allow mathematically justifying the reliability of the obtained result in the case of an unknown distribution of random noise and a small number of observations, its assessment is the basis of the method of sign-perturbed sums. The necessary condition for the minimum of the sum in expression (1.9) can be written as follows:

$$\sum_{i=1}^{N}\left(\sigma_{*i}-\varphi(\tau,\dot{\varepsilon}_i)\right)\frac{d\varphi(\tau,\dot{\varepsilon}_i)}{d\tau}=0, \tag{1.10}$$

where the analytical expression for the derivative can be obtained by direct differentiation of expression (1.7):

$$\frac{d\varphi(\tau,\dot{\varepsilon})}{d\tau}=\begin{cases}\dfrac{E\dot{\varepsilon}}{2}, & \dot{\varepsilon}\le\dfrac{2\sigma_c}{E\tau},\\[2ex] \dfrac{1}{\sqrt{2\tau}}\sqrt{\sigma_c E\dot{\varepsilon}}, & \dot{\varepsilon}>\dfrac{2\sigma_c}{E\tau}.\end{cases} \tag{1.11}$$

In the method of sign-perturbed sums, the expression on the left side of formula (1.10) is designated as the base sum $H_0(\tau)$, which can be calculated for an arbitrary value of the determining parameter of the system τ:

$$H_0(\tau) = \sum_{i=1}^{N} \left(\sigma_{*i} - \varphi(\tau, \dot{\varepsilon}_i)\right) \frac{d\varphi(\tau, \dot{\varepsilon}_i)}{d\tau}. \qquad (1.12)$$

Next, it is necessary to select the level of reliability, or confidence probability by specifying the values of two natural parameters M and q, specifying the probability, with which the confidence interval T will contain the true value of the parameter τ_*:

$$Prob\{\tau_* \in \mathrm{T}\} = 1 - \frac{q}{M}.$$

In the randomized part of the SPS method, the number M also determines the number of sign-perturbed sums that must be composed randomly by generating $M - 1$ sets of N random numbers β_{ij} taking the values ± 1 with probability $\frac{1}{2}$

$$Prob\{\beta_{ij} = 1\} = Prob\{\beta_{ij} = -1\} = \frac{1}{2}, \qquad i = 1 \ldots N, j = 1 \ldots M - 1.$$

Thus, it is possible to obtain $M - 1$ sign-perturbed sums $H_j(\tau)$:

$$H_j(\tau) = \sum_{i=1}^{N} \beta_{ij} \left(\sigma_{*i} - \varphi(\tau, \dot{\varepsilon}_i)\right) \frac{d\varphi(\tau, \dot{\varepsilon}_i)}{d\tau}, \qquad j = 1 \ldots M - 1. \qquad (1.13)$$

The intuitive idea of the method is that if we calculate the base sum and sign-perturbed sums for the true value of the sought parameter τ_*, then, provided that the random noise is symmetric, there should be no fundamental difference between their absolute values. Indeed, after substituting the true value of τ_* into expressions (1.12) and (1.13), taking into account equality (1.8), we can obtain the following relationships:

$$H_0(\tau_*) = \sum_{i=1}^{N} \big((\varphi(\tau_*, \dot{\varepsilon}_i) + v_i) - \varphi(\tau_*, \dot{\varepsilon}_i)\big) \frac{d\varphi(\tau_*, \dot{\varepsilon}_i)}{d\tau} = \sum_{i=1}^{N} v_i \frac{d\varphi(\tau_*, \dot{\varepsilon}_i)}{d\tau} \tag{1.14}$$

and

$$H_j(\tau_*) = \sum_{i=1}^{N} \beta_{ij} \big((\varphi(\tau_*, \dot{\varepsilon}_i) + v_i) - \varphi(\tau_*, \dot{\varepsilon}_i)\big) \frac{d\varphi(\tau_*, \dot{\varepsilon}_i)}{d\tau} = \sum_{i=1}^{N} \beta_{ij} v_i \frac{d\varphi(\tau_*, \dot{\varepsilon}_i)}{d\tau}, \qquad j = 1 \dots M - 1. \tag{1.15}$$

Since it is assumed that the noise $v_i = \pm|v_i|$ is symmetrical, the expressions on the right-hand sides of relations (1.14) and (1.15) are essentially the same:

$$H_0(\tau_*) = \sum_{i=1}^{N} (\pm|v_i|) \frac{d\varphi(\tau_*, \dot{\varepsilon}_i)}{d\tau} = \sum_{i=1}^{N} \beta_{ij} (\pm|v_i|) \frac{d\varphi(\tau_*, \dot{\varepsilon}_i)}{d\tau} = H_j(\tau_*),$$

therefore $|H_0(\tau)|$ can equally likely be both greater and less than any $\big|H_j(\tau)\big|$. This property of the base sum and the sign-perturbed sums calculated for the true value of the target parameter is the key feature of the SPS method.

Formal steps of the method of sign-perturbed sums

The following formal steps of the method of sign-perturbed sums can be distinguished:

1) Select the values of natural parameters $M > q > 0$ in a way to obtain the desired level of reliability of the result:

$$\mathrm{p} = 1 - \frac{\mathrm{q}}{\mathrm{M}}.$$

2) Generate $N(M-1)$ random numbers β_{ij} equal to ± 1 with probability $\frac{1}{2}$.

3) Specify a discrete set of trial values of the desired parameter $\{\tau_k\}, \tau_k \in \mathbb{R}^+$ with the required step size.

4) For each τ_k, run the procedure $SPS\_Indicator(\tau_k)$ to check whether the trial value τ_k falls within the confidence interval T or not.

The pseudocode for the $SPS\_Indicator(\tau_k)$ procedure is given in Table 1.1:

Table 1.1. Procedure $\boldsymbol{SPS\_Indicator(\tau_k)}$

$\boldsymbol{SPS\_Indicator(\tau_k)}$	
1.	Calculate the residuals $\delta_i(\tau_k) = \sigma_{*i} - \varphi(\tau_k, \dot{\varepsilon}_i)$
2.	Using the generated set of random signs, calculate the base sum $$H_0(\tau_k) = \sum_{i=1}^{N} \left(\sigma_{*i} - \varphi(\tau_k, \dot{\varepsilon}_i)\right) \frac{d\varphi(\tau_k, \dot{\varepsilon}_i)}{d\tau}$$ and $M-1$ sign-perturbed sums $$H_j(\tau_k) = \sum_{i=1}^{N} \beta_{ij} \left(\sigma_{*i} - \varphi(\tau_k, \dot{\varepsilon}_i)\right) \frac{d\varphi(\tau_k, \dot{\varepsilon}_i)}{d\tau}, \qquad j = 1 \ldots M-1$$
3.	Sort the values $\left\|H_j(\tau_k)\right\|$, $j = 1 \ldots M-1$ in ascending order. If some values are equal, they should be arranged arbitrarly relative to each other
4.	Calculate the rank $\Re(\tau_k)$ as the sequential number of the sum $\|H_0(\tau_k)\|$ in the ordered set $\left\{\left\|H_j(\tau_k)\right\|\right\}_{j=0}^{M-1}$
5.	If $\Re(\tau_k) \leq M - q$, then $\boldsymbol{SPS\_Indicator(\tau_k) = 1}$, which means that $\tau_k \in$ T, in the opposite case $\boldsymbol{SPS\_Indicator(\tau_k) = 0}$

Since the SPS method was initially developed by the authors for a linear model function, it becomes necessary to prove its applicability for the model function $\varphi(\tau, \dot{\varepsilon})$, which determines the rate dependence of strength using the incubation time criterion.

Statement. *If* the measurement noise values v_i are independent random variables with a symmetric (relative to zero) distribution and the model function $\varphi(\tau, \dot{\varepsilon})$ is defined by relation (1.7),

then

- probability $Prob\{\tau_* \in \mathrm{T}\} = 1 - \frac{q}{M}$

  (provided that the confidence interval T is constructed according to the steps 1-4 of the algorithm of sign-perturbed sums method described above);
- the confidence interval T is bounded.

Proof. To prove the level of reliability of the obtained estimate, it is necessary to formalize the reasoning given above to describe the intuitive idea of the method. If the trial value $\tau_k = \tau_*$ coincides with the true value, then all discrepancies will be determined only by random noisev_i:

$$\left.\begin{array}{l} \sigma_{*i} = \varphi(\tau_*, \dot{\varepsilon}_i) + v_i \\ \delta_i(\tau_*) = \sigma_{*i} - \varphi(\tau_*, \dot{\varepsilon}_i) \end{array}\right\} \Longrightarrow \delta_i(\tau_*) = -v_i.$$

Under the assumption of symmetry of the random distribution of noise v_i, it can be represented as follows:

$$v_i = \gamma_i |v_i|,$$

where the random variable γ_i is equal to the sign of the random noise and takes on values of ±1 with equal probability. That is,

$$Prob\{\gamma_i = 1\} = Prob\{\gamma_i = -1\} = \frac{1}{2}.$$

Then the expressions for the base sum and sign-perturbed sums can be written in the following form:

$$H_0(\tau_*) = \sum_{i=1}^{N} \gamma_i |v_i| \frac{d\varphi(\tau_*, \dot{\varepsilon}_i)}{d\tau},$$

$$H_j(\tau_*) = \sum_{i=1}^{N} \beta_{ij}\gamma_i |v_i| \frac{d\varphi(\tau_*, \dot{\varepsilon}_i)}{d\tau}.$$

Since γ_i and β_{ij} are independent random variables, it can be argued that the random variable $\gamma_i\beta_{ij}$ also has a symmetric distribution, like β_{ij}:

$$Prob\{\gamma_i\beta_{ij} = 1\} = Prob\{\gamma_i\beta_{ij} = -1\} = \frac{1}{2}.$$

In this case, the expressions for the base sum and sign-perturbed sums actually coincide, which means that $|H_0(\tau_*)|$ can equally likely occupy any position in the ordered set $\{|H_j(\tau_k)|\}_{j=0}^{M-1}$. Therefore

$$Prob\{\Re(\tau_*) \le M - q\} = 1 - \frac{q}{M}.$$

This means that the procedure $\boldsymbol{SPS\_Indicator}(\boldsymbol{\tau}_*) = \mathbf{1}$ will include the true value of the target parameter τ_* in the confidence interval T with the same probability.

The proof of the boundedness of the confidence interval T is conveniently given when $\alpha = 1$, since in this case there is an analytical expression for the model function $\varphi(\tau, \dot{\varepsilon})$ (1.7). However, even in the case when $\alpha = const > 0$, the idea of the proof does not change.

1. First of all, note that, based on the mechanical meaning of the problem under consideration, positive are both the incubation time parameter $\tau > 0$ and the strain rate $\dot{\varepsilon} > 0$. Consequently, for any positive values of τ and $\dot{\varepsilon}$, according to the right-hand side of expression (1.11), the derivative of the model function is also

positive: $\frac{d\varphi(\tau,\dot{\varepsilon})}{d\tau} > 0$. Therefore, for the same loading rate $\dot{\varepsilon} > 0$, we have $\varphi(\tau_1, \dot{\varepsilon}) > \varphi(\tau_2, \dot{\varepsilon})$, provided that $\tau_1 > \tau_2$.

2. Formula (1.7) also allows calculating a set of values $\{\tau_i\}_{i=1}^N$ that correspond to the model curves of the rate dependence of strength, each of which will pass through the corresponding experimental point $\{(\sigma_{*i}, \dot{\varepsilon}_i)\}_{i=1}^N$.

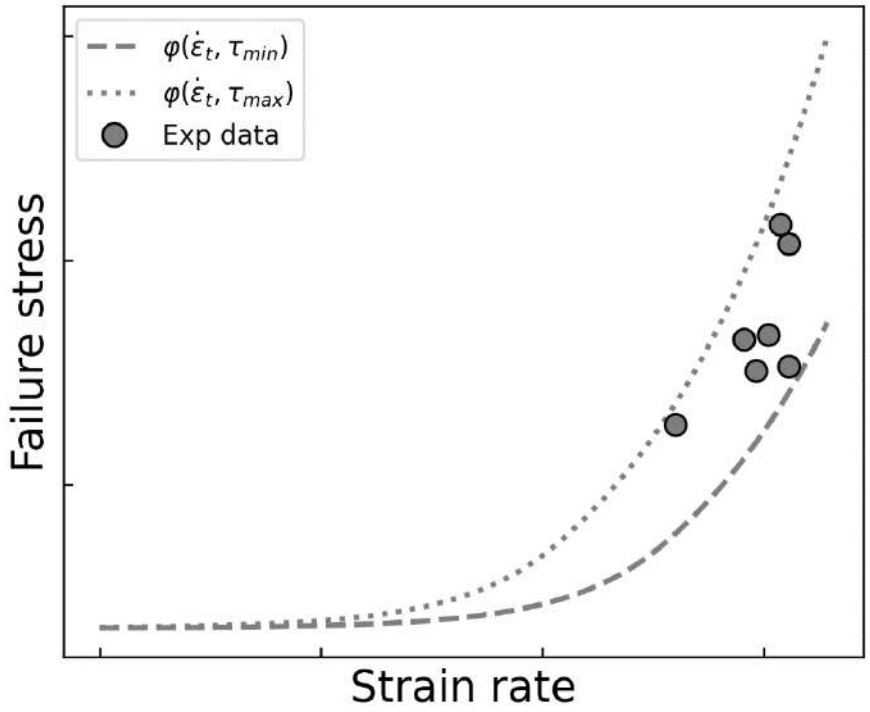

Figure 1.2 Calculated curves of strain rate dependences of strength for values of incubation time τ_{min} and τ_{max}.

3. Denote $\tau_{min} = \min\{\tau_i\}_{i=1}^N$, and $\tau_{max} = \max\{\tau_i\}_{i=1}^N$. According to item 1, all experimental data points of dynamic tests $\{(\sigma_{*i}, \dot{\varepsilon}_i)\}_{i=1}^N$ will be located on the graph between the model curves corresponding to the values of τ_{min} and τ_{max}.(see Figure 1.2).

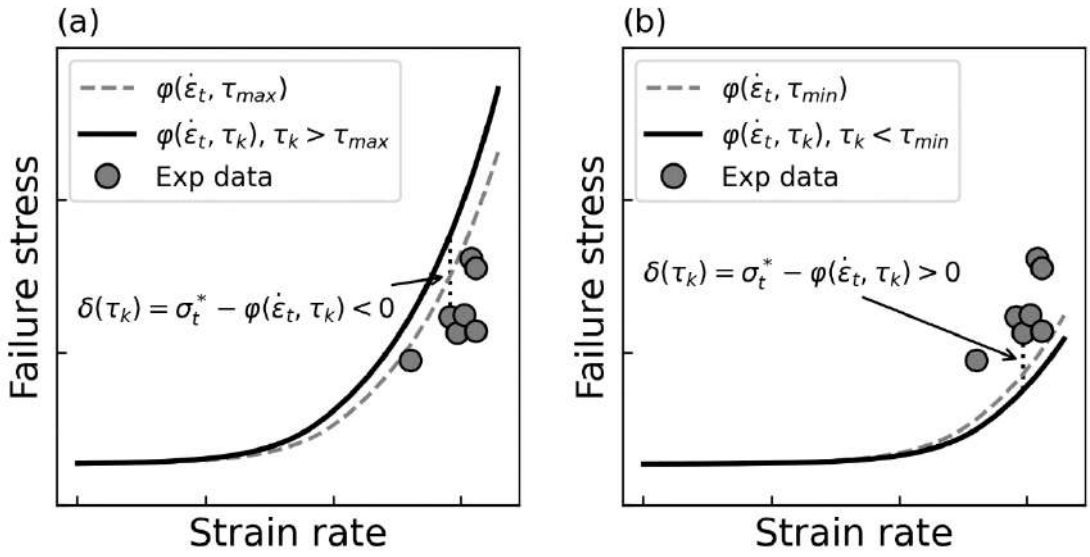

Figure 1.3 Shift of the calculated curves of strain rate dependence of strength: (a) as τ_k increases, (b) as τ_k decreases.

4. From item 3 it follows that for any $\tau_{max}^+ > \tau_{max}$ all residuals will be of the same sign, namely negative: $\delta_i(\tau_{max}^+) = \sigma_{*i} - \varphi(\tau_{max}^+, \dot{\varepsilon}_i) < 0$ (see Figure 1.3(a)).

Similarly, for any $\tau_{min}^- > \tau_{min}$ all residuals will be of the same sign, namely positive: $\delta_i(\tau_{min}^-) = \sigma_{*i} - \varphi(\tau_{min}^-, \dot{\varepsilon}_i) > 0$ (see Figure 1.3(b)).

5. Thus, for any $\tau_k \notin [\tau_{min}, \tau_{max}]$ it turns out that in the base sum

$$H_0(\tau_k) = \sum_{i=1}^{N} \delta_i(\tau_k) \frac{d\varphi(\tau_k, \dot{\varepsilon}_i)}{d\tau}$$

all residuals are summed up with one sign, since the derivative for all values of $\dot{\varepsilon}_i$ is positive: $\frac{d\varphi(\tau, \dot{\varepsilon}_i)}{d\tau} > 0$. At the same time in the sign-perturbed sums

$$H_j(\tau_k) = \sum_{i=1}^{N} \beta_{ij} \delta_i(\tau_k) \frac{d\varphi(\tau_k, \dot{\varepsilon}_i)}{d\tau}$$

part of the residuals is taken with the opposite sign, since $\beta_{ij} = \pm 1$,

This allows us to assert that in the case when the trial value τ_k differs sufficiently "strongly" from the true value τ_*, then the base sum will, with a high probability, be greater or equal in absolute value than the perturbed sums:

$$|H_0(\tau_k)| \geq \left|H_j(\tau_k)\right|, \qquad \tau_k \notin [\tau_{min}, \tau_{max}].$$

Equality is only possible if in some of the randomly generated sets of signs all the signs are the same. The probability of such an event is $\frac{M-1}{2^{N-1}}$.

Thus, we can conclude that for $\tau_k \notin [\tau_{min}, \tau_{max}]$ the base sum $|H_0(\tau_k)|$ will with a high degree of probability occupy the last place in the ordered set $\left\{\left|H_j(\tau_k)\right|\right\}_{j=0}^{M-1}$, and the rank for the corresponding trial values τ_k will be equal to M:

$$\Re(\tau_k) = M.$$

Therefore, for $\tau_k \notin [\tau_{min}, \tau_{max}]$ the $\boldsymbol{SPS\_Indicator(\tau_k) = 0}$ for any values of the parameter $q \geq 1$, and it will exclude such trial values from the confidence interval T. This means that the boundedness of the confidence interval obtained as a result of applying the method of sign-perturbed sums is proven.

1.3 Application of the SPS method to problems of fracture of brittle materials under high-speed impact

To test the performance of the method of sign-perturbed sums, data from dynamic tests performed by various authors for a number of brittle materials, such as various types of rocks, concrete, and ice at various temperatures, were processed.

Fracture of rocks

The developed method for assessing the value of the incubation time of fracture was applied to process the data of dynamic tests of rocks. The data of measurements of dynamic tensile strength under spalling conditions were used. Figure 1.4 shows a comparison of the calculated strength rate dependence for granite with experimentally measured data [101].

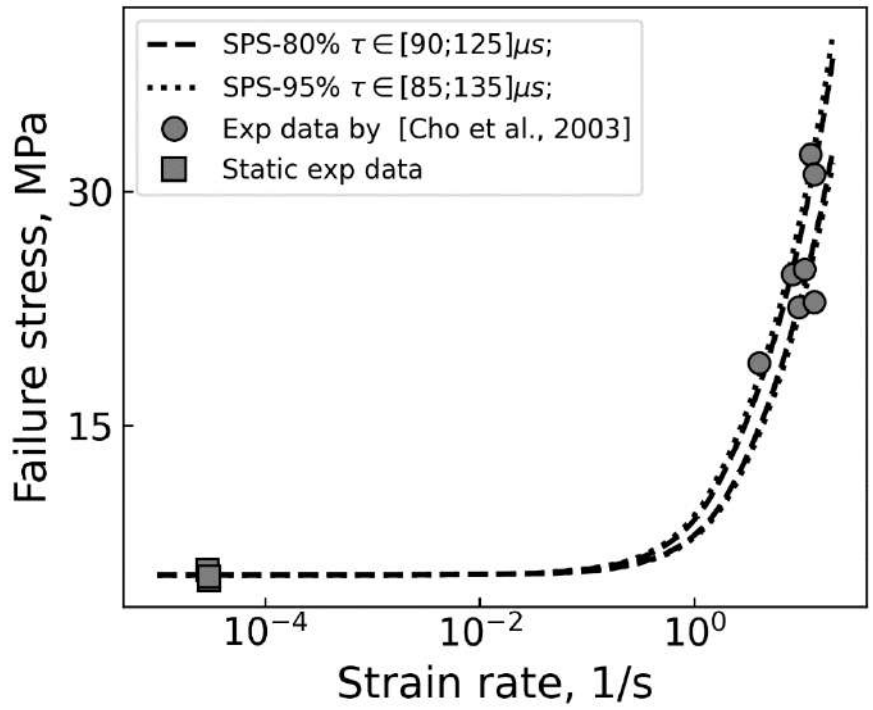

Figure 1.4 Tensile strain rate dependence of strength for granite [101]. Calculated values: dashed line – $\tau_{0.8} \in [90; 125]$μs , dotted line – $\tau_{0.95} \in [85; 135]$μs, σ_c=5.4 MPa.

For the calculations the value of the critical stress $\sigma_c = 5.4\,MPa$ was chosen, which was equal to the experimentally measured static strength of the material. For the incubation time τ we took the values that correspond to the boundaries of the confidence intervals obtained by the SPS method with different levels of confidence probability: 80% – $\tau_{0.8} \in [90; 125]$μs and 95% – $\tau_{0.95} \in$

$[85; 135]$μs. It can be noted that for the selected values of confidence probability, there is a good match between the calculated curves and the experimentally measured dynamic branch of the strain rate dependence of strength.

Comparison of the obtained confidence intervals shows that an increase in the level of confidence probability leads to a natural increase in their width. However, even with a sufficiently high level of confidence probability of 95%, the error in estimating the incubation time of the relative mean value is only about 23%, which may be quite acceptable for engineering practice.

Also processed were experimental data obtained in spallation tests on tuff [101]. In this case, the value of the critical stress $\sigma_c = 2.0\ MPa$ for calculations was also chosen at the level of the experimentally measured static strength of the material.

The incubation time τ values were estimated using the SPS method for two confidence levels: 95% and 99%. Figure 1.5 shows the calculated curves of strain rate dependence of strength, which were obtained for the boundary values of the resulting confidence intervals: $\tau_{0.95} \in [601; 1247]\mu s$ and $\tau_{0.99} \in [564; 1453]\mu s$. As in the case of granite, good quantitative agreement can be seen between the model curves and the experimental results. However, in this case, for a confidence level of 95%, a slightly larger error (about 35%) in estimating the incubation time was obtained.

It can be noted that the values of incubation time determined from the results of processing the test data for tuff turned out to be an order of magnitude higher than those obtained for granite. This result correlates well with the mechanical meaning of incubation time, the value of which is determined by the rate of preparatory processes for fracture at the microstructural level. In this sense, a

significantly higher value of incubation time for tuff with its porous microstructure seems natural.

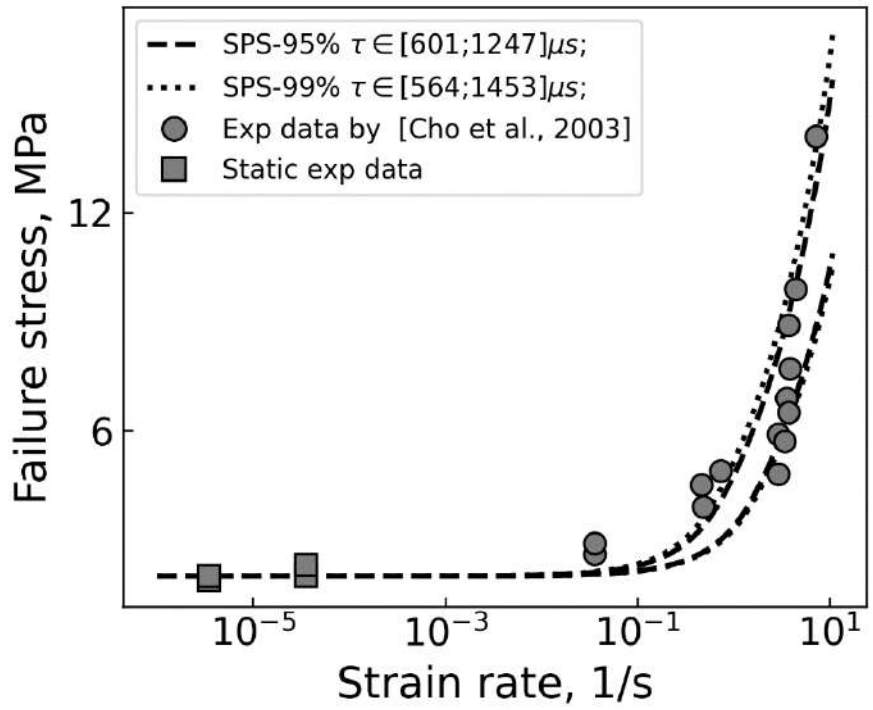

Figure 1.5. Strain rate dependence of tensile strength for tuff [101]. Calculated values: dashed line – $\tau_{0.95} \in [601; 1247]$ μs and dotted line – $\tau_{0.99} \in [564; 1453]$μs, σ_c=2.0 MPa.

The results of the evaluation of the values of incubation time for granite and tuff demonstrated above indicate good prospects for the use of the proposed method in practice. It is evident that at a sufficiently high level of confidence probability of 95%, errors in the evaluation of incubation time are obtained that are quite acceptable for engineering calculations. However, the question of choosing the optimal level of confidence probability, at which the desired level of error in the evaluation of τ will be obtained, remains open.

Fracture of ice at different temperatures

Experimental data from dynamic tests conducted on samples of distilled ice at different temperatures were processed [102]. Table 1.2 shows the values of the incubation time of fracture obtained using the SPS method with a confidence level of 90%.

Table 1.2 Results of the assessment of the incubation time of fracture for ice [102] using the SPS method. Confidence level 90%.

T, °C	τ_{min}, мкс	τ_{max}, мкс	τ_{avg}, мкс
−125	7.5	12.9	10.2
−80	9.0	14.8	11.9
−50	7.1	13.3	10.2
−15	6.3	12.8	9.6
−10	6.8	15.0	10.7

The possibility of obtaining an estimate in the form of a confidence interval made it possible to find that there is a mutual intersection of such intervals calculated for different temperatures and, thus, to state that the value of the incubation time weakly depends on temperature. So, it turned out that the test data for all temperatures can be approximately described by one pair of model curves constructed for the average values of the boundaries of the obtained confidence intervals.

Figure 1.6 shows the dependence of the dynamic multiplier DIF for distilled ice in the entire range of test temperatures. One can see that many experimental points do not fall within the band limited by the curves, which were calculated for the average values of the boundaries of the obtained intervals of incubation time

values. This may be due to the fact that there is a weak dependence of the incubation time on temperature, as well as to a relatively low value of the confidence probability.

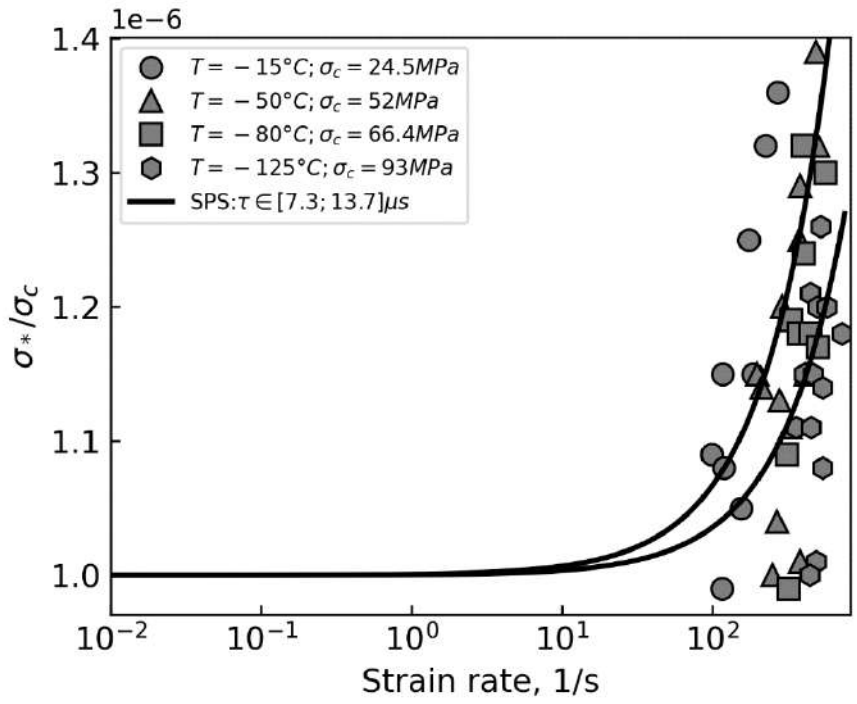

Figure 1.6. Dynamic factor DIF dependence on the strain rate for distilled ice. Model curves are plotted for $\tau \in [7.3; 13.7]\mu s$, points correspond to experimental data from [102].

The possibility of obtaining an estimate in the form of a confidence interval made it possible to find that there is a mutual intersection of such intervals calculated for different temperatures and, thus, to state that the value of the incubation time weakly depends on temperature. So, it turned out that the test data for all temperatures can be approximately described by one pair of model curves constructed for the average values of the boundaries of the obtained confidence intervals.

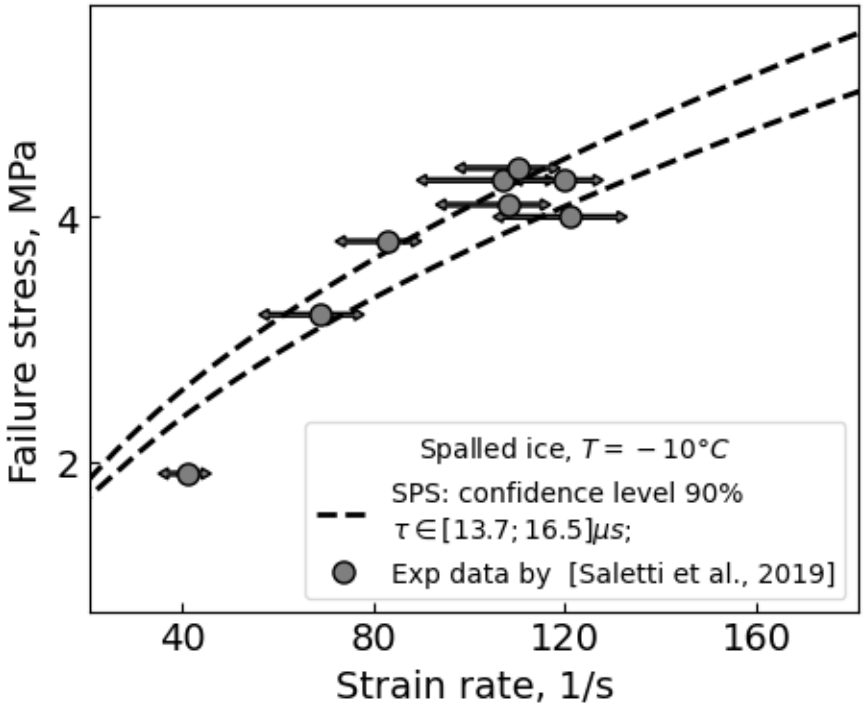

Figure 1.7 Strain rate dependence of strength for polycrystalline ice. Model curves in the figure are indicated by a dashed line for $\tau \in [13.7; 16.5] \mu s$, the points correspond to experimental data from [103].

Next, the SPS method was used to process data obtained in dynamic tensile tests of cylindrical polycrystalline ice specimens under spallation conditions [103]. For calculations, the critical stress σ_c=1.0 MPa was chosen at the level of the experimentally measured static strength of the material. The incubation time values were estimated for a confidence level of 90%. Figure 1.7 shows the estimated strain rate dependences of strength constructed for the boundary values of the confidence interval [13.7;16.3] μs. Note that the resulting error in estimating the incubation time was only 9%.

It can be noted that the model curves describe well not only the experimental values of dynamic strength, but also the scatter of possible values of strain rates shown by the authors of the experiment (see Figure 1.7). This observation

indirectly confirms the validity of the scatter of incubation time values obtained by the SPS method. Thus, it can be assumed that in other cases of application of the proposed method, the resulting scatter of incubation time values will be determined by the heterogeneity of the properties of the material under study.

It should be noted that the proposed method has also been successfully applied to estimate the incubation time values of various metals, alloys, and plastics [93, 92, 94, 95, 96]. In all cases, it was possible to obtain an estimate of the incubation time values with a relative error of no more than 20-30%, with high confidence levels of over 90%. The simplicity of the method allows us to hope that in the future the incubation time criterion can be used as the basis for new practical standards for measuring the strength of materials under high rate loading.

From a fundamental point of view, the importance of the developed method lies in the fact that the knowledge of the exact values of the incubation time makes it possible to calculate the fracture conditions under arbitrary time dependences describing the loading. Thus, for example, under impulse loading in the conditions of a spalling test scheme, it is possible to determine the spalling section or the zone of multiple spalling [104], as well as to reveal such an effect as delayed fracture, which occurs under threshold impacts [105].

1.4 Conclusions to Chapter 1

A new method for estimating the value of incubation time has been developed, based on the randomized method of sign-perturbed sums.

A detailed analysis of the main idea of the method is given, and a theorem on the fulfillment of the conditions of applicability of this method for the problem under study and on the limitations of the resulting estimate is proved.

The effectiveness of the proposed method is demonstrated using experimental data for various materials.

Interval assessment of the incubation time value allows us to draw additional conclusions about the strength properties of the material, which may not be obvious from a point assessment:

- - The confidence interval can be used to calculate the accuracy of the incubation time estimate.
- - Additional conclusions can be drawn about the strength properties of the material that are not obvious from the single value estimate.

The applicability of the proposed method was tested not only for brittle materials, but also for processing data of high-speed tests of metal and polymer specimens.

The proposed method for estimating the incubation time values can be further used in the development of new standards for determining the strength properties of materials under high-speed loading.

Chapter 2 Dynamic fracture of liquid

The use of the incubation time criterion is not limited to solving problems of brittle material failure under dynamic impact. The concept underlying the criterion that any transient process requires some time to originate and develop allows solving problems related to liquid cavitation. This chapter will show how the incubation time criterion can be used to study critical conditions for the occurrence of acoustic and pulsed cavitation. A method for assessing the effect of weak ultrasonic fields on the equilibrium conditions of the liquid and vapor phases will also be considered.

The results shown in Chapter 2 were presented in the following papers [49, 73, 74, 72, 75].

2.1 Incubation time criterion for predicting acoustic cavitation

The structural-temporal approach can be effectively used in problems of predicting critical loading conditions of continuous liquid media, under which their fracture or, in other words, a violation of continuity occurs. This process of fracture of liquids is called cavitation, which is usually described as the nucleation, subsequent growth and abrupt collapse of a vapor-gas bubble arising in the region where tensile stresses exist, or in terms of hydromechanics, in a zone of reduced pressure [106, 107, 108].

The various physical effects that occur during cavitation of a liquid stipulate great scientific and applied interest in studying the properties and features of this phenomenon. It is enough to list the main areas of research directly related to cavitation to see the relevance of its study. For example, cavitation is actively used

in sonochemistry [109, 110], medicine [111, 112], food industry [113], to influence microorganisms and biomaterials [114, 115]. In metallurgy, cavitation is used to obtain an improved structure of alloys [116, 117]. The cavitation process plays a great role in the study of phase transitions [118, 119], with special attention paid to cavitation in cryogenic liquids [120, 121].

Depending on how the local zone of negative pressure appears, cavitation is divided into hydrodynamic and acoustic. Hydrodynamic cavitation occurs in layers of liquid located in the immediate vicinity of a rapidly moving surface of a solid. In acoustic cavitation, the initiator of the growth of a vapor-gas bubble is the stretching phase of the acoustic effect [122, 123]. It can be noted that from the point of view of fracture mechanics, the division of cavitation into hydrodynamic and acoustic is in some sense nominal, since, for example, an acoustic wave in a liquid occurs as a result of the movement of the surface of a waveguide. In any case, regardless of the method of cavitation initiation, the time profile of the pressure leading to a violation of the continuity of the liquid can usually be calculated with a sufficiently high degree of accuracy. Therefore, from the point of view of fracture mechanics, the cavitation process can be considered as a process of liquid destruction caused by some mechanical action, as a result of which a local decrease in pressure occurs in the liquid for some time.

To determine the critical conditions for the onset of cavitation, the incubation time criterion can be written as follows:

$$\frac{1}{\tau}\int_{t-\tau}^{t} sign\big(P(\xi)\big)\left(\frac{|P(\xi)|}{P_c}\right)^{\alpha} d\xi \le 1, \qquad (2.1)$$

where $P(t)$ is the time profile of pressure in the liquid; while the cavitation incubation time τ, the static cavitation threshold P_c and the dimensionless parameter α are the macro parameters of the liquid determining its strength. Note

that in further analysis, for convenience, it is assumed that by analogy with the tensile stress in a solid, the tensile pressure in the liquid, is considered as positive, and the compressive pressure – as negative.

The mechanical meaning of the parameters of criterion (2.1) remains approximately the same as in the case of brittle fracture, however, a specific feature associated with the behavior of liquid continuous media can be noted: the value of the parameter α is to some extent determined by the viscosity of the liquid. In his work, A.A. Gruzdkov [110], having analyzed the Rayleigh equation describing the oscillations of a vapor-gas bubble in a liquid, showed that for water it is justified to choose the value of the parameter $\alpha = 1/2$, while for more viscous media, such as glycerin, the parameter α can be considered equal to one.

2.2 Pulse induced cavitation

In the case of pulse cavitation, the low-pressure region arises when the compressive pulse is reflected from the free surface as a stretching pulse. In order to simplify the analysis, all subsequent considerations are made for a liquid at a certain constant temperature $T = const$, which will mean the absence of temperature dependences for the incubation time τ and the static cavitation threshold P_c. Also, for certainty, the time profile of the loading effect will be presented as a triangular linearly decaying pulse:

$$P(t) = A\left(1 - \frac{1}{t_0}\right)[H(t) - H(t - t_0], \qquad (2.2)$$

where $\boldsymbol{A}$ is the pulse amplitude, t_0 is its duration, and $H(t)$ is the Heaviside function. The time profile of the pressure in the liquid at some distance x from the free surface is the sum of the initial and reflected pulses:

$$P(x,t) = A\left(\left(1-\frac{t}{t_0}-\frac{x}{ct_0}\right)\left[H\left(t+\frac{x}{c}\right)-H\left(t+\frac{x}{c}-t_0\right)\right]\right.$$
$$\left.-\left(1-\frac{t}{T}+\frac{x}{ct_0}\right)\left[H\left(t-\frac{x}{c}\right)-H\left(t-\frac{x}{c}-t_0\right)\right]\right) \qquad (2.3)$$
$$= Af(x,t),$$

where c is the velocity of an acoustic wave in a liquid. Just as in the case of acoustic cavitation, the smallest value of the amplitude A_* at which the growth and collapse of cavitation bubbles occurs will be referred to as the threshold of pulsed cavitation.

The dependence of the pulse cavitation threshold on the duration of the load pulse can also be calculated using the incubation time criterion. Since the pressure in the resulting pulse (2.3) takes both positive and negative values, then for the correct calculation of the cavitation threshold, for example, for water at $\alpha = \frac{1}{2}$, it is necessary to take into account the presence of the multiplier $sign\big(P(\xi)\big)$ in criterion (2.1).

After substituting the expression for pressure (2.3) into criterion (2.1), the following expression is obtained for calculating the threshold of pulsed cavitation:

$$\left(\frac{A_*}{P_c}\right)^{\alpha} = \frac{\tau}{I_{max}}, \qquad (2.4)$$

where

$$I_{max} = \max_t \int_{t-\tau}^{t} sign(f(x,\xi))|f(x,\xi)|^{\alpha} d\xi.$$

It should be noted that the maximum of the integral I_{max} can be reached for the first time in different cross-sections x, depending on the ratio of the pulse duration t_0 and the incubation time τ. If $t_0 > \tau$, which means that the compression

pulse is long enough, the maximum I_{max} will be reached for the first time when the reflected pulse with the tensile pressure stops adding up to the incident one. This will happen for the first time in the cross-section $x = \frac{ct_0}{2}$ at time instant $t = \frac{t_0}{2}$. In this case, only one Heaviside function $H\left(t - \frac{x}{c} - t_0\right)$ in formula (2.3) takes a value equal to zero, and then the maximum of the integral will be calculated as follows:

$$I_{max} = \int_{\frac{t_0}{2}}^{\frac{t_0}{2}+\tau} \left(\frac{3}{2} - \frac{\xi}{t_0}\right)^{\alpha} d\xi = \frac{t_0}{\alpha+1}\left(1 - \left(1 - \frac{\tau}{t_0}\right)\right). \qquad (2.5)$$

For relatively short loading pulses when $t_0 < \tau$, the duration of the influence of the compressive component of the action on the integral value exceeds the pulse duration. In this case, the maximum of the integral will be reached for the first time in the section $x = \frac{ct_0}{2}$ at time instant $t = \frac{\tau}{2}$:

$$I_{max} = \int_{\frac{\tau}{2}}^{\frac{\tau}{2}+t_0} \left(1 - \frac{\xi}{t_0} + \frac{\tau}{2t_0}\right)^{\alpha} d\xi = \frac{t_0}{\alpha+1}. \qquad (2.6)$$

Substituting formulae (2.5) and (2.6) into expression (2.4) allows us to obtain an analytical expression for the pulse cavitation threshold for a triangular-shaped loading pulse:

$$\left(\frac{A_*}{P_c}\right)^{\alpha} = \begin{cases} (\alpha+1)\frac{\tau}{t_0}, & t_0 < \tau, \\ (\alpha+1)\frac{\tau}{t_0}\left(1 - \left(1 - \frac{\tau}{t_0}\right)^{\alpha+1}\right)^{-1}, & t_0 \geq \tau. \end{cases} \qquad (2.7)$$

In order to use the obtained result when calculating the threshold of pulsed cavitation for a specific liquid, it is necessary to know the values of its strength

parameters τ and P_c. The value of the static cavitation threshold P_c can be independently measured experimentally at an equilibrium decrease in pressure, while the value of the incubation time τ can be determined only by comparing the predicted values of the cavitation threshold with the results of dynamic tests. For this purpose, as for the previously considered case of fracture of solids at a constant rate of stress growth, it is convenient to use the method of sign-perturbed sums.

Analysis of expression (2.7) shows that the dependence of the cavitation threshold A_* on the duration of the loading pulse t_0 is monotonically decreasing. As it was proven earlier in Chapter 1, a bounded confidence interval is obtained when using the SPS method for a monotonically increasing model function that determines the strain rate dependence of strength. In order to obtain a suitable form of the model function that determines the value of the cavitation threshold in the case of pulsed loading, it is sufficient to introduce a new dimensionless parameter $\kappa = \frac{\tau}{t_0}$, which is in a sense an analogue of the average loading rate under pulsed action. Then expression (2.7) can be rewritten as follows:

$$\left(\frac{A_*}{P_c}\right)^{\alpha} = \varphi(\kappa) = \begin{cases} \dfrac{(\alpha+1)\kappa}{1-(1-\kappa)^{\alpha+1}}, & \kappa \le 1, \\ (\alpha+1)\kappa, & \kappa > 1, \end{cases} \qquad (2.8)$$

where, the function $\varphi(\kappa(t_0, \tau))$ completely satisfies the necessary conditions of the SPS method. This allows us to consider the results of measuring the cavitation threshold under pulse loading in the form of the following observation model:

$$y_i = \varphi\left(\kappa\left(t_{0_i}, \tau\right)\right) + v_i, \qquad i = 1..N, \qquad (2.9)$$

where $y_i = \left(\frac{A_{*i}}{P_c}\right)^{\alpha}$ is an experimentally observed value, which is determined by the value of the cavitation threshold A_{*i} depending on the duration of the loading pulse

t_{0_i} and the internal parameter τ, the value of which is to be estimated, v_i is the random noise, *N* is the number of measurements.

For additional clarity, the meaning of expression (2.9) can be defined in terms of a control theory problem as follows. Let the cavitation process in a liquid be a dynamic system whose properties are determined by the value of the internal parameter of the system τ. The current state of the system is determined by the cavitation threshold A_*, the value of which is a response to an external action specified by the control parameter t_0. In this case, all measurements of the current state of the system, that is, A_{*i}, contain random noise v_i. If we take into account that all systematic errors are eliminated and the experiment is carried out as carefully as possible, then it is reasonable to assume that v_i are random variables with a distribution symmetrical with respect to zero.

To estimate the incubation time, the data from pulsed cavitation experiments conducted for degassed water were selected [125]. As noted above, in the case of water, the parameter α should be taken equal to ½ . Based on the results of using the SPS method, in accordance with the procedure described in Chapter 1, the following estimate of the incubation time values was obtained in the form of a confidence interval $\tau \in [15.5; 17.0]\ \mu s$ with a confidence level of 95%. The value of the static cavitation threshold was chosen as $P_c = 1\ atm$.

The dependences of the cavitation threshold calculated according to formula (2.8) for the boundary values of the confidence interval are shown by solid lines in Figure 2.1. It is worth noting that there is a good correspondence between the calculated curves and experimental points, and that, the possible error in the estimate is relatively small, about 5%, despite the high level of reliability.

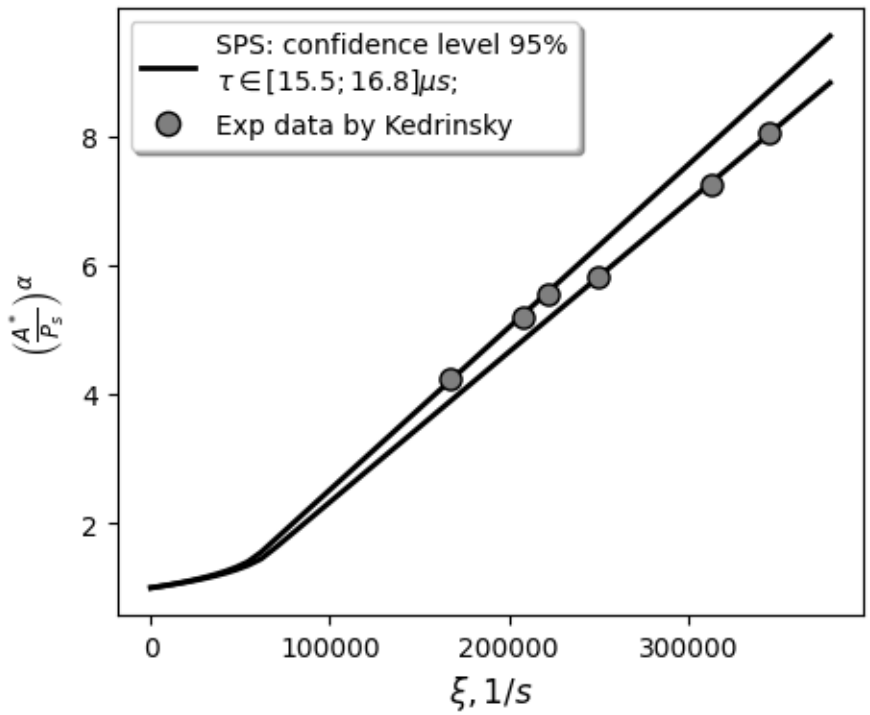

Figure 2.1 Dependence of the cavitation threshold on the “average strain rate” of loading under pulsed action. Lines are the calculated curves for the boundary values of the confidence interval $\tau \in [15.5; 17.0]$μs, points are experimental data from work [125].

For the found values of the incubation time, it is also possible to construct, using relation (2.7), the dependence of the cavitation threshold on the duration of the loading pulse (see Figure 2.2).

Note the good agreement between the calculated curves and the experimental data on pulsed cavitation. However, a comparison with the experiment of the calculated curves obtained for the same values of incubation time $\tau \in [15.5; 17.0]\ \mu s$, but in the case of ultrasonic cavitation, is also of great interest.

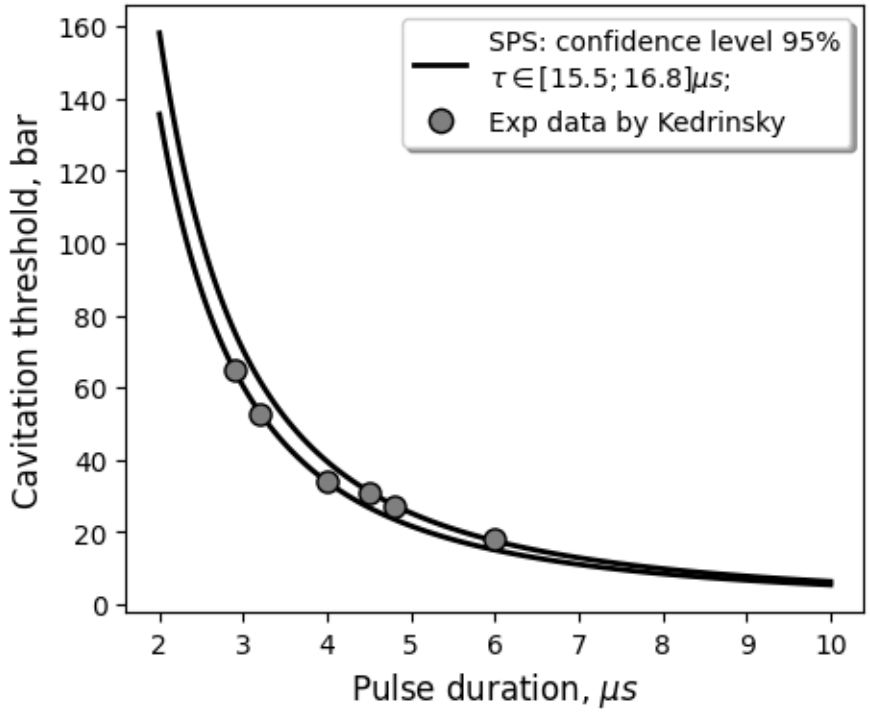

Figure 2.2 Dependence of the pulsed cavitation threshold on the duration of the loading pulse. Lines are calculated curves for the boundary values of the confidence interval $\tau \in [15.5; 17.0]\mu s$, points are experimental data from work [125].

2.3 Ultrasonic cavitation

Ultrasonic harmonic vibrations of the surface of a solid body immersed in a liquid and called a vibrator, create a high-frequency acoustic wave, the pressure in which can be expressed with a high degree of accuracy as follows:

$$P(t) = A\sin(\omega t), \qquad (2.10)$$

where A is the pressure amplitude, the value of which depends on the power of the vibrator, and ω is the vibration frequency. Thus, in a certain microvolume of liquid located in the path of propagation of the acoustic wave, negative pressure will

periodically arise once in time period $\frac{\pi}{\omega}$. If the amplitude of the wave A is large enough, then the growth and subsequent collapse of vapor-gas bubbles may occur in the liquid, which will cause the onset of acoustic cavitation. In this case, the cavitation threshold is the minimum value of the acoustic wave amplitude A_*, with which the pressure decreases sufficiently for the cavitation process to begin. Experimental studies show that with an increase in the frequency of the acoustic wave, there is a tendency for the cavitation threshold to increase, while in the high-frequency range there is also a significant scatter of the observed values. The incubation time criterion, written in the form (2.15) and taking into account the temperature dependencies (2.14) and (2.13), allows us to determine the dependence $A_*(\omega)$ by substituting the expression for the pressure in the acoustic wave (2.10) into criterion (2.1):

$$\left(\frac{A_*}{P_c}\right)^{\alpha} = \frac{\frac{\omega\tau}{2}}{\int_0^{\frac{\omega\tau}{2}} \psi(\xi)d\xi}, \qquad (2.11)$$

where $\psi(\xi) = sign(\cos\xi)|\cos\xi\,|^{\alpha}$. It is also worth noting that in the resulting expression the right-hand side tends to unity under the condition $\tau\to 0$, which means that at an infinitely small value of the incubation time, the cavitation strength of the liquid is determined only by the value of the static cavitation threshold.

Besides, it is easy to see that for a certain relationship between the frequency of the acoustic wave and the value of the incubation time, the integral on the right side of expression (2.11) becomes zero, namely when:

$$\frac{\omega\tau}{2} = 2\pi n, \qquad n \in \mathbb{N}.$$

In this case, according to formula (2.11), one should expect infinitely large values of the acoustic cavitation threshold A_* (see Fig. 2.3), which is not observed

experimentally. Therefore, to calculate the frequency dependence of the cavitation threshold, one can assume that, due to the heterogeneity of the mechanical properties of the liquid, the incubation time τ can equally likely take a value from a certain interval $[\tau_{min}\,;\,\tau_{max}]$. Then the cavitation threshold can be determined according to the weak link principle, as the smallest value of all those calculated for $\tau \in [\tau_{min}\,;\,\tau_{max}]$

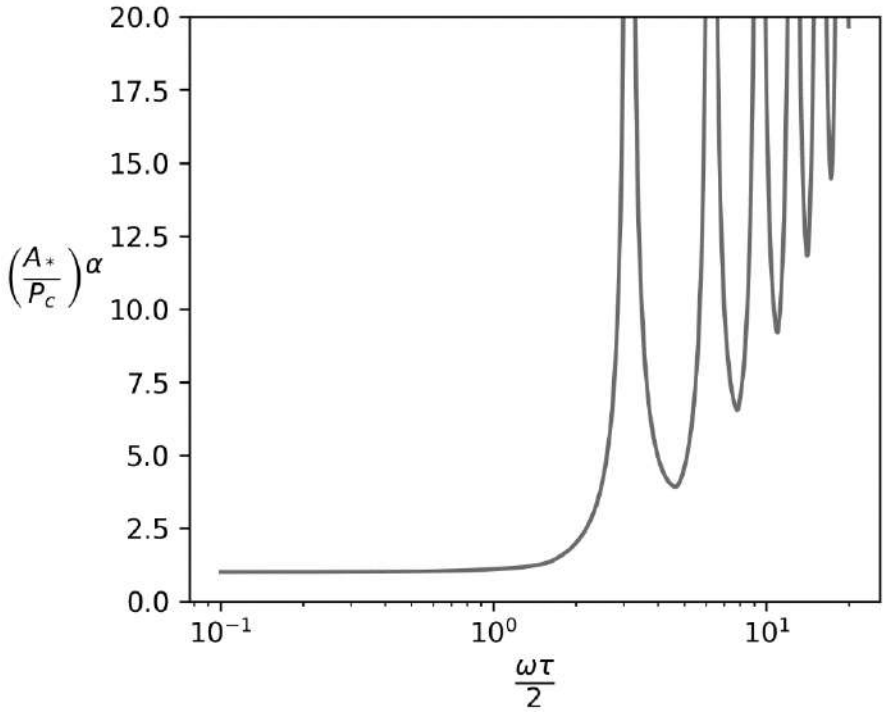

Figure 2.3 Dependence of the acoustic cavitation threshold on frequency in dimensionless form ($\alpha = \frac{1}{2}$).

$$\left(\frac{A_*}{P_c}\right)^{\alpha} = \min_{\tau\in[\tau_{min}\,;\,\tau_{max}]}\left(\frac{\frac{\omega\tau}{2}}{\int_0^{\frac{\omega\tau}{2}}\psi(\xi)d\xi}\right). \qquad (2.12)$$

It was shown earlier that the incubation time value estimate in the form of a certain interval can be obtained using the method of sign-perturbed sums. It was shown that for the correct use of the SPS method it is necessary that the model function be monotonically increasing relative to the control parameter, which in this case is the

frequency of the acoustic wave ω. However, it is easy to see that the dependence determined by the relation (2.11) is a non-monotonic function, therefore it is impossible to estimate the incubation time values directly from the acoustic cavitation test data. Therefore, the calculation of the dependence of the threshold of acoustic cavitation of water is carried out for the interval of incubation time values obtained when processing the test data on the initiation of cavitation by shock pulses under spallation conditions.

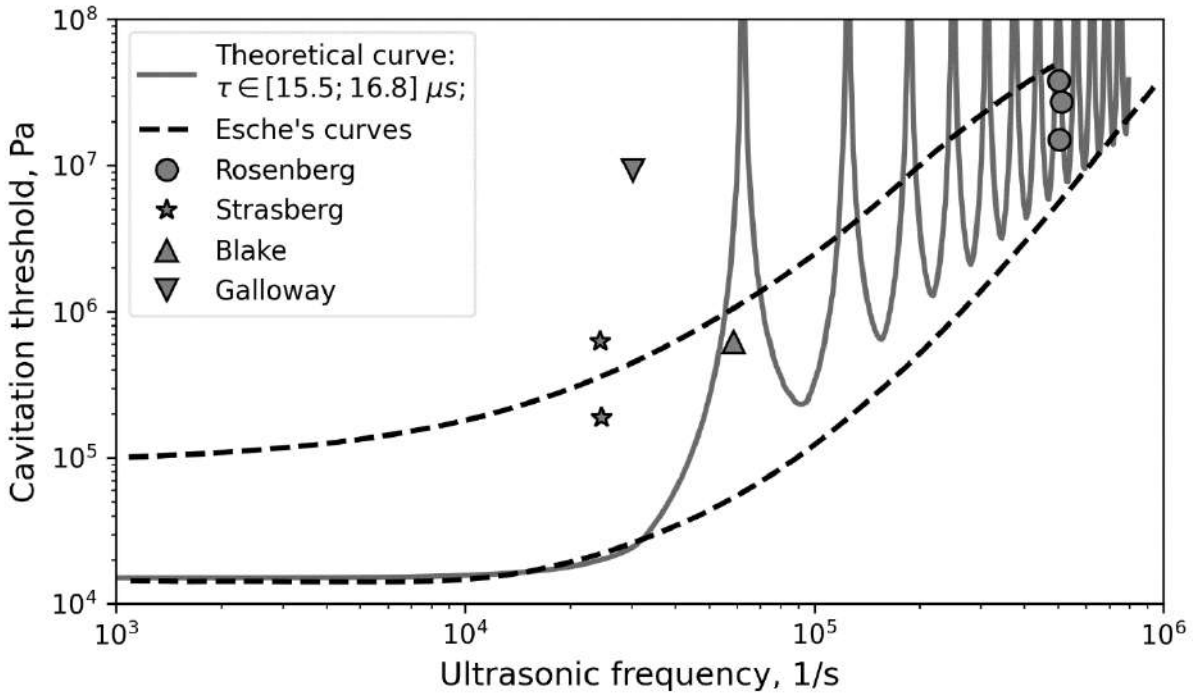

Figure 2.4 Calculated dependence of the acoustic cavitation threshold for water. Calculated curves are solid lines, Esche's curves are dashed lines, points are experimental data of other authors.

The calculation results are presented in Figure 2.4, which supplies a comparison of the calculated curves obtained according to (2.12) for the values of the incubation time $\tau \in [15.5; 16.8]\mu s$ and $P_c = 0.15\ atm$ together with Esche's curves, which he used to designate the range of values of the acoustic cavitation threshold.

It can be noted that for the calculated curves of the acoustic cavitation threshold, there is good qualitative and quantitative agreement with the experimentally obtained Esche's curves. It is important that the calculation of the acoustic cavitation threshold is made for the same values of incubation time that were obtained from the results of tests conducted within the framework of a completely different experimental scheme - pulsed loading of water. The non-monotonic behavior of the calculated curves shows that the experimentally observed scatter of values can be associated not only with the heterogeneity and high mobility of the liquid medium, but can also be directly caused by the specifics of the loading process.

While the interval for the incubation time τ and the value of α were the same, values for the static cavitation threshold were chosen different: $P_c = 0.15\ atm$ for the case of acoustic cavitation and $P_c = 1\ atm$ for pulsed cavitation. These values correspond respectively to the levels of the lower and upper Esche's curves at low frequencies about 1 kHz. Such a scatter of experimentally measured values of the static cavitation threshold is apparently associated with the presence of metastable states in the liquid under slow excitation. Therefore, to predict the frequency dependence of the acoustic cavitation threshold or the dependence of the pulsed cavitation threshold on pulse duration, we chose the values of P_c, for which the agreement with the experimental data was achieved in the best way.

2.4 Dependence of the cavitation threshold on temperature and background pressure

In the previous paragraphs, all calculations of the threshold of acoustic and pulse cavitation were carried out for constant values of the parameters of the incubation time criterion - τ, P_c and α. However, the cavitation properties of a

liquid can depend on many factors, such as temperature and background pressure, the degree of degassing, the presence of impurities, their concentration and average size. However, if we consider a liquid as a homogeneous continuous medium, then the key parameters will be only the temperature and background pressure.

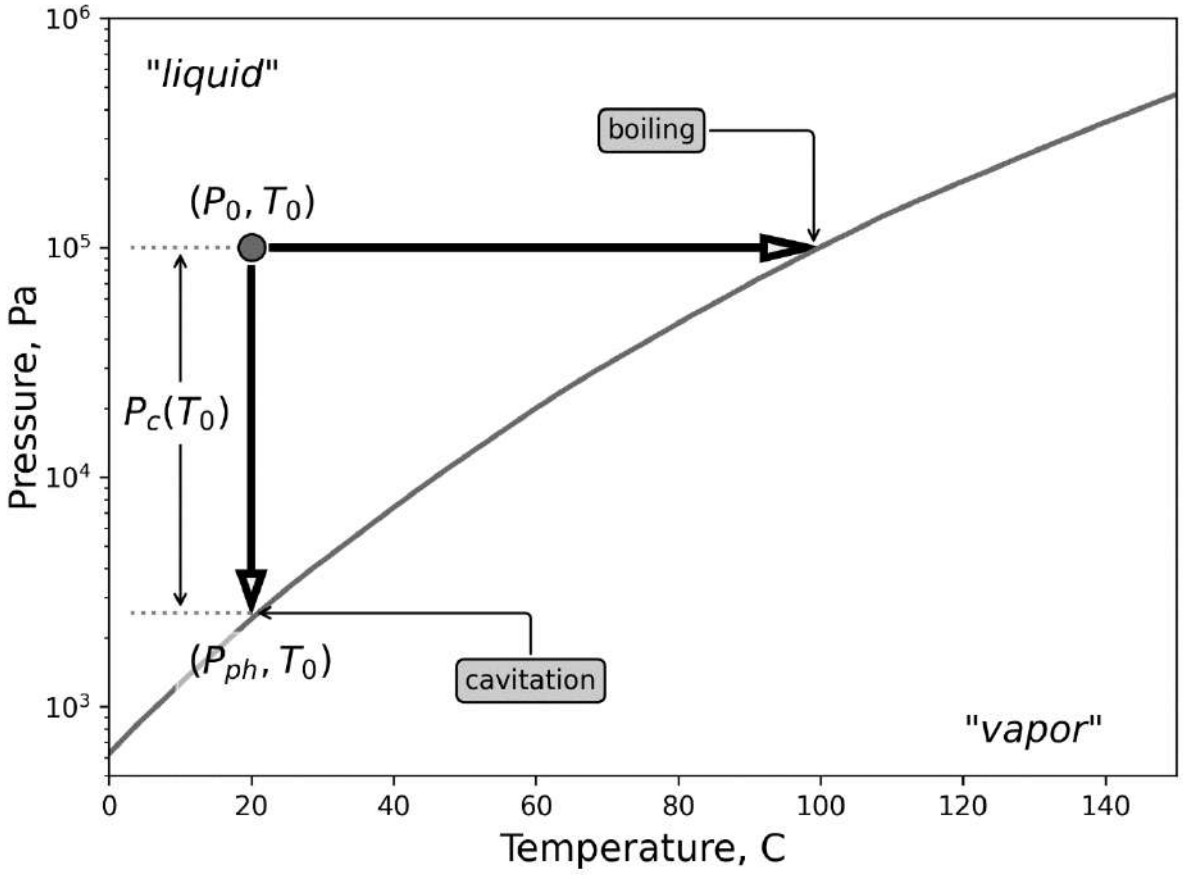

Figure 2.5 Interpretation of the cavitation process as a phase transformation from a liquid to a gaseous state using the example of a diagram for water.

Failure of liquid continuity during cavitation is always accompanied by the formation of a vapor-gas phase. From this point of view, the phenomenon of cavitation can be considered as the transition of a continuous medium from a liquid to a vapor state, only not as a result of heating, as in the boiling process, but as a result of a local decrease in pressure. In this case, the formation, growth and subsequent collapse of vapor-gas bubbles, which is essentially the cavitation of

liquids, can occur without any mechanical action, for example, only under heating. In this case, the value, by which the liquid temperature must be increased directly depends on the background pressure. Thus, to use the incubation time criterion in cavitation problems, it is necessary to determine the dependence of the incubation time criterion parameters on temperature and background pressure.

Figure 2.5 shows the liquid-vapor phase equilibrium diagram for water. If the current state of the liquid is characterized by pressure and temperature (P_0, T_0), then to form a new phase, i.e. cavitation, it is necessary to apply an external action that locally reduces the pressure to a level determined by the phase equilibrium curve.

Thus, for an arbitrary temperature T, the value of the static threshold P_c can be defined as the difference between the current value of the pressure in the liquid P_0 and the corresponding pressure level on the phase equilibrium curve $P_{ph}(T)$:

$$P_c(T) = P_0 - P_{ph}(T). \qquad (2.13)$$

For the incubation time, the type of temperature dependence $\tau(T)$ can be selected based on the following considerations. As noted earlier, the incubation time determines a certain characteristic time required for the processes to occur at the microstructural level that precede the failure at the macrolevel. An increase in temperature increases the mobility of molecules, facilitating the acceleration of the processes of structural reorganization at the microlevel. Thus, it can be concluded that the value of the incubation time will decrease with an increase in the temperature of the liquid medium. Therefore, as a dependence of the incubation time on temperature, a relationship of the type proposed by Arrhenius for determining the reaction rate dependence on temperature was adopted:

$$\tau(T) = \tau_0 \exp\left(\frac{G}{kT}\right), \qquad (2.14)$$

where τ_0 is the characteristic value of the cavitation incubation time, $k = 1{,}3807 \times 10^{23} J/K$ is the Boltzmann constant, and G is the energy required to initiate cavitation in a certain elementary volume. It can be assumed that the effect of the background pressure P_0 on the value of the incubation time τ is not as significant as the effect of temperature, so as a simple approximation it can be neglected. Thus, the incubation time criterion can be written in the following form:

$$\frac{1}{\tau(T)} \int_{t-\tau(T)}^{t} \left(\frac{P(\xi)}{P_c(T)}\right)^{\alpha} d\xi \leq 1. \qquad (2.15)$$

where $P_c(T)$ and $\tau(T)$ are determined by relations (2.13) and (2.14). By analogy with relation (2.12), one can calculate the temperature dependence of the acoustic cavitation threshold for some constant frequency of the ultrasonic wave ω:

$$\left(\frac{A_*(T)}{P_c(T)}\right)^{\alpha} = \min_{\tau(T)\in[\tau_{min}\,;\,\tau_{max}]} \frac{\frac{\omega\tau(T)}{2}}{\int_0^{\frac{\omega\tau(T)}{2}} \psi(\xi)d\xi}. \qquad (2.16)$$

Since in this case the range of possible values for $\tau(T)$ is unknown, it can be determined as follows:

$$[\tau_{min}\,;\,\tau_{max}] = \left[\left(1-\frac{\delta}{2}\right)\tau(T);\ \left(1+\frac{\delta}{2}\right)\tau(T)\right],$$

where δ defines a certain scatter of values. The confidence interval for possible values of the incubation time, which was previously obtained using the SPS method, turned out to be quite narrow. The deviation of the interval boundary values from the average value was not more than 5%. However, with such a value of δ, the calculated values of the frequency dependence of the acoustic cavitation threshold in the vicinity of frequencies $\omega_n = 4\pi n/\tau$, where n is a natural number,

go quite far beyond the experimental Esche's band, see Figure 2.4. Therefore, for further calculation of the temperature dependence of the cavitation threshold, the value of δ was chosen with a reserve of 20%.

Figure 2.6 shows the calculated curves of the temperature dependence of the acoustic cavitation threshold, calculated for water at different levels of background pressure. The calculation was performed for the ultrasound frequency ω=25.5 kHz, with the following parameter values $\tau_0 = 3.7\,\mu s$, and $G = 1475 \times 10^{-23} J$. Comparison with the experimental data from work [126] showed that the proposed method allows one to qualitatively predict a decrease in the cavitation threshold with increasing temperature, as well as its increase with increasing background pressure.

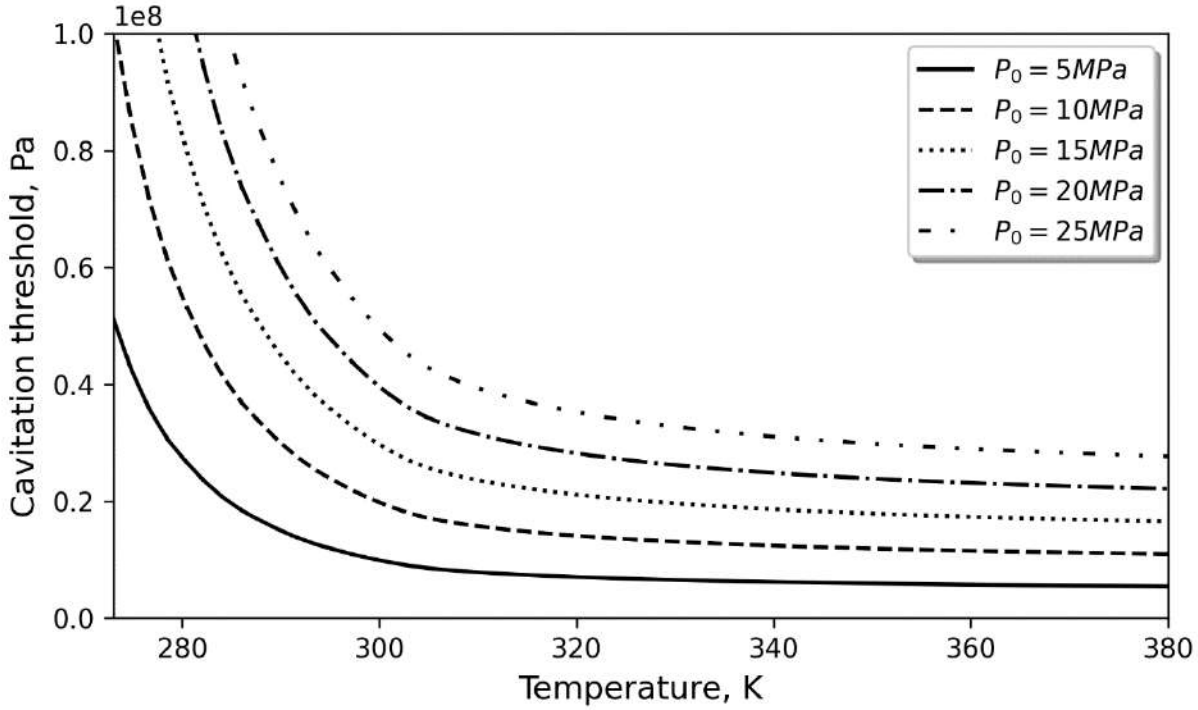

Figure 2.6 Temperature dependence of the acoustic cavitation threshold in water at different values of background pressure.

To achieve the best quantitative fit for different values of background pressure P_0, different values of activation energy G were chosen, which are given in Table 2.1.

Table 2.1 Dependence of activation energy on background pressure in water

P_0, МПа	5	10	15	20	25
$G, 10^{-23}$ Дж	1510	1490	1475	1470	1460

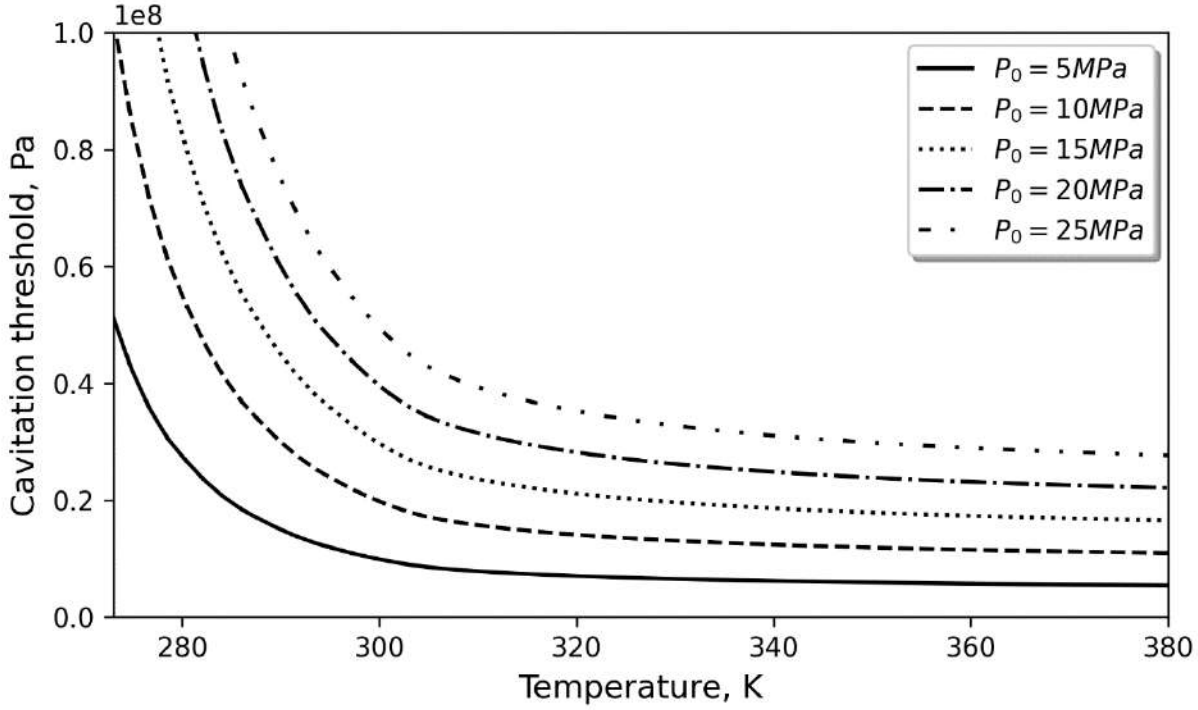

Figure 2.7 Temperature dependence of the acoustic cavitation threshold in water calculated for different values of background pressure. Calculated curves are solid lines, dots are experimental data from [126].

The calculation results for variable activation energy are shown in Figure 2.7. In this case, one can already note a good match between the experimental data and the calculated curves. This shows the need to take into account the influence of background pressure not only on the value of the static cavitation threshold P_c, but also on the value of the incubation time τ, through the dependence of the activation energy on the background pressure.

Comparison of the obtained results with experimental data showed that the proposed method allows one to fairly accurately predict the threshold of acoustic cavitation for different values of the ultrasonic wave frequency, as well as the parameters of the liquid state – its temperature and background pressure.

2.5 Influence of ultrasound on phase equilibrium conditions

The representation of the cavitation phenomenon as a phase transformation from a liquid to a vapor state allows, as shown above, not only to effectively predict the value of the acoustic cavitation threshold, but also, conversely, to evaluate the influence of an ultrasonic wave on the conditions of phase equilibrium. Indeed, if an acoustic wave with an amplitude lower than the threshold value propagates in a continuous liquid medium, then in this case the conditions of phase equilibrium will differ from the initial ones, when the same medium is in an unloaded state.

Let an acoustic wave propagate in a liquid, the amplitude of which is less than the threshold value:

$$P(T) = A_0 \sin \omega t\,, \qquad A_0 < A_*.$$

In this case, a local pressure decrease by the value A_0 periodically occurs in the medium, but this does not allow us to conclude that at this time instant the conditions of phase equilibrium should also be shifted by the value A_0. In order to estimate the equilibrium decrease in the pressure level created by an acoustic wave with a pressure amplitude of A_0, we can use the relation (2.16). The left-hand side of this expression, which depends only on the time profile of the impact and the incubation time for a continuous medium, is a value that determines the ratio of the threshold amplitude of the sound wave to the static cavitation threshold. In other

words, this ratio shows how much greater the amplitude of the acoustic wave A must be than the value by which the background pressure must be lowered under equilibrium conditions in order for liquid cavitation to occur. That is, the action of an acoustic wave with a threshold amplitude A_* is equivalent, from the point of view of phase transformation, to an equilibrium decrease in pressure by the value of the static cavitation threshold P_c. Thus, expression (2.16) can be rewritten as follows:

$$\left(\frac{A_0}{P_{eq}(T)}\right)^{\alpha} = \min_{\tau(T)\in[\tau_{min}\,;\,\tau_{max}]} \frac{\frac{\omega\tau(T)}{2}}{\int_0^{\frac{\omega\tau(T)}{2}} \psi(\xi)d\xi}, \qquad (2.17)$$

where $P_{eq}(T)$ is the value, by which the background pressure in the liquid at temperature T decreases on average when an acoustic wave with amplitude A_0 and frequency ω propagates in the liquid. If we consider a liquid, through which the acoustic wave with a subthreshold pressure amplitude propagates as a new continuous medium, then the conditions of phase equilibrium for it will be determined as follows:

$$\tilde{P}_{ph}(T) = P_{ph}(T) + P_{eq}(T), \qquad (2.18)$$

where $\tilde{P}_{ph}(T)$ and $P_{ph}(T)$ are the pressure levels for the phase transformation of a continuous medium in the case of the action of an ultrasonic wave and without it, respectively.

Figure 2.8 shows an example of calculation using formulae (2.17) and (2.18) of “corrected” phase equilibrium diagrams for water, in which propagates an acoustic wave with an amplitude of $\mathrm{A}_0 = 0.25\ MPa$ and frequency in the range $\omega = 10 - 70\ kHz$. The results presented in the graph (2.8) show that for a certain ratio of the values of the problem parameters the deviation of the phase transition

pressure from the standard phase diagram can be significant and reach more than half of the wave amplitude A_0.

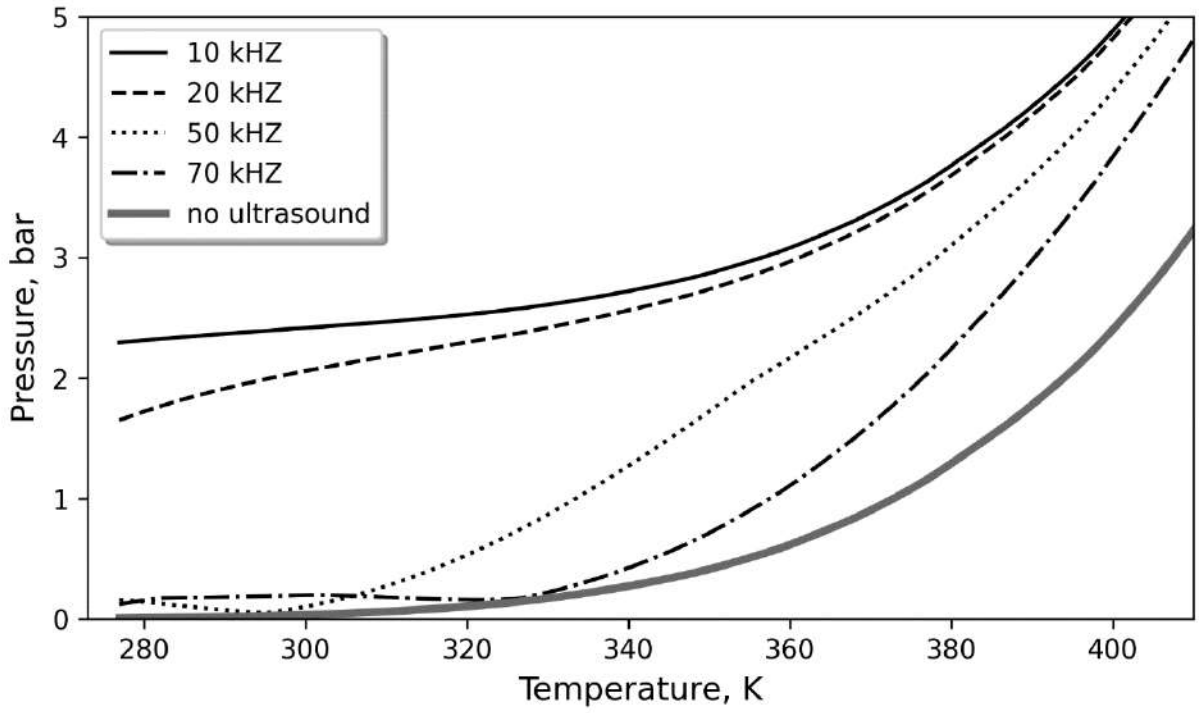

Figure 2.8 “Corrected” phase equilibrium diagrams for water in which an acoustic wave with an amplitude of $A_0 = 0.25\ MPa$ and a frequency in the range $\omega = 10 - 70\ kHz$ propagates

Figure 2.8 shows that the level of influence of the ultrasonic wave on the phase equilibrium conditions decreases with increasing wave frequency (with the same oscillation amplitude). Within the framework of the model, this can be explained by the fact that at low frequencies, the pressure in the acoustic wave changes slowly on the scale of the incubation time. In this case, the value $P_{eq}(T)$ tends to the amplitude A_0. At high frequencies, the time interval τ fits almost the entire period of oscillations, and the value of $P_{eq}(T)$ turns out to be insignificant. With increasing temperature, the value of the incubation time decreases, and in this case, even for high frequencies, the value of $P_{eq}(T)$ becomes comparable with A_0.

2.6 Energy consumption analysis of the cavitation bubble collapse

In problems related to the phenomenon of liquid cavitation, besides determining the threshold values of the loading effect, the issue of cavitation erosion is particularly important [127]. When a cavitation bubble collapses, a strong pulse action occurs, leading to micro fracture of a nearby solid surface, for example, the surface of a waveguide in the case of ultrasonic cavitation or a turbine blade in hydrodynamic cavitation. Since the number of collapsing bubbles in the process of developed cavitation is usually very large, this can ultimately lead to significant damage of the surface of a solid body located in the cavitating liquid. Experimental studies show that the intensity of the erosive destruction process during acoustic cavitation depends on the frequency and amplitude of the ultrasonic wave. In the work [128] the authors experimentally measured the amplitude of the pulse stress arising during the collapse of a bubble and showed that its value increases with an increase in the amplitude or frequency of ultrasound. A qualitative explanation of this phenomenon can be obtained by analyzing the energy intensity of the cavitation process. During an experimental study of acoustic cavitation, M.G. Sirotyuk identified the following scheme for the growth and collapse of vapor-gas bubbles [129]. During the action of the stretching phase of the ultrasonic wave, the formation and subsequent growth of a vapor-gas bubble occurs, which then collapses almost immediately with the onset of the action of the compression stage. Thus, it turns out that all the energy accumulated during the growth of the vapor-gas bubble is almost instantly released, creating a powerful erosive effect. To estimate the amount of energy spent on the formation of the bubble and the amount of energy that accumulates until its collapse, one can use the technique shown in Section 2.3.

The stretching stage of an ultrasonic wave with a frequency ω corresponds to a sinusoidal pulse with a duration $\frac{t_0}{2} = \frac{\pi}{\omega}$ and an amplitude A, which is given as follows:

$$P(t) = \left[H(t) - H\left(t - \frac{t_0}{2}\right)\right] A \sin\left(2\pi \frac{t}{t_0}\right). \quad (2.19)$$

After substituting expression (2.19) into criterion (2.1), we can obtain the following expression for the threshold values of the amplitude depending on the pulse duration:

$$\left(\frac{A_*}{P_c}\right)^{\alpha} = \frac{1}{\max\limits_{t} \int_{t-\tau}^{\mathrm{t}} \left[H(t) - H\left(t - \frac{t_0}{2}\right)\right] \left(\sin\left(2\pi \frac{\xi}{t_0}\right)\right)^{\alpha} d\xi}. \quad (2.20)$$

The integral on the right side of expression (2.20) cannot be calculated analytically in the general case (for example, it was shown earlier that for water the parameter α should be chosen equal to ½), therefore, for the simplicity of further reasoning, it is convenient to take the value of the parameter $\alpha = 1$. In this case, the following analytical relationship can be obtained for the threshold pulse amplitude:

$$\tilde{A}_* = \frac{A_*}{P_c} = \begin{cases} \pi/\tilde{t}_0, & \tilde{t}_0 \le 2, \\ \dfrac{\pi/\tilde{t}_0}{\sin\left(\pi/\tilde{t}_0\right)}, & \tilde{t}_0 > 2, \end{cases} \quad (2.21)$$

where $\tilde{t}_0 = \frac{t_0}{\tau}$ is the normalized pulse duration. We note an interesting feature of the obtained dependence for the pulsed cavitation threshold (2.21). If we consider it as a function of the corresponding frequency $\tilde{\omega} = \frac{2\pi}{\tilde{t}_0}$, it turns out that expression (2.21) will define the lower envelope of the non-monotonic curve calculated using

formula (2.11) for the frequency dependence of the cavitation threshold (see Figure 2.9).

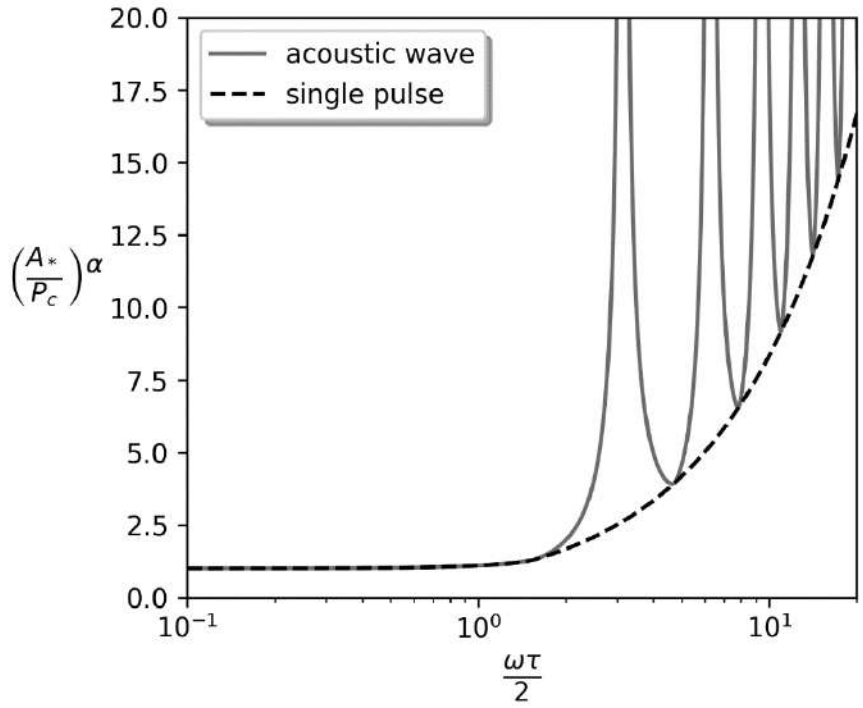

Figure 2.9 Frequency dependence of the cavitation threshold, continuous line – calculation for the entire acoustic wave taking into account the presence of the compressive phase, dotted line – calculation with an account of only a single stretching pulse.

In order to calculate the specific energy capacity of the cavitation process, one can calculate the amount of energy that an ultrasonic wave manages to transfer before time instant t_*, at which the cavitation bubble appears:

$$E_1 = \int_0^{t_*} \frac{P^2(\xi)}{\rho c} d\xi, \qquad (2.22)$$

where ρ and c are the density and velocity of sound propagation in a cavitating liquid. The dimensionless time instant of fracture $\tilde{t}_* = \frac{t_*}{\tau}$ depending on the

parameters of the fracturing pulse can also be calculated using the incubation time criterion:

$$\tilde{t}_* = \begin{cases} \frac{1}{\tilde{\omega}} \arccos\left(1 - \frac{\tilde{\omega}}{\tilde{A}}\right), & \tilde{t}_0 \le 2, \\ \frac{1}{2} + \frac{1}{\tilde{\omega}} \arcsin\left(\frac{\tilde{\omega}}{2\tilde{A}} \frac{1}{\sin\left(\tilde{\omega}/2\right)}\right), & \tilde{t}_0 > 2. \end{cases} \quad (2.23)$$

Substituting expressions (2.19) into formula (2.22) and subsequent integration allows us to obtain the following expression for the energy accumulated by the sound wave before the onset of cavitation:

$$E_1 = \frac{\tau P_c^2 \tilde{A}^2}{2\rho c} \left(\tilde{t}_* - \frac{\sin(2\tilde{\omega}\tilde{t}_*)}{2\tilde{\omega}}\right). \quad (2.24)$$

Thus, after substituting the expression for the fracture time (2.23) into formula (2.24), we can calculate the dependence of the amount of energy spent on initiating a cavitation bubble on the parameters of the fracturing pulse: its amplitude and duration. Figure 2.10 shows a qualitative graph of this dependence in dimensionless coordinates. For convenience, the frequency of the corresponding ultrasonic wave is used instead of the pulse duration. The energy value is also indicated in dimensionless form after normalization by the value $E_0 = \frac{\tau {P_c}^2}{2\rho c}$, which has the dimension of energy, the value of which is determined by the parameters of the cavitating liquid.

Note that the dependences of the cavitation generation energy on the amplitude corresponding to the sections of the surface shown in Figure 2.10 by planes $\omega\tau = const$ in a certain range of low frequencies are not monotonic. However, starting from a certain frequency value, this dependence becomes monotonically increasing and with a further increase in frequency its nature does not change.

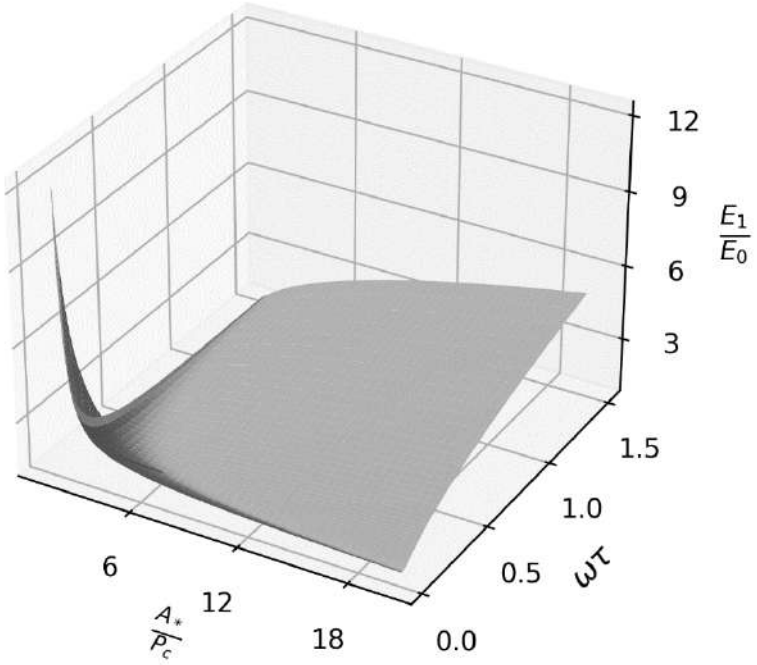

Figure 2.10 Energy of cavitation onset depending on the pulse amplitude and the frequency of the corresponding acoustic wave.

The obtained dependence of the energy spent on the occurrence of cavitation qualitatively agrees with the results of experimental observations [129]. It can also be noted that the obtained estimate of the energy intensity of the cavitation process is indirectly confirmed by experimental results on measuring the intensity of the effects formed during the collapse of cavitation bubbles [128].

2.7 Conclusions to Chapter 2

A method for determining the strength parameters of a material based on the method of sign-perturbed sums used to processing the time dependence of strength, experimentally observed in tests under pulse loading has been developed.

Based on the incubation time criterion, a model has been developed that predicts the dependence of the acoustic cavitation threshold on the frequency of the ultrasonic wave.

The calculated curves of the frequency dependence of the acoustic cavitation threshold for degassed water showed good qualitative and quantitative agreement with the experimentally observed Esche's curves. The calculation was carried out for the values of incubation time found by processing the time dependence of the cavitation threshold obtained within the framework of another experimental scheme.

The influence of equilibrium parameters of the continuous medium state – temperature and external hydrostatic pressure – on the values of model strength parameters is investigated. Temperature dependences for incubation time and critical stress are proposed.

The effectiveness of the proposed models was demonstrated on the example of problems related to determining the threshold of acoustic and pulsed cavitation of liquids.

An analytical model has been developed that evaluates the influence of a background acoustic ultrasonic field on the phase equilibrium conditions of a continuous medium.

A method is proposed for assessing the energy capacity of the acoustic cavitation process, depending on the frequency of the initiating ultrasonic wave.

Chapter 3 Peculiarities of continuous media fracture energy consumption under high-speed loading

The growth of the critical stress level with increasing loading rate indicates that other properties can also change dramatically when the loading mode is changed from low to high-rate loading. One of the key parameters is the energy consumption of the fracture process. In this chapter, the energetic characteristics of the high-speed impact fracture process of a continuous elastic medium are analyzed within the framework of the incubation time approach.

The results of Chapter 3 were presented in the following papers [116, 117, 118, 119, 120, 121, 50, 122].

3.1 Optimization of energy consumption in fracture by impact of a rigid particle on an elastic half-space

One of the simplest ways to create a high-rate action on an elastic solid medium is to impact it with another body of greater stiffness. As a result of the impact, tensile stresses are applied to the surface of the solid medium in the vicinity of the contact zone, leading to fracture. For spherical and cylindrical impactors, Hertz's hypothesis is applicable, according to which the force of the contact interaction depends on the depth of penetration of the impactor into the solid medium. Using this hypothesis, it is possible to calculate $\sigma(t)$, the time profile of the fracture stresses that lead to the initiation of surface cracks and initial fracture. The amplitude and duration of the impact are determined by the impact velocity V_0 and the radius of the spherical particle R. In the case of impact with a cylindrical particle, R is the radius of the cylinder base. In this case, the incubation time criterion allows us to calculate the values of the load impact characteristics V_0

and R that correspond to the initiation of threshold fracture pulses on the elastic medium:

$$\max_{t} \int_{t-\tau}^{t} \sigma(R, V_0, \xi) d\xi = \sigma_c \tau, \tag{3.1}$$

where τ and σ_c are strength parameters of the medium, parameter $\alpha = 1$.

Impact by spherecal particle

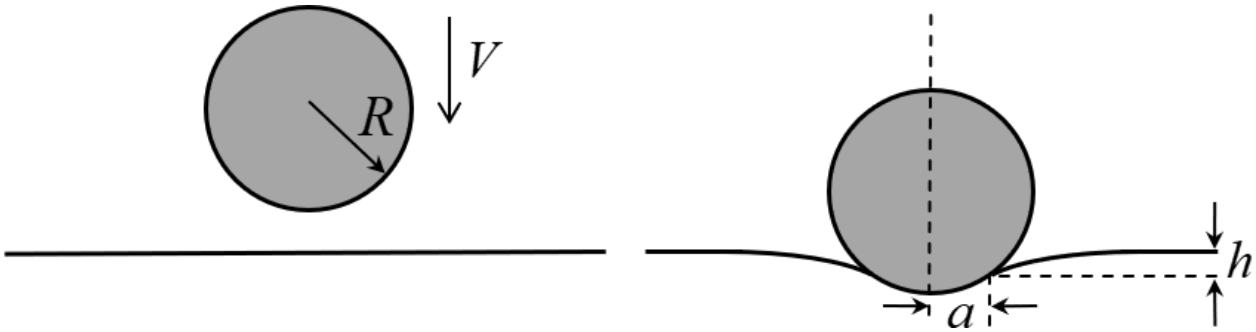

Figure 3.1 General scheme of the impact of a spherical particle on an elastic half-space.

The Hertz hypothesis for the contact force P when a spherical particle impacts the surface of an elastic half-space (see Figure 3.1) is as follows:

$$P(t) = k_b h^{\frac{3}{2}}(t), \tag{3.2}$$

where h is the penetration depth of the particle inside the surface, k_b is a constant coefficient whose value is determined by the elastic properties of the half-space, Young's modulus E and Poisson's ratio ν, and the particle radius R

$$k_b = \frac{4\sqrt{R}E}{3(1-\nu^2)}.$$

To determine the time dependence of $h(t)$ when the particle interacts with the surface after the impact with velocity V_0, it is necessary to solve the equation of motion with the following initial conditions:

$$\begin{cases} m\dfrac{d^2h(t)}{dt^2} = -P(t) = -k_b h^{\frac{3}{2}}(t) \\ \left.\dfrac{dh(t)}{dt}\right|_{t=0} = V_0 \\ h(0) = 0 \end{cases} . \qquad (3.3)$$

Equation (3.3) is nonlinear and does not have an exact analytical solution, but it can be integrated once using a standard technique by multiplying its left and right parts by $\frac{dh(t)}{dt}$.

$$\frac{1}{2}\left(\frac{dh(t)}{dt}\right)^2 = -\frac{2k_b}{5m}h^{\frac{5}{2}}(t) + C_1$$

From the initial conditions it can be seen that the integration constant $C_1 = V_0$. In this case, the time dependence of the particle velocity in the contact process is determined by the following relation:

$$V(t) = \frac{dh(t)}{dt} = \sqrt{V_0^2 - \frac{4k_b}{5m}h^{\frac{5}{2}}(t)}\,. \qquad (3.4)$$

The maximum penetration depth h_0 is reached at the moment when $V(t) = 0$, so it follows from expression (3.4) that

$$h_0 = \left(\frac{5V_0^2 m}{4k_b}\right)^{\frac{2}{5}}. \qquad (3.5)$$

Considering relation (3.5) for the maximum depth h_0, expression (3.4) can be re-written as follows

$$\frac{dh(t)}{dt} = V_0 \sqrt{1 - \left(\frac{h(t)}{h_0}\right)^{\frac{5}{2}}}. \tag{3.6}$$

After the separation of the variables and the subsequent integration, we can write the following expression that links the process time and the penetration depth:

$$t = \frac{h_0}{V_0} \int_0^{\gamma} \frac{d\gamma'}{\sqrt{1 - (\gamma')^{\frac{5}{2}}}} + C_2, \tag{3.7}$$

where the dimensionless quantity $\gamma = \frac{h(t)}{h_0}$. At the initial time $t = 0$, the penetration depth $h(0) = 0$, hence the integration constant $C_2 = 0$. Let the duration of the impact be equal to t_0, then the maximum value of the penetration depth h_0 will correspond to the time $t = \frac{t_0}{2}$, and then $\gamma\left(\frac{t_0}{2}\right) = 1$. Then, according to relation (3.7), for the approximate calculated value of the definite integral, we can obtain the following expression for the duration of the impact:

$$t_0 = 2\frac{h_0}{V_0} \int_0^{1} \frac{d\gamma'}{\sqrt{1 - (\gamma')^{\frac{5}{2}}}} \approx 2.94\frac{h_0}{V_0}. \tag{3.8}$$

The solution of problem (3.3) can be represented with a high degree of accuracy in the following form:

$$h(t) = [H(t) - H(t - t_0)]h_0 \sin\left(\frac{\pi t}{t_0}\right), \tag{3.9}$$

where $H(t)$ is the Heaviside function. Tensile stresses resulting from an impact on the surface of an elastic half-space can be expressed by the contact force $P(t)$ and the radius of the contact area $a(t)$ [123]:

$$\sigma(t) = \frac{1-2\nu}{2}\frac{P(t)}{\pi a^2(t)}, \tag{3.10}$$

where

$$a(t) = \left(3P(t)(1-\nu^2)\frac{R}{4E}\right)^{\frac{1}{3}}. \tag{3.11}$$

Substituting the contact force $P(t)$ according to Hertz's hypothesis (3.2) into the expression obtained by substituting (3.11) into (3.10) gives the following expression for the stress pulse:

$$\sigma(t) = \frac{1-2\nu}{2\pi}\frac{k_b}{R}\sqrt{h(t)}\,. \tag{3.12}$$

Substituting the obtained solution of the motion equation (3.9) into expression (3.12) allows us to completely determine the time profile of the tensile stresses that initiate the fracture of the elastic half-space:

$$\sigma(t) = \frac{1-2\nu}{2\pi}\frac{k_b}{R}\sqrt{h_0}[H(t)-H(t-t_0)]\sqrt{\sin\left(\frac{\pi t}{t_0}\right)}. \tag{3.13}$$

After substituting of the expression (3.13) into the condition (3.1), the following relation is obtained, which establishes the relationship between the parameters of the problem at which the threshold fracture pulses occur:

$$\frac{1-2\nu}{2\pi}\frac{k_b}{R}\sqrt{h_0}\max_t\left(\frac{1}{\tau}\int_{t-\tau}^{t}[H(\xi)-H(\xi-t_0)]\sqrt{\sin\left(\frac{\pi\xi}{t_0}\right)}\,d\xi\right) = \sigma_c. \tag{3.14}$$

It is convenient to pass to dimensionless analogues of the main parameters of the problem in order to simplify further calculations:

$$\tilde{t}_0 = \frac{t_0}{\tau}; \qquad \tilde{V}_0 = \frac{V_0}{c_\rho}; \qquad \tilde{R} = \frac{R}{\tau c_\rho}, \tag{3.15}$$

where c_ρ is the propagation velocity of longitudinal waves in an elastic medium, which is determined by the elastic properties and the density of the medium ρ_m as follows:

$$c_\rho = \sqrt{\frac{E(1-\nu)}{\rho_m(1+\nu)(1-2\nu)}}. \tag{3.16}$$

Note that the maximum of the integral in expression (3.14) is reached at $t = \frac{(t_0+\tau)}{2}$, then, taking into account the notations introduced earlier, it can be rewritten as follows:

$$\alpha_b \tilde{V}_0^{\frac{2}{5}} \int_{\frac{\tilde{t}_0-1}{2}}^{\frac{\tilde{t}_0+1}{2}} [H(\xi) - H(\xi - \tilde{t}_0)] \sqrt{\sin\left(\pi \frac{\xi}{\tilde{t}_0}\right)}\, d\xi = 1, \tag{3.17}$$

where α_b is a dimensionless coefficient obtained by substituting the expressions for k_b and h_0 into condition (3.14), taking into account that the mass of the incident particle $m = 4/3\pi\rho R^3$ can be expressed by its volume and density:

$$\alpha_b = \frac{(1-2\nu)}{2\pi\sigma_c}\, c_\rho^{\frac{2}{5}} (E^4\rho)^{\frac{1}{5}} \left(\frac{4}{3}(1-\nu^2)\right)^{\frac{4}{5}} \left(\frac{5\pi}{3}\right)^{\frac{1}{5}}.$$

The expression (3.17) allows us to calculate, for an arbitrary dimensionless impact duration $\tilde{t}_0$, the threshold amplitude of the pulse and thus the threshold velocity of the impactor $\tilde{V}_0^*(\tilde{t}_0)$ corresponding to this amplitude.

The impact duration $\tilde{t}_0$ can also be expressed in terms of the particle radius R and the impact velocity V_0, using expressions (3.5) and (3.8):

$$\tilde{t}_0 = \frac{t_0}{\tau} \approx 3.2 \frac{1}{\tau} \left(\frac{\pi\rho(1-\nu^2)}{E} \right)^{\frac{2}{5}} \frac{R}{V^{\frac{1}{5}}}. \quad (3.18)$$

After substituting the dependence $\tilde{V}_0^*(\tilde{t}_0)$ into expression (3.18), we can calculate the threshold particle radius $\tilde{R}^*(\tilde{t}_0)$, which will also correspond to the threshold impact initiated by the impact:

$$\tilde{R}^*(\tilde{t}_0) = \frac{\tilde{t}_0}{\beta_b} \left(\tilde{V}_0^*(\tilde{t}_0) \right)^{\frac{1}{5}}, \quad (3.19)$$

where β_b is a dimensionless coefficient:

$$\beta_b = 3.2 \left(\pi(1-\nu^2) \frac{\rho c_\rho^2}{E} \right)^{\frac{2}{5}}.$$

Thus, expressions (3.17) and (3.19) allow us to calculate the threshold radius $\tilde{R}^*(\tilde{t}_0)$ and particle impact velocity $\tilde{V}_0^*(\tilde{t}_0)$ at which a threshold impact of duration $\tilde{t}_0$. occurs on the surface of the medium.

The kinetic energy of the particle allows us to estimate the energy input for the fracture initiated by the impact method of energy supply. For the impact of a spherical particle, its value is equal to:

$$W = \frac{2}{3} \pi\rho R^3 V_0^2. \quad (3.20)$$

Substituting the dependencies $\tilde{R}^*(\tilde{t}_0)$ and $\tilde{V}_0^*(\tilde{t}_0)$ into the energy expression allows us to estimate the energy consumption for the initiation of threshold fracture pulses as a function of their duration $\tilde{t}_0$:

$$\widetilde{W}^*(\tilde{t}_0) = \frac{W(\tilde{t}_0)}{w} = \left(\tilde{R}^*(\tilde{t}_0)\right)^3 \left(\tilde{V}_0^*(\tilde{t}_0)\right)^2, \qquad (3.21)$$

where $w = \frac{2}{3}\pi\rho\tau^3 c_\rho^5$ is a parameter with the dimension of energy, the value of which is determined by the parameters of the elastic medium and the density of the impacting particle.

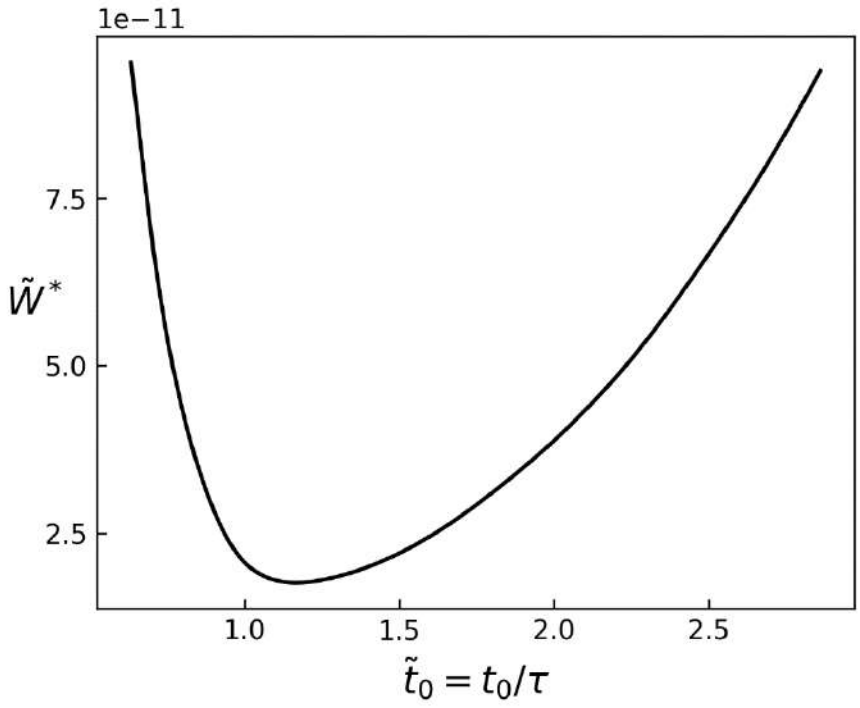

Figure 3.2 The kinetic energy of a spherical particle as a function of the duration of a threshold pulse initiated by an impact on the surface of an elastic half-space.

Figure 3.2 shows the dependence of the kinetic energy of a spherical particle on the duration of a threshold pulse occurring on the surface of an elastic half-space after impact. A notable feature of this dependence is a characteristic minimum at pulse durations t_0 close to the value of the incubation time τ. This means that the choice of loading mode, in order to minimize the energy consumption for fracture, must focus on impact durations close to the incubation time.

Impact by cylindrical particle

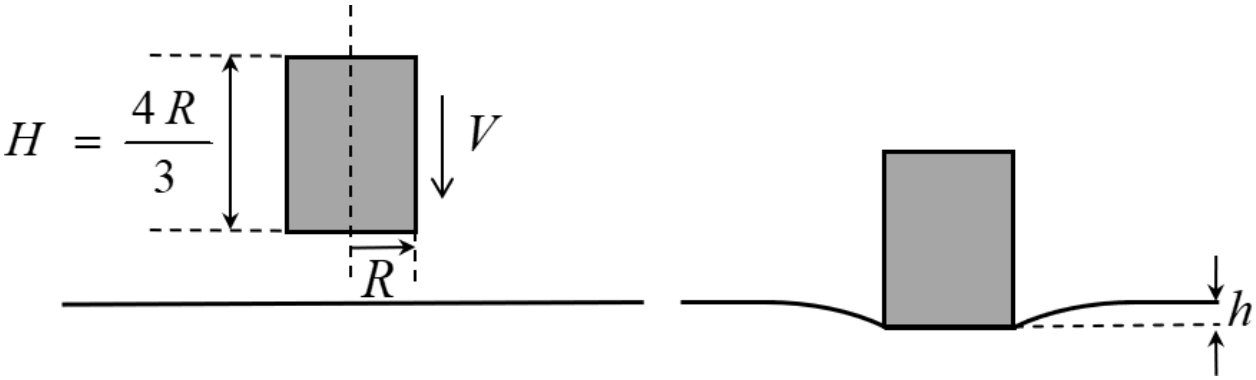

Figure 3.3 General scheme of the impact of a cylindrical particle on an elastic half-space.

A seemingly simpler case is observed when a half-space is impacted by a rigid cylindrical particle (see Figure 3.3), for which Hertz's hypothesis for the contact force P is as follows:

$$P(t) = k_c h(t), \qquad (3.22)$$

where h is the penetration depth of the particle inside the surface, k_c is a constant coefficient whose value is also determined by the elastic properties of the half-space, Young's modulus E and Poisson's ratio ν, and the base radius R

$$k_c = \frac{2RE}{1-\nu^2}.$$

To find the time dependence of the penetration depth of the impactor into the half-space, it is again necessary to solve the equation of motion with similar initial conditions:

$$\begin{cases} m\dfrac{d^2h(t)}{dt^2} = -P(t) = -k_c h(t) \\ \left.\dfrac{dh(t)}{dt}\right|_{t=0} = V_0 \\ h(0) = 0 \end{cases} . \qquad (3.23)$$

For the cylindrical particle, the equation (3.23) has a simple analytical solution:

$$h(t) = h_0 \sin\left(\pi \frac{t}{t_0}\right), \qquad (3.24)$$

where the contact time t_0 and the maximum penetration depth h_0 are defined as follows:

$$h_0 = V_0 \sqrt{\frac{m}{k_c}}, \qquad (3.25)$$

$$t_0 = \pi \sqrt{\frac{m}{k_c}}. \qquad (3.26)$$

For the cylinder impact, the contact area value does not depend on time and is determined only by the radius R. Therefore, the maximum tensile stresses can be calculated using the formula [123]:

$$\sigma(t) = \frac{1-2\nu}{2} \frac{P(t)}{\pi R^2}, \quad r \to R + 0. \qquad (3.27)$$

After substituting the expression for the impact pulse (3.27) into the criterion (3.1), taking into account that the maximum of the integral is also reached at the time $t = \frac{(t_0+\tau)}{2}$, we obtain the following relationship between the parameters of the problem in the case of threshold impacts:

$$\alpha_c \tilde{V}_0 \int_{\frac{\tilde{t}_0-1}{2}}^{\frac{\tilde{t}_0+1}{2}} [H(\xi) - H(\xi - \tilde{t}_0)] \sin\left(\pi \frac{\xi}{\tilde{t}_0}\right) d\xi = 1, \qquad (3.28)$$

where α_c is a dimensionless coefficient obtained by assuming that the volume of the cylindrical particle is equal to the volume of the spherical particle, that is, the cylinder height $H = \frac{4}{3}R$:

$$\alpha_b = \frac{(1-2\nu)c_\rho}{2\sigma_c} \sqrt{\frac{8E\rho}{3\pi(1-\nu^2)}}.$$

Таким образом, выражение (3.28) также позволяет вычислить пороговую скорость цилиндрического ударника $\tilde{V}_0^*(\tilde{t}_0)$.для произвольной безразмерной длительности воздействия $\tilde{t}_0$. Соответствующее значение порогового радиуса $\tilde{R}^*(\tilde{t}_0)$ можно вычислить аналогичным образом, как и в случае сферического ударника:

Thus, expression (3.28) also allows us to calculate the threshold velocity of the cylindrical impactor $\tilde{V}_0^*(\tilde{t}_0)$ for any dimensionless impact duration $\tilde{t}_0$. The corresponding value of the threshold radius $\tilde{R}^*(\tilde{t}_0)$ can be calculated in the same way as for a spherical impactor:

$$\tilde{R}^*(\tilde{t}_0) = \frac{\tilde{t}_0}{\beta_c}, \qquad (3.29)$$

with β_c being a nondimensional factor:

$$\beta_c = \pi c_\rho \sqrt{\frac{2\pi}{3} \frac{\rho(1-\nu^2)}{E}}.$$

Note that for the cylindrical impactor, there is a one-to-one correspondence between the base radius and the pulse duration, and between the impact velocity

and the fracture pulse amplitude. In the case of the spherical impactor, the impact velocity influences on not only the amplitude but also the duration.

Since the volume of the cylinder was chosen to be equal to that of the sphere, the energy dependence of the impact load can be calculated by substituting the new expressions for $\tilde{V}_0^*(\tilde{t}_0)$ and $\tilde{R}^*(\tilde{t}_0)$ into equation (3.21).

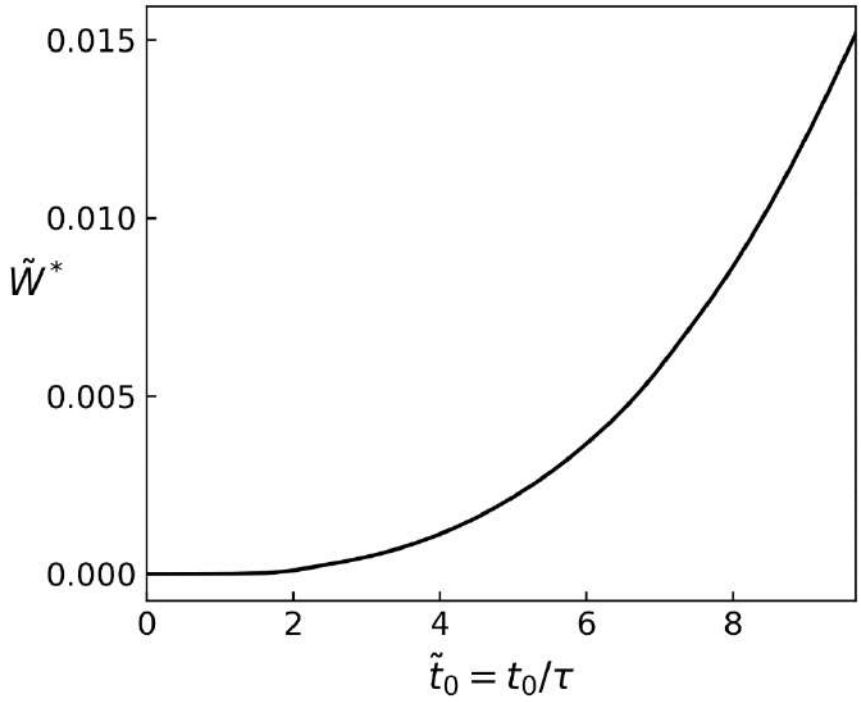

Figure 3.4 Dependence of the kinetic energy of the cylindrical particle on the duration of a threshold pulse initiated by an impact on the surface of an elastic half-space.

The threshold energy dependence shown in Figure 3.4 has no local minimum, unlike the case of the spherical impactor, and the energy input tends to zero as the particle radius decreases. In order to find the reasons for such a fundamental difference observed in these two cases, it is necessary to investigate another intermediate shape of the impactor, which in limit cases may correspond to a cylinder or a sphere.

Impact by a particle in the form of a revolution surface

The main difference between the contact conditions of the spherical particle and the cylindrical particle is the non-stationary contact surface, which leads to the existence of optimal impact durations in terms of energy consumption. In order to verify this assumption, we have considered another case of the impact by a particle whose contact surface is a rotation figure of an exponential function curve given by the following equation:

$$z = Br^4 \tag{3.30}$$

To make the mass of such an impactor equal to the mass of the spherical one, the coefficient B should be set equal to $B = \frac{2}{R^3}$.

According to Staermann's theory of quasi-static impact, the pressure distribution in the contact area can be calculated by the formula:

$$p(r) = \frac{5}{3}\left(\left(\frac{r}{a}\right)^2 + \frac{1}{2}\right)\sqrt{1 - \left(\frac{r}{a}\right)^2}\,\frac{P}{\pi a^2}, \qquad r \in [0, a]. \tag{3.31}$$

Using the solution of the Businesq's problem of a concentrated force, we can determine that the maximum tensile stresses will be radial stresses, which are found by the same formula as in the case of the spherical particle impact:

$$\sigma(t) = \frac{1 - 2\nu}{2}\frac{P(t)}{\pi a^2(t)},$$

where the radius $a(t)$ of the contact area and the contact force $P(t)$ are calculated as follows:

$$a(t) = \left(\frac{15(1-\nu)^2}{64\,E} + \frac{P(t)}{B}\right)^{\frac{1}{5}}, \tag{3.32}$$

$$P(t) = k\big(h(t)\big)^{\frac{5}{4}}, \qquad k = \frac{8E}{1-\nu^2}\left(\frac{3}{2A}\right)^{\frac{1}{4}}\left(\frac{1}{5}\right)^{\frac{5}{4}}. \tag{3.33}$$

The solution of the corresponding equation of motion can be written in the standard form

$$h(t) = h_0 \sin\left(\pi\frac{t}{t_0}\right),$$

for which, the pulse duration t_0 and the maximum penetration depth h_0 are determined accordingly:

$$h_0 = \left(\frac{9}{8}\frac{mV_0^2}{k}\right)^{\frac{4}{9}}, \tag{3.34}$$

$$t_0 = \frac{h_0}{V_0}\frac{8\sqrt{\pi}}{9}\frac{\Gamma(4/9)}{\Gamma(17/19)}, \tag{3.35}$$

where $\Gamma(x)$ is the Euler Gamma function.

The use of the incubation time criterion allows us to obtain a similar condition for determining the threshold velocity $\tilde{V}_0^*(\tilde{t}_0)$ as a function of the loading pulse duration. Substituting the expression for the fracture pulse (3.12) into the criterion (3.1), taking into account relations (3.32) - (3.35), we obtain the following expression:

$$\alpha_{rs}\tilde{V}_0^{\frac{2}{3}}\int\limits_{\frac{\tilde{t}_0-1}{2}}^{\frac{\tilde{t}_0+1}{2}}[H(\xi)-H(\xi-\tilde{t}_0)]\left(\sin\left(\pi\frac{\xi}{\tilde{t}_0}\right)\right)^{\frac{3}{4}}d\xi = 1, \tag{3.36}$$

where the dimensionless coefficient α_{rs} is determined by the problem parameters as follows:

$$\alpha_{rs} = \frac{(1-2\nu)}{2\pi\sigma_c}\, c_\rho^{\frac{2}{3}} \left(\frac{8E}{1-\nu^2}\right)^{\frac{2}{3}} \left(\frac{3}{2}\,\pi\rho\right)^{\frac{1}{3}} \left(\left(\frac{1}{5}\right)^5 \left(\frac{8}{15}\right)^{\frac{3}{2}} \frac{3}{2}\right)^{\frac{1}{15}} 2^{\frac{1}{9}}.$$

To calculate the threshold for the radius $\tilde{R}^*(\lambda)$ we use the equation

$$\tilde{R}^*(\tilde{t}_0) = \frac{\tilde{t}_0}{\beta_c} \tilde{V}_0^{\frac{1}{9}}(\tilde{t}_0), \qquad (3.37)$$

where

$$\beta = \frac{8\sqrt{\pi}}{9} \left(\frac{c_\rho^2\,\rho}{E}\right)^{\frac{8}{9}} \frac{\Gamma(4/9)}{\Gamma(17/19)} \left(5^{\frac{5}{4}}\,\frac{1-\nu^2}{8}\pi\right)^{\frac{4}{9}} 2^{\frac{1}{9}}.$$

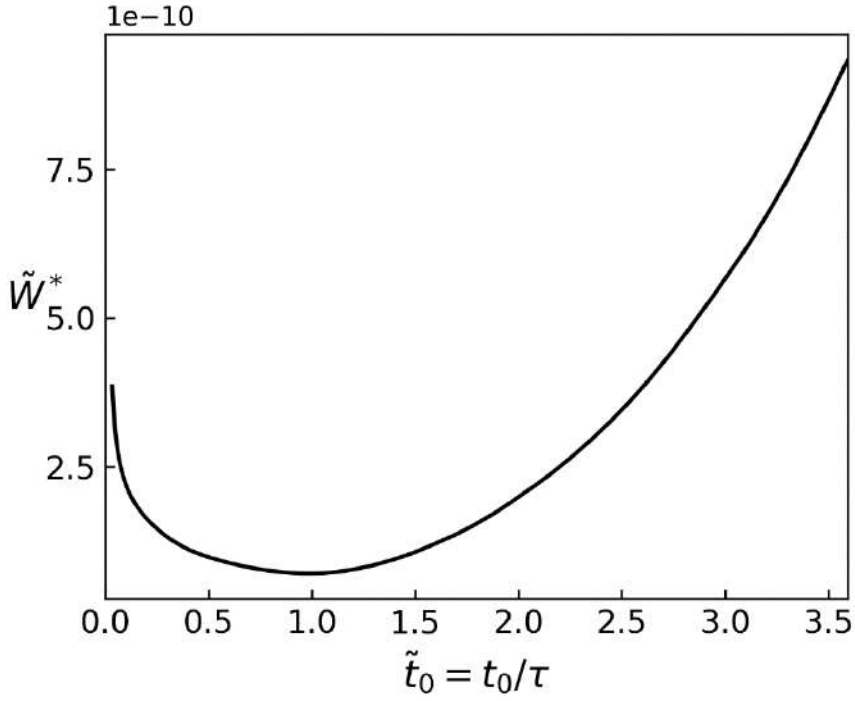

Figure 3.5 Dependence of the kinetic energy of the particle with a contact surface profile given by the function z=Br^4 on the duration of a threshold pulse initiated by an impact on the surface of an elastic half-space.

A similar dependence of energy consumption under impact loading can be calculated by substituting the expressions for $\tilde{V}_0^*(\tilde{t}_0)$ and $\tilde{R}^*(\tilde{t}_0)$, determined

according to (3.36) and (3.37), into formula (3.21). The resulting dependence of the kinetic energy on the threshold pulse duration is shown in Figure 3.5. As in the case of the spherical impactor, it has the same local minimum for the fracture pulse durations, which values is around τ.

A more general case was analyzed in [124], where the latter problem was investigated in a more general formulation. The contact surface was given by equation:

$$z = B^{1-\lambda} r^{\lambda}, \qquad (3.38)$$

where B is a constant of length dimension and the shape parameter $\lambda > 1$. This choice of equation is due to the fact that in the limiting case as $\lambda \to \infty$ the shape of the contact surface tends to be cylindrical, while for values $\lambda \sim 2$ its shape is close to spherical. It turned out that there is a critical value $\lambda^* = 5.5$ which determines the type of dependence of the threshold energy on the fracture pulse duration:

$$\begin{cases} \widetilde{W}^*(\tilde{t}_0) \underset{\tilde{t}_0 \to 0}{\longrightarrow} \infty, & \lambda < \lambda^* \\ \widetilde{W}^*(\tilde{t}_0) \underset{\tilde{t}_0 \to 0}{\longrightarrow} const, & \lambda = \lambda^* \\ \widetilde{W}^*(\tilde{t}_0) \underset{\tilde{t}_0 \to 0}{\longrightarrow} 0, & \lambda > \lambda^* \end{cases}$$

In other words, for $\lambda < 5.5$ the dependence of the threshold energy on the impact duration has a local minimum, as in the case of the spherical impactor, and for $\lambda > 5.5$ the value of the threshold energy tends to zero as the impact duration decreases, as in the case of the cylindrical impactor. The results obtained show the need for additional research to determine the nature of this critical value $\lambda^* = 5.5$, since at first sight it may seem to be some universal value, since all calculations of the threshold energy have been performed in dimensionless form.

3.2 Peculiarities of dynamic impact loading. Supersonic and subsonic interaction

One of the key factors in the contact interaction of the impactor with an elastic medium is the velocity of the contact region boundary, and its ratio to the velocity of longitudinal waves in the elastic medium is also of fundamental importance. For example, it has been shown in [125] and [126] that under dynamic contact conditions, a supersonic stage can be observed in which the contact region grows faster than the propagation of elastic waves caused by the contact interaction. Later, in [127], Borodich gave a proof based on geometric considerations that for any convex smooth surface, in particular for a spherical surface, there are always two stages of contact interaction: supersonic and subsonic. In the first stage, the growth rate of the contact boundary exceeds the speed of longitudinal waves in the elastic medium, and conversely, in the second stage, the boundary grows slower than the propagation speed of the interaction signal. Let the time moment t_* correspond to the transition of the contact interaction process from the supersonic to the subsonic stage.

Then it can be assumed that the application of the Hertz and Staermann approaches is justified only at $t > t_*$, since they were proposed for quasi-static equilibrium conditions. Therefore, for a more correct analysis of the threshold energy, a different contact interaction condition should be used for the supersonic stage when $t < t_*$. In the following analysis, we use the solution of the dynamic contact problem obtained by Borodich on the basis of general principles that have also been used by other researchers of dynamic contact problems with moving boundaries [128], [129], [130].

Supersonic stage

The influence of the consideration of the supersonic stage on the peculiarities of the threshold energy behavior is studied for the contact surface, the shape of which is given by equation (3.38):

$$z = B^{1-\lambda} r^{\lambda}.$$

In this case, the area of the contact zone S depends on the penetration depth h as follows:

$$S(h) = \pi B^{2-\frac{2}{\lambda}} r^{\frac{2}{\lambda}}. \tag{3.39}$$

In [124] it was shown that if we represent a particle as a generalized ellipsoid whose surface in the contact region is described by equation (3.38), then in this case the mass of the particle should be calculated as follows

$$m = \frac{4\pi}{3} B^3 \rho_1 \lambda^{-\frac{\lambda+2}{\lambda-1}} \Gamma\left(\frac{2}{\lambda}\right) \Gamma\left(\frac{1}{\lambda}\right) \Gamma\left(\frac{3}{\lambda}\right)^{-1}, \tag{3.40}$$

where ρ_1 is the particle density.

According to the solution proposed by Borodich [127], the time dependence of the penetration depth can be expressed implicitly:

$$t(h) = \int_0^h \frac{dh'}{V_0 - \frac{\rho c_\rho \pi}{m\mu} B^{3-\mu} h'^{\mu}}, \qquad \mu = \frac{\lambda+2}{\lambda}, \quad 1 < \mu < 3, \tag{3.41}$$

where, as before, V_0 is the initial velocity of the impactor, c_ρ is the velocity of propagation of the elastic wave, and ρ is the density of the elastic medium. After a

series of algebraic transformations, expression (3.41) can be rewritten in the following form:

$$t(h) = \frac{h_s}{V_0}\int_0^{\frac{h}{h_s}} \frac{d\xi}{1-\xi^{\mu}},$$
$$h_s = B\left(\frac{\mu m V_0}{\rho c_\rho \pi} B^{-3}\right)^{1/\mu}. \qquad (3.42)$$

The expression (3.42) implicitly defines a function $F_\mu(\gamma)$ that relates the penetration depth h to the time t:

$$F_\mu(\gamma) = \int_0^{\gamma} \frac{d\xi}{1-\xi^{\mu}},\ 0 < \gamma < 1. \qquad (3.43)$$

It is important to note that $F_\mu\ (\gamma)$ is a monotonically increasing function from zero to infinity for all values $1 < \mu < 3$ at $0 < \gamma < 1$. This allows us to state that for each specific shape of the impactor there will exist an inverse function F_μ^{-1} that determines the time dependence of $h(t)$. Thus, the contact interaction between a convex impactor and an elastic half-space in the supersonic phase is determined according to the following relationship:

$$h_d(t) = h_s F_\mu^{-1}\left(\frac{V_0}{h_s} t\right). \qquad (3.44)$$

Then, the impact velocity $V_d\ (t)$ and the contact force $P_d(t)$ can be defined as follows:

$$V_d(t) = \dot{h}_d(t),$$
$$P_d(t) = \rho c_\rho \pi V_d(t) B^2 \left(\frac{h_d(t)}{B}\right)^{\mu-1}. \qquad (3.45)$$

The end time of the supersonic stage t^* can be found based on the equality condition between the propagation velocity of the contact region boundary and the longitudinal wave velocity c_ρ , and calculated as a solution of equation:

$$\dot{a}\,(t_*) = c_\rho = \sqrt{\frac{E}{\rho}}. \qquad (3.46)$$

For the chosen shape of the impactor, the left part of equation (3.46) can be rewritten as follows:

$$\dot{a}\,(t_*) = \frac{1}{\lambda}\big(h_d(t_*)\big)^{\frac{1}{\lambda}-1} B^{\frac{\lambda-1}{\lambda}} V_0 \left(1 - \left(\frac{h_d(t_*)}{h_s}\right)^{\mu}\right) = \sqrt{\frac{E}{\rho}}. \qquad (3.47)$$

Thus, equation (3.47) allows us to estimate the transition time t_* and, consequently, to calculate the boundary values of the penetration depth $h_* = h_d(t_*)$, the contact radius $a_* = a_d(t_*)$, and the impactor velocity $V_* = V_d(t_*)$. It can also be noted that $t_* \to 0$ as $\rho \to 0$, which means that there is no supersonic stage for an elastic medium with infinite longitudinal wave propagation velocity.

It should be noted that there is no exact analytical solution for the stresses generated by the impact during the supersonic phase. Therefore, at this stage, only a numerical evaluation of the threshold energy is possible, which significantly complicates the overall calculation algorithm.

Subsonic stage. Staermann's solution

The contact interaction in the subsonic stage at $t > t_*$ can be described according to the Staermann approach in the same way as in [124]:

$$P_{qs}(t) = k_1 \left(h_{qs}(t)\right)^{\frac{\lambda+1}{\lambda}}, \tag{3.48}$$

where

$$k_1 = \frac{E}{1-\nu^2} B^{\frac{\lambda-1}{\lambda}} \frac{2^{\frac{2}{\lambda}} \lambda^{\frac{\lambda-1}{\lambda}}}{\lambda+1} \Gamma\left(\frac{\lambda}{2}\right)^{-\frac{2}{\lambda}} \Gamma(\lambda)^{\frac{1}{\lambda}}.$$

The time dependence of the penetration depth at the loading stage can be found from the solution of the equation of motion with appropriate initial conditions defined at the supersonic interaction stage:

$$\begin{cases} m\dfrac{d^2 h_{qs}(t)}{dt^2} = -P_{qs}(t) = -k_1 h_{qs}^{\beta}(t), \ \ \beta = \dfrac{\lambda+1}{\lambda} \\ \left.\dfrac{dh_{qs}(t)}{dt}\right|_{t=t_*} = V_* \\ h_{qs}(t_*) = h_* \end{cases}. \tag{3.49}$$

As in the case of the spherical impactor, equation (3.49) does not have an analytical solution, but can be integrated by multiplying both parts by $\frac{dh_{qs}}{dt}$:

$$\frac{m}{2}\left(V_{qs}^2 - V_*^2\right) = -\frac{k_1}{\beta+1}\left(h_{qs}^{\beta+1} - h_*^{\beta+1}\right). \tag{3.50}$$

Substituting $V_{qs} = 0$ in relation (3.50) allows us to calculate the maximum penetration depth h_0:

$$h_0 = \left(\frac{(\beta+1)mV_*^2}{2k_1} + h_*^{\beta+1}\right)^{\frac{1}{\beta+1}}. \tag{3.51}$$

Formal integration of expression (3.50) allows us to write down the following relation for the time dependence of the penetration depth $h_{qs}(t_*)$ during the subsonic stage:

$$\int_{t_*}^{t} dt = t - t_* = \Delta t = h_0 \sqrt{\frac{m(\beta+1)}{2k_1 h_0^{\beta+1}}} U_\beta\left(\frac{h_{qs}}{h_0}\right), \qquad (3.52)$$

where

$$U_\beta\left(\frac{h_{qs}}{h_0}\right) = \int_{\frac{h_*}{h_0}}^{\frac{h_{qs}}{h_0}} \frac{d\xi}{\sqrt{1-\xi^{\beta+1}}}.$$

Thus, expression (3.52) allows us to estimate the time interval t_{qs} during which the penetration depth reaches its maximum value h_0:

$$\int_{t_*}^{t_0} dt = t_0 - t_* = t_{qs} = h_0 \sqrt{\frac{m(\beta+1)}{2k_1 h_0^{\beta+1}}} U_\beta(1), \qquad (3.53)$$

where t_0 is the duration of the loading phase. Taking into account expression (3.51), we can rewrite (3.53) in the following form:

$$t_0 = t_* + \frac{h_0}{V_*} \sqrt{1 - \frac{2k_1 h_*^{\beta+1}}{(\beta+1)mV_*^2 + 2k_1 h_*^{\beta+1}}}\, U_\beta(1), \qquad (3.54)$$

During unloading, when the impactor moves in the opposite direction, there is no supersonic stage. Therefore, to find the contact interaction conditions, it is necessary to solve the equation of motion (3.49) again with new boundary conditions:

$$\begin{cases} m\dfrac{d^2 h_{qs}(t)}{dt^2} = -P_{qs}(t) = -k_1 h_{qs}^{\beta}(t), \;\; \beta = \dfrac{\lambda+1}{\lambda} \\ \left.\dfrac{dh_{qs}(t)}{dt}\right|_{t=t_0} = 0 \\ h_{qs}(t_0) = h_0 \end{cases} . \qquad (3.55)$$

The first integration of equation (3.55) allows us to determine the velocity of the impactor in the reverse direction during unloading.

$$\frac{dh_{qs}(t)}{dt} = \sqrt{\frac{2k_1 h_0^{\beta+1}}{m(\beta+1)}} \sqrt{1 - \left(\frac{h_{qs}(t)}{h_0}\right)^{\beta+1}} . \qquad (3.56)$$

Therefore, the contact end time t_{**} can be calculated as follows:

$$t_{**} - t_0 = h_0 \sqrt{\frac{m(\beta+1)}{2k_1 h_0^{\beta+1}}} \int_0^1 \frac{d\xi}{\sqrt{1-\xi^{\beta+1}}}, \qquad (3.57)$$

It should also be noted that the duration of the unloading process $t_{**} - t_0$ exceeds the duration of the loading phase t_0, because

$$h_0 \sqrt{\frac{m(\beta+1)}{2k_1 h_0^{\beta+1}}} \int_0^1 \frac{d\xi}{\sqrt{1-\xi^{\beta+1}}} > t_*.$$

Design of a continuous solution for the supersonic and subsonic stages

The time dependencies of the penetration depth and the impactor velocity in the supersonic and subsonic phases are continuous functions by virtue of the conditions for the construction of the defining relations obtained on the basis of the Borodich solution and the quasi-static Staermann approximation. However, due to the fundamental difference between these approaches for the time dependence of the contact zone radius, the transient moment t_* is a first-order breakpoint, which is in contradiction with the physics of the process. Therefore, to construct a continuous solution, it is necessary to introduce a smoothing function $0 \le \chi(t) \le 1$ on the interval $[0.95t_*; 1.05t_*]$, which ensures a continuous transition from the supersonic to the subsonic stage:

$$\chi(t) = \begin{cases} 1, & 0 < t < 0.95t_*, \\ 0, & 1.05t_* > t. \end{cases} \qquad (3.58)$$

This function can be used to link expressions not only for the radius of the contact zone $a(t)$, but also for the contact force $P(t)$:

$$\begin{aligned} a(t) &= a_d(t)\chi(t) + a_{qs}(t)(\chi(t)-1), \qquad 0 < t < t_{**}, \\ P(t) &= P_d(t)\chi(t) + P_{qs}(t)(\chi(t)-1), \qquad 0 < t < t_{**}. \end{aligned} \tag{3.59}$$

In addition, the same function $\chi(t)$ allows us to approximate the mean pressure in the contact zone:

$$p_0(t) = \frac{P_d(t)}{\pi a_d^2(t)}\chi(t) + \frac{P_{qs}(t)}{\pi a_{qs}^2(t)}(\chi(t)-1), \qquad 0 < t < t_{**}. \tag{3.60}$$

The solution proposed by Borodich does not include a special estimation of the surface stresses for the supersonic case, so in a first approximation we can use the same method as for the subsonic case. In this case, the pressure distribution in the contact area is calculated as follows:

$$\sigma_z(r_0,t) = p(r_0,t) = \frac{\lambda+1}{2}p_0(t)\int_0^{\sqrt{1-r_0^2}}(r_0^2+\xi^2)d\xi, \tag{3.61}$$

where $r_0 = r_0(r,t) = \frac{r}{a(t)}$ is a dimensionless coordinate. The expression for radial ultimate stresses can be approximated in a similar manner:

$$\sigma_r(r_0,t) = \begin{cases} p(r_0,t) + \dfrac{1-2\nu}{r_0^2}\displaystyle\int_0^{r_0}\eta p(\eta)d\eta, & r_0 \le 1, \\ \dfrac{1-2\nu}{r_0^2}\displaystyle\int_0^{1}\eta p(\eta)d\eta, & r_0 > 1. \end{cases} \tag{3.62}$$

The maximum radial stress occurs at the contact boundary when $r_0 = 1$:

$$\sigma_r(1,t) = (1-2\nu)\int_0^1 \eta p(\eta)d\eta = \frac{(1-2\nu)P(t)}{2\pi a^2(t)}. \tag{3.63}$$

Thus, for any time during the contact interaction, the expressions (3.60), (3.61) and (3.63) allow us to approximate the maximum level of the fracture stresses at the surface of the elastic medium. In this case, at the edges of the interaction time interval, the solution will be exact, since it is constructed on the basis of the Borodich exact solution for the supersonic stage, and on the basis of the quasi-static Staermann approach for the subsonic stage.

It should also be noted that expression (3.61) defines the maximum failure stresses at different points of the half-space surface for each instant of time. Therefore, the result of using this expression in the incubation time criterion as a time profile of the loading action will be a lower estimate of the threshold amplitude.

Threshold energy calculation

As in the previous cases, the thresholds of the problem parameters are calculated using the incubation time criterion. However, the obtained expression (3.63) does not allow us to calculate the time dependence of the fracture stresses in an explicit form. Therefore, to determine the threshold impact velocity V_0^* as a function of the impact duration t_{**}, it is convenient to introduce the following function:

$$\Upsilon_{t_{**}}(V_0) = \frac{1}{\tau\sigma_c} \max_{t\in[0,t_{**}]} \left(\int_{t-\tau}^{t} \sigma(\xi) d\xi \right) - 1. \qquad (3.64)$$

The function $\Upsilon_{t_{**}}(V_0)$ can be used in the iterative algorithm to find the threshold velocity V_0^* with the required accuracy $\delta > 0$, because by definition it has the following property:

$$\Upsilon_{t_{**}}(V_0) = \begin{cases} > 0, & V_0 = V_0^* + \delta, \\ \equiv 0, & V_0 = V_0^*, \\ < 0, & V_0 = V_0^* - \delta. \end{cases} \quad (3.65)$$

The formal steps of the algorithm to calculate the threshold velocity are summarized in Table 3.1 Formal steps of the procedure to determine the threshold velocity V_0^*.

Table 3.1 Formal steps of the procedure for determining the threshold velocity $\boldsymbol{V_0^*}$ for a given pulse duration $\boldsymbol{t_{**}}$

1.	For some value of the pulse duration t_{**}, determine the initial approximation of the threshold velocity V_p using the quasi-static solution (see [124]).
2.	Set the interval of test values in some steps $$V_\delta = [V_p - \delta, V_p + \delta],$$ which probably includes the desired value V_0^*.
3.	Using the equations from Section 3.2, determine the time dependence of the stresses for each value of V_δ.
4.	For each value of V_δ, compute the function $\Upsilon_{t_{**}}(V_0)$. Using property (3.65), define a new, narrower interval for trial values
5.	Repeat steps 2-4 to obtain the desired value of V_0^* with the required accuracy.
6.	Calculate the value of the threshold energy W for the value of V_0^* found.

The computational complexity of the proposed algorithm does not allow us to obtain the dependence of the threshold energy W on the pulse duration t_{**} with a good degree of discretization. Therefore, calculations of the threshold velocity and then the threshold energy were performed for a limited set of values of t_{**}..

Figure 3.6 shows the results of the calculations for different values of the parameter $\lambda < \lambda^* = 5.5$ at different density ratios of the elastic medium and the impactor. The gabbro-diabase with the following parameter values $E = 6.2 \times 10^9 Pa$, $\nu = 0.26$, $\sigma_c = 44.04 \times 10^6 Pa$ was chosen as the elastic medium. The value of the impactor density was chosen to be $\rho_1 = 2400\ kg/m^3$.

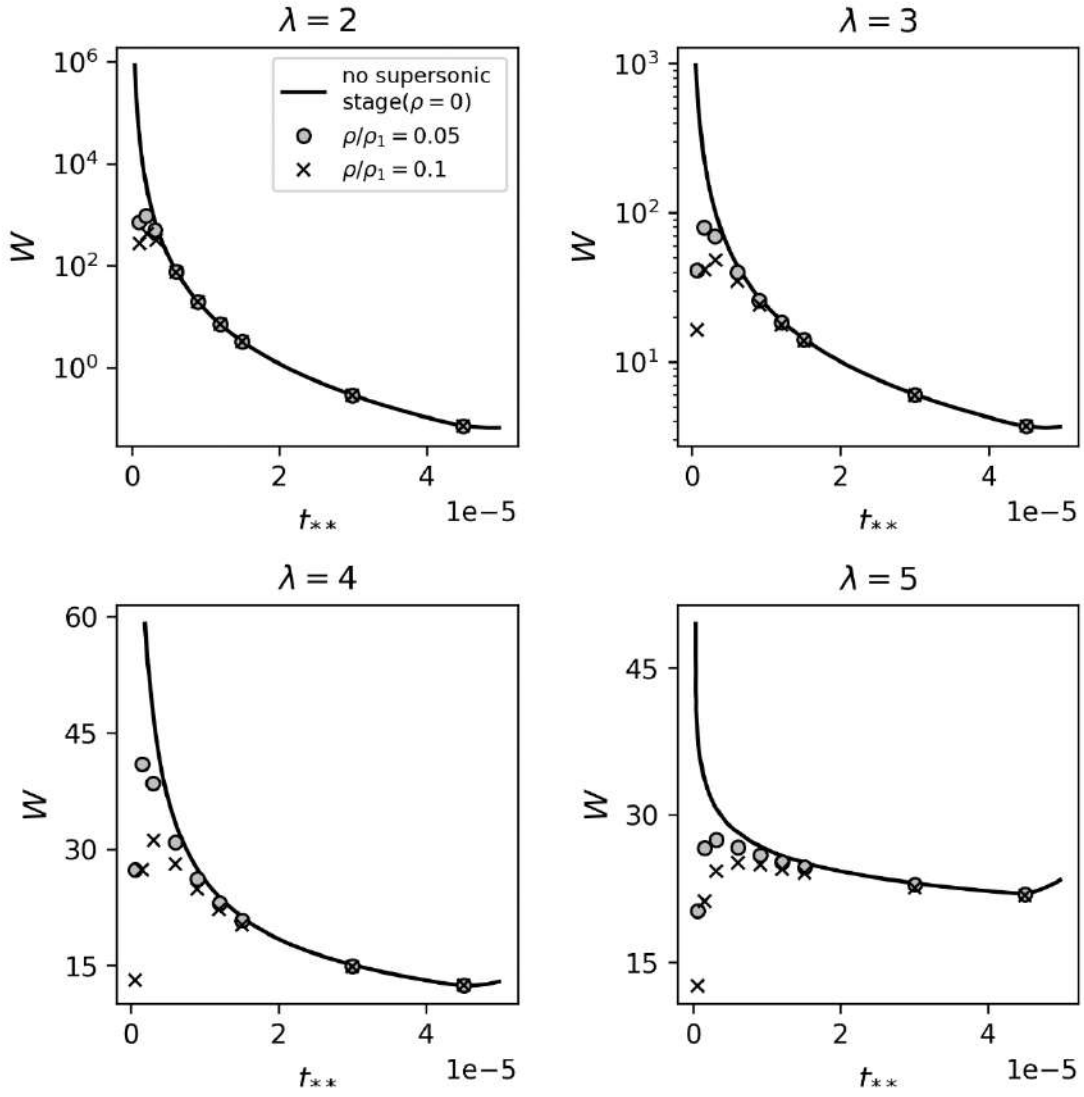

Figure 3.6 Threshold energy as a function of impact duration for different elastic medium and impactor density ratios at $\lambda = \{2,3,4,5\}$.

The calculations show that as the contact time increases, the values of the threshold energy, taking into account the presence of the supersonic stage, tend to the values calculated in the quasi-static approximation, which in Figure 3.6 corresponds to the solid curve obtained at $\rho = 0$. However, as the contact time decreases, the value of the threshold energy begins to rapidly approach zero, and the lower the velocity of the elastic wave propagation, the faster the value of the threshold energy decreases.

It should be noted that taking into account the supersonic stage of the contact interaction leads to a decrease of the threshold energy at values of the parameter $\lambda < \lambda^*$. Thus, the previously found value $\lambda^* = 5.5$ is critical one only in the framework of quasi-static analysis.

3.3 Optimization of energy consumption in the technology of ultrasonically assisted processing of materials

The previously described dependence of the energy consumption of the fracture process on the impact duration can be used to explain the effectiveness of the technology of ultrasonically assisted (UA) processing of materials. It should be noted that high-frequency vibrations are widely used in various applied technologies, in particular, ultrasound is used for cleaning and degreasing of machine parts, intensification of chemical reactions, degassing and structuring of melts, as well as in many types of mechanical processing of metals. In this paragraph, we will consider the reasons related to ultrasonic assisted turning or drilling of solids.

Ultrasonic vibrations strongly affect the behavior of the material during the technological process: there is a significant reduction in the force applied during machining, and the quality of the cut surface is improved [131, 132, 133]. For

example, it has been observed that the overlap of ultrasonic vibrations in the tool direction during turning or drilling, leads to a significant reduction in the force applied to the tool. This effect makes it possible to produce parts from high-strength, difficult-to-machine materials that are difficult or even almost impossible to treat using conventional methods [134].

One of the main ways to study the ultrasonic assisted process is numerical modeling using the finite element method, which allows to directly describe the interaction between the cutting tool and the processed material. Due to the complexity of the geometry of the process zone and the kinematics of the chip formation process, it is necessary to use models that take into account the three-dimensional nature of the cutting force, the stress-strain state and also the temperature field to study even the traditional cutting process [135]. Often, computational schemes assume that chip separation occurs along some predetermined surfaces, which can significantly limit the volume of material to be described. Therefore, a number of computational schemes have used a different mechanism for the formation of a new surface [136], which is related to the formation of new features due to large deformations resulting from the penetration of the tool into the material being machined. Among other things, finite element analysis can take into account the interaction of thermal and mechanical processes in the cutting zone [137].

There are several hypotheses that qualitatively explain the intensification of the fracture process in the presence of additional ultrasonic vibrations, the most important of which can be attributed to a change in the effective deformation properties of the material or a decrease in the friction between the tool and the processed material. However, the previously obtained evaluation of the threshold energy input for the fracture of the elastic material by the solid particle impact gives a fundamentally different explanation of the effectiveness of the ultrasonic

assisted processing of materials. It can be assumed that the addition of ultrasonic vibrations transforms the material processing into a shock-pulse mode [138], which, as it was shown earlier, reduces the energy consumption of the fracture process.

Ultrasonically assisted turning of Inconel 718

The analysis of the energy consumption of the ultrasonic assisted machining can be demonstrated using at the difficult-to-machine alloy Inconel 718. The choice of this material is stipulated by the fact that for it experimental dependencies of cutting forces on the material rate for various values of frequency and amplitude of applied vibrations are known. In addition, there are a number of finite element studies that examine the behavior of this material during chip formation and the stress-strain state in the cutting zone. For example, in a two-dimensional FEM model of orthogonal ultrasonic turning, a cycle of ultrasonic vibrations is numerically analyzed in detail for [139]. In subsequent works by these authors (e.g., [140, 141]), this model is generalized to the three-dimensional case for a comparative description of conventional and ultrasonic-assisted cutting processes. Based on the modeling results, a significant reduction of the force acting on the cutting tool was demonstrated, and the influence of the amplitude of ultrasonic vibrations on the level of this force was also studied. In these works, it was shown that the numerical results of the modeling agree well with the experimental measurements carried out by the same authors on a special installation for ultrasonic-assisted turning of metals.

Therefore, the main feature of ultrasonic-assisted turning that needs to be explained is the reduction of the cutting force. It should also be noted that this effect decreases with the feed rate and finally disappears when a certain critical

speed is reached. Experimental studies show that at a critical feed rate, the tool simply does not have time to break away from the material due to oscillations, so the impact component of the process disappears [132]. This suggests that it is most likely the impact method of striking the material that leads to a decrease in cutting force.

To explain the effect of force reduction in vibration-assisted machining, it is necessary to recall the results presented in section 3.1. As was shown in the case of impact-type contact interaction, the minimum impact energy at which a threshold fracture impulse occurs in an elastic medium depends significantly on its duration. Consequently, it can be assumed that the application of ultrasound simply transfers the fracture of the processed material to a more energy-efficient mode. It is also reasonable to assume that the force applied to the tool is composed of a dynamic component responsible for the destruction of the material in the impact mode and a constant component F_0 associated with the kinematics of the cutting process. The value of this constant force can be measured experimentally and the value of the dynamic component can be estimated by assuming that the energy W^* that must be supplied to the material to generate the threshold fracture pulse is equal to its work at a displacement equal to the amplitude of the imposed oscillations A_{us}. We can then obtain the following expression for the total force F acting on the tool:

$$F = \frac{W^*}{A_{us}} + F_0. \qquad (3.66)$$

As it was mentioned earlier, increasing the feed rate leads to a growth of the contact time between the tool and the material, and thus the duration of the loading action. Therefore, when the critical level r_c is reached, the loading duration approaches a certain threshold value t_0^c, above which the material reacts to the load as if it were static. Therefore, at feed rates exceeding r_c, the value of the cutting

force will be the same as in conventional cutting. Thus, the following formula can be proposed to calculate the loading time as a function of the feed rate r_c:

$$t_0 = \frac{1}{f} + \frac{r}{r_c}\left(t_0^c - \frac{1}{2f}\right), \tag{3.67}$$

where f is the frequency of the imposed oscillations.

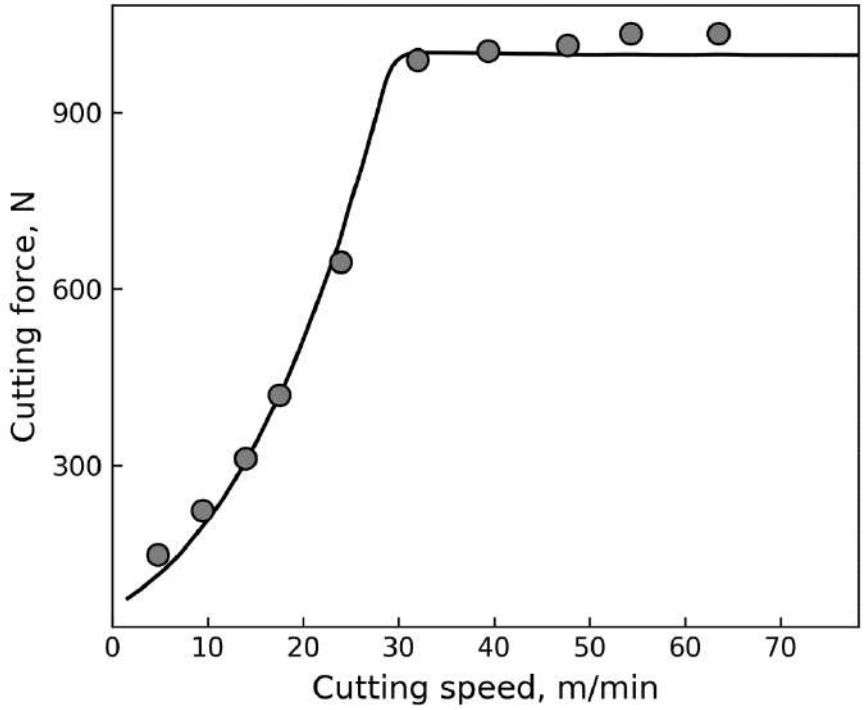

Figure 3.7 Cutting force versus cutting rate for Inconel 718 alloy: $f = 20\,kHz$, $A_{us} = 25\ \mu m$.

Figure 3.7 shows a comparison of the calculated dependence of cutting force on tool feed rate for Inconel 718 alloy with experimentally measured values. The following values of the problem parameters were used in the calculation: $E = 205\,GPa, \nu = 0.284, \sigma_c = 700\,MPa$ and $\tau = 8$ μs. The choice of such a value of the incubation time is due to the following reasons. Previously in [142] it was shown that the minimum energy required to produce a shock fracture is obtained at a pulse duration two to three times higher than τ. Since the oscillation frequency in

the experiment was equal to $20\,kHz$, the minimum duration of the impact is approximately half the oscillation period $\frac{1}{2f} = 25\,\mu s$.

Assuming that the lowest power consumption corresponds to pulses with a duration close to the minimum, it turns out that the value of the incubation time should be taken equal to one third of this value. Thus, for the selected parameters, a good quantitative agreement was obtained between the calculations and the test results.

It should be noted that all calculations of the threshold energy in expression (3.66) are performed for the case of impact by the spherical particle. It is determined by the results given in Section 3.2, where it was shown that for smooth contact surfaces the dependence of the threshold energy on the impact duration is not qualitatively different from the case with a spherical surface.

Ultrasonically assisted turning of aluminum

Another material where the main effect of UA machining is also remarcable is aluminum. Despite its relatively low strength, aluminum, as well as the alloy Inconel 718, becomes very “ductile” during conventional turning. As a result, it requires relatively high machining forces, while the quality of the machined surface suffers greatly. The use of additional vibration avoids these disadvantages.

Figure 3.8 shows the dependence of the cutting force on the vibration amplitude calculated by formula (3.20) in comparison with the experimental data [132]. A good quantitative agreement was obtained for the following values of the problem parameters: $E = 70\,MPa$, $\nu = 0.33$, $\sigma_c = 100\,MPa$ and $\tau = 12\,\mu s$, $F_0 = 10\,N$.

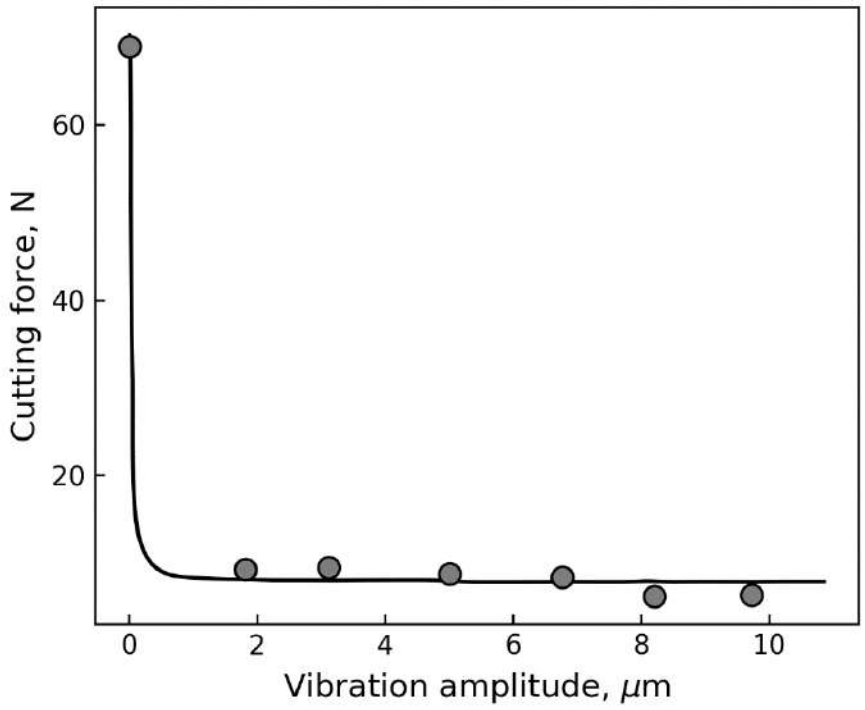

Figure 3.8 Effect of ultrasonic vibration amplitude on the magnitude of cutting force for aluminum alloy: $f = 20\ kHz$.

It should be noted that, according to expression (3.20), the absolute value of the threshold energy W^* depends not only on the parameters of the fractured material, but also on the density of the impacting particle ρ. Thus, in the particle impact problem, this parameter sets a general level of impact intensity. Therefore, its value can be related to such a process parameter as the cutting depth. In fact, the greater the cutting depth, the greater the force that must be applied to the tool. In the calculations shown in Figure 3.8, the value of ρ was chosen assuming that the depth of cut is $0.05\ mm$.

Figure 3.9 shows the dependence of cutting force on machining rate for aluminum [132]. for different values of cutting depth. All the calculated curves are in good agreement with the real test data. It should be noted that the calculations for all values of the cutting depth were performed with the same constant values of the parameter set as for the amplitude dependence, except for the static component

of the total force $F_0 = 3\ N$, as well as the parameter ρ. The value of the latter was chosen for each depth to obtain the best agreement with the experimental data.

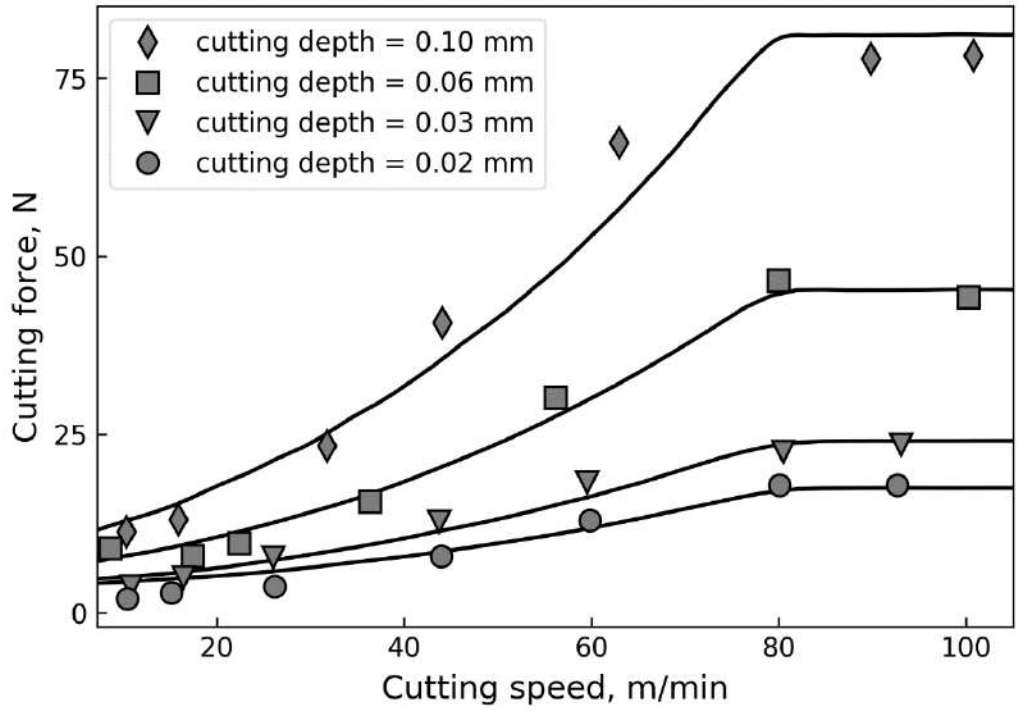

Figure 3.9 Dependence of cutting force versus machining rate for aluminum for different values of cutting depth: $f = 20\ kHz$, $A_{us} = 10\ \mu m$, $F_0 = 3\ N$. The calculated curves are obtained for values $\tau = 12\ \mu s$, $\sigma_c = 100\ MPa$, experimental data from [132].

Thus, based on the results obtained in the study of the energy consumption for the fracture process under pulse loading, it has been possible to construct a fairly simple model of ultrasonically assisted machining process, which allows us to describe quantitatively the dependence of the cutting force on the material feed rate. The assumption that additional vibrations shift the fracture process to a more energetically optimal mode is also indirectly confirmed by the improvement in the quality of the machined surface. Excessive energy delivered to the fracture zone at high impact durations, characteristic of the traditional method, is dissipated in

excessive heating of the workpiece and undesirable destruction, which ultimately results in excessive roughness of the resulting surface.

Apart from the ultrasonically assisted turning, a similar model has been developed for modeling rock fracture in underwater mineral extraction [143]. It should be noted that a similar optimization of fracture energy consumption occurs in problems related to the determination of adhesive bond strength. Using similar computational methods, it has been found that the additional vibrations can significantly reduce the bond strength [144, 145, 146, 147].

3.4 Conclusions to Chapter 3

The study of the energy inputs necessary for the initiation of the dynamic threshold fracture pulses, initiated by the impact of a solid body with an elastic medium, has been carried out.

The analytical model constructed within the framework of the incubation time criterion allowed to reveal the existence of energy-optimal modes of impact loading.

The dependence of the threshold value of the energy input into the medium on the duration of the fracture pulse was studied for different shapes of a rigid impactor.

It has been shown that the different type of dependence obtained for spherical and cylindrical impactors is obtained only in the framework of quasi-static analysis using the Hertz hypothesis on the magnitude of the contact force.

The constructed model of the threshold energy estimation, in which the supersonic phase is taken into account, has shown that for real bodies the dependence of the threshold energy is similar to the case of the spherical impactor.

Based on the performed energy consumption analysis, the analytical model of ultrasonically assisted machining has been constructed. The dependence of the cutting force on the machining rate, which qualitatively and quantitatively agrees with the results of experimental studies, has been obtained.

Chapter 4 Competition of microstructural mechanisms of inelastic deformation of continuous media

In this chapter the proposed method of determining the values of strength parameters using the SPS method is generalized for the two-dimensional case, in which the values of not only the incubation time but also the critical stress are estimated. This modification of the method enabled us to address a new issue pertaining to the identification of the strain rate sensitivity of the fracture mode, given that the material fracture mechanisms differ under slow and high strain rate loading.

The results presented in Chapter 4 were published in the following works: [88, 98].

4.1 Estimation of material strength parameters from dynamic test data

As demonstrated in preceding chapters, the critical stress σ_c and incubation time τ are parameters of paramount importance within the structure-time approach. As previously demonstrated, the strain rate dependences of strength indicate that the critical stress level under slow loading is solely determined by the value of σ_c, whereas the influence of the parameter τ is evident under high-speed loading. It is important to note, however, that under impact loading, the critical stress level also depends on the parameter σ_c. This indicates that the experimentally determined ultimate stress level under high-speed loading provides information not only about the incubation time τ, but also about the critical stress σ_c. It can thus be concluded that when processing data from only dynamic tests of a given material, it is theoretically possible to estimate not only τ, but also σ_c.

Two-dimensional case: estimation of the incubation time and critical stress

In order to estimate the critical stress parameter from data obtained exclusively from impact tests, it is again proposed to use the sign-perturbed sum method. As demonstrated in Chapter 1, the SPS method enables the estimation of the value of incubation time τ in the form of a confidence interval that encompasses the true value of the parameter with a pre-specified probability level. It is assumed that the value of the critical stress, σ_c, is a known quantity that has been measured independently under slow loading of the material. In other words, the problem has been considered to be one-dimensional, with the parameter sought being a scalar quantity. In this section, we investigate the two-dimensional case in which the sought parameter $\vartheta = (\tau, \sigma_c)$ contains two components. In this case, the true value of the desired parameter $\vartheta_* = (\tau_*, \sigma_{c_*})$ will be estimated as a confidence region T on the plane (τ, σ_c).

As previously stated, it is assumed that the dynamic tensile strength test results, which are to be evaluated in terms of their strength characteristics, are a set of N values of dynamic tensile strength measured for different values of strain rate:

$$\sigma_{*i} = \sigma_{*i}(\dot{\varepsilon}_i), \qquad i = 1 \dots N.$$

For convenience, the measured values of dynamic strength σ_{*i} are represented as the results of the following observation model:

$$\sigma_{*i} = \varphi\left(\tau_*, \sigma_{c_*}, \dot{\varepsilon}_i\right) + v_i, \qquad i = 1 \dots N, \tag{4.1}$$

where the true values of the incubation time and critical stress parameters, designated as τ_* and σ_{c_*}, are to be determined. Furthermore, it is assumed that the disturbances, designated as v_i, are random variables with an unknown symmetric distribution. As previously stated, the model function $\varphi(\tau, \sigma_c, \dot{\varepsilon})$ describing the

strain rate dependence of the ultimate stress level at the moment of fracture is determined by formula (1.7):

$$\sigma_*(\dot{\varepsilon}) = \varphi(\tau, \sigma_c, \dot{\varepsilon}) = \begin{cases} \sigma_c + \dfrac{E\dot{\varepsilon}\tau}{2}, & \dot{\varepsilon} \le \dfrac{2\sigma_c}{E\tau}, \\ \sqrt{2\sigma_c \tau E \dot{\varepsilon}}, & \dot{\varepsilon} > \dfrac{2\sigma_c}{E\tau}. \end{cases}$$

In the two-dimensional case, the formal steps of the sign-perturbed sum method, with a few exceptions, are largely consistent with those described above for the one-dimensional case:

1) select the values of natural parameters $M > q > 0$, so as to obtain the desired level of reliability of the result:
$$\mathrm{p} = 1 - \frac{\mathrm{q}}{\mathrm{M}}$$
2) Generate $N(M-1)$ random numbers β_{ij} taking values ± 1 with probability $\frac{1}{2}$.
3) Define a discrete set of trial values of the desired parameter:
$$\{(\tau_k, \sigma_{c_l})\}, \qquad (\tau_k, \sigma_{c_l}) \in \mathbb{R}^2, \;\; k = 1 \dots K, l = 1 \dots L$$
4) For each σ_{c_l} construct the corresponding confidence interval T_l by testing each value of τ_k using the $SPS\_Indicator(\tau_k)$, which determines whether or not the trial value τ_k falls within the confidence interval T_l (see Table 1.1 in Section 1.2)
5) Construct the confidence region T as the union of confidence intervals: $\mathrm{T} = \bigcup_l \mathrm{T}_l$

It should be noted that the aforementioned algorithm does not constitute a comprehensive analogy of the two-dimensional case described by the authors of the SPS method in the original paper for a linear model function. This is due to the presence of a normalizing multiplier, the calculation of which for a nonlinear

function in the non-dimensional case requires additional computational resources. In the one-dimensional case, the aforementioned multiplier is simply equal to the partial derivative of $\frac{d\varphi(\tau,\dot{\varepsilon}_i)}{d\tau}$.

In Section 0, it was proved that the function $\varphi(\tau,\sigma_c,\dot{\varepsilon})$ possesses all the necessary properties for the appropriate application of the sign-perturbed sum method, thereby yielding a bounded interval estimate for the incubation time. The proof is based on the existence of a positive derivative of the function $\varphi_{\tau,\sigma_c}(\dot{\varepsilon})$ with respect to the parameter τ: $\frac{d\varphi(\tau,\sigma_c,\dot{\varepsilon})}{d\tau} > 0$. It is evident that the partial derivative of the parameter σ_c is also a positive quantity $\frac{d\varphi(\tau,\sigma_c,\dot{\varepsilon})}{d\sigma_c} > 0$. Consequently, for a constant loading rate $\dot{\varepsilon} = const > 0$, furthermore, for a constant value of incubation time $\tau = const > 0$, it can be demonstrated that $\varphi(\tau,\sigma_{c_1},\dot{\varepsilon}) > \varphi(\tau,\sigma_{c_2},\dot{\varepsilon})$, provided that $\sigma_{c_1} > \sigma_{c_2}$. Consequently, employing analogous reasoning, it can be demonstrated that the resulting confidence region derived from the SPS method will be bounded.

Furthermore, the boundedness of the confidence region will be a consequence of the intrinsic constraints associated with the mechanical interpretation of the critical stress σ_c. In accordance with the incubation time criterion, the parameter σ_c accounts for the ultimate stress level under slow loading. Consequently, the trial values σ_{c_l} should not be selected that exceed the experimentally determined values of the dynamic strength of the material σ_{*i}.

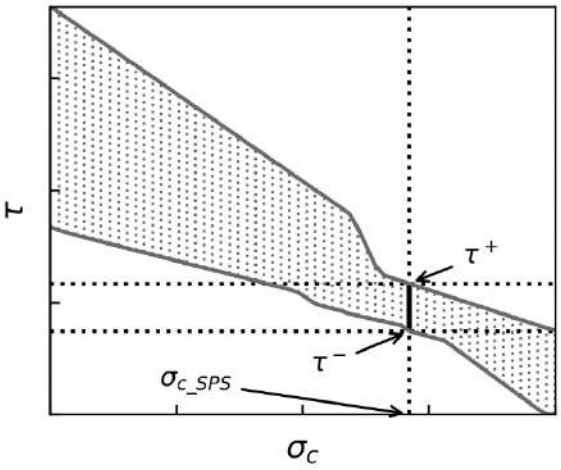

Figure 4.1 Typical view of the confidence region. The thick line indicates the smallest section of the confidence region, which corresponds to the optimum value of the critical stress σ_{c_SPS}

Figure 4.1 illustrates the typical confidence region resulting from the proposed method. As the trial values of σ_{c_l} increase, the magnitude of the corresponding incubation time value decreases on average. This observation precludes the possibility of concluding that there is a unique critical stress value. However, if we look at the estimated scatter of the incubation time values, or in other words the width of the corresponding confidence interval T_l, we can see that its dependence on $\sigma_{c_l}$is not monotonic.

Indeed, in the majority of cases where the experimental points obtained in dynamic tests establish a distinctive trend for the strain rate dependence of the material strength, there is a value $\sigma_{c_l} = \sigma_{c\_SPS}$ at which the width of the confidence interval T_l is at its narrowest. In Figure 4.1, this interval is indicated by a thick black line. The following section will demonstrate that the model curves corresponding to the boundaries of the τ_l^- and τ_l^+ interval, for this value of σ_{c_l}, provide the most accurate description of the experimentally observed rate

dependence of the strength. Therefore, this value of σ_{c_l} can be considered the optimal critical stress value for the tested material:

$$\sigma_{c\_SPS} = \sigma_{c_l}:\ |\mathrm{T}_l| = [\tau_l^+ - \tau_l^-] \to \min_l\ . \tag{4.2}$$

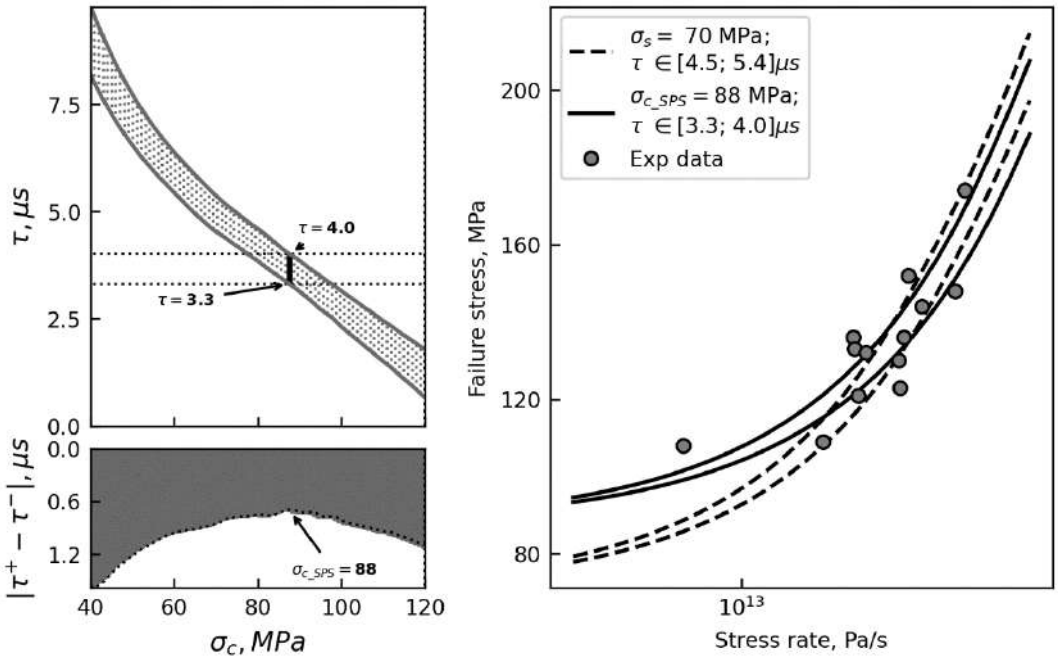

Figure 4.2 Results of processing data from dynamic compression tests on sandstone [9]. Top left: confidence region T on the (τ, σ_c) plane, bottom left: diagram showing the value of $|\mathrm{T}_l|$ for different values of σ_{c_l}. Right: comparison of calculated rate dependences of strength with experimental data, solid line is plotted for $\sigma_c = \sigma_{c\_SPS}$, dashed line – for $\sigma_c = \sigma_s$ measured under low strain rate loading.

Figure 4.2 depicts the outcomes of the analysis conducted on the experimental data obtained from dynamic compression tests of sandstone [9]. The upper left plot, which depicts the general view of the confidence region T on the (τ, σ_c) plane, is complemented from below by a diagram that illustrates the width$|\mathrm{T}_l|$ of the confidence region as a function of the trial value σ_{c_l}. The arrows indicate the optimal value of the critical stress, $\sigma_{c\_SPS} = 88\ MPa$, and the limits of

the corresponding confidence interval for the incubation time, $\tau \in [3.3; 4.0]\ \mu s$. Note that the ultimate stress level for this material, as measured under slow loading, is $\sigma_s = 70\ MPa$. If we assume that the critical stress parameter σ_c is equal to the ultimate stress parameter σ_s, then the confidence interval is obtained as $\tau \in [4.5; 5.4]\ \mu s$. The graph on the right illustrates a comparison of the strain rate dependence of strength, calculated for different critical stress values. The dashed line is for the critical stress value $\sigma_c = \sigma_s$, while the solid line – $\sigma_c = \sigma_{c\_SPS}$.

Note that on the logarithmic scale, which displays a wide range of loading rates from 10^7 to $10^{13}\ Pa/s$ for both cases, there is a notable concordance between the calculated dependences and the experimentally measured values. Nevertheless, in order to discern the distinction, it is essential to reorganize these dependences on a linear scale within a more restricted range of loading rates, which were realized in the experiment (see Figure 4.3).

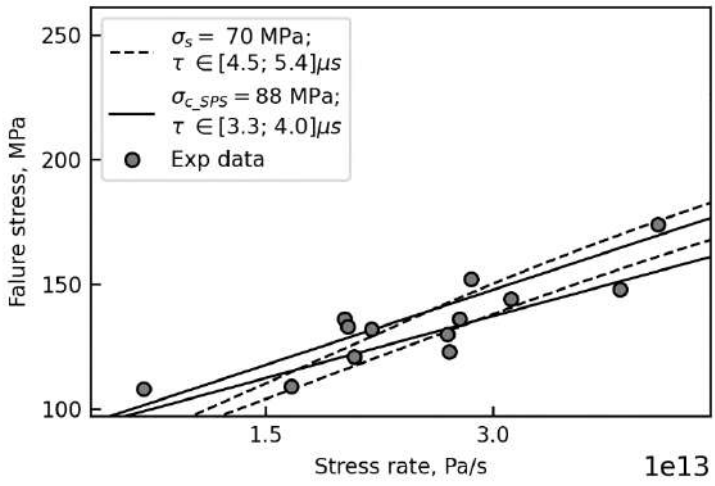

Figure 4.3 Comparison of calculated loading rate dependences of strength for sandstone with experimental data [9]; solid line is plotted for the parameters $\sigma_c = \sigma_{c\_SPS} = 88MPa$, $\tau \in [3.3; 4.0]\ \mu s$, dashed line – for $\sigma_c = \sigma_s = 70MPa$, $\tau \in [4.5; 5.4]\ \mu s$

It can be observed that the model curves (solid lines) calculated for the value $\sigma_c = \sigma_{c\_SPS}$, exhibit a greater degree of alignment with the trend indicated by the experimental points than those calculated for the value $\sigma_c = \sigma_s$. In this instance, the discrepancy is relatively insignificant, given that the width of the confidence interval for the incubation time remains largely unchanged for critical stress values between 70 and 100 MPa (see left bottom plot of Figure 4.2).

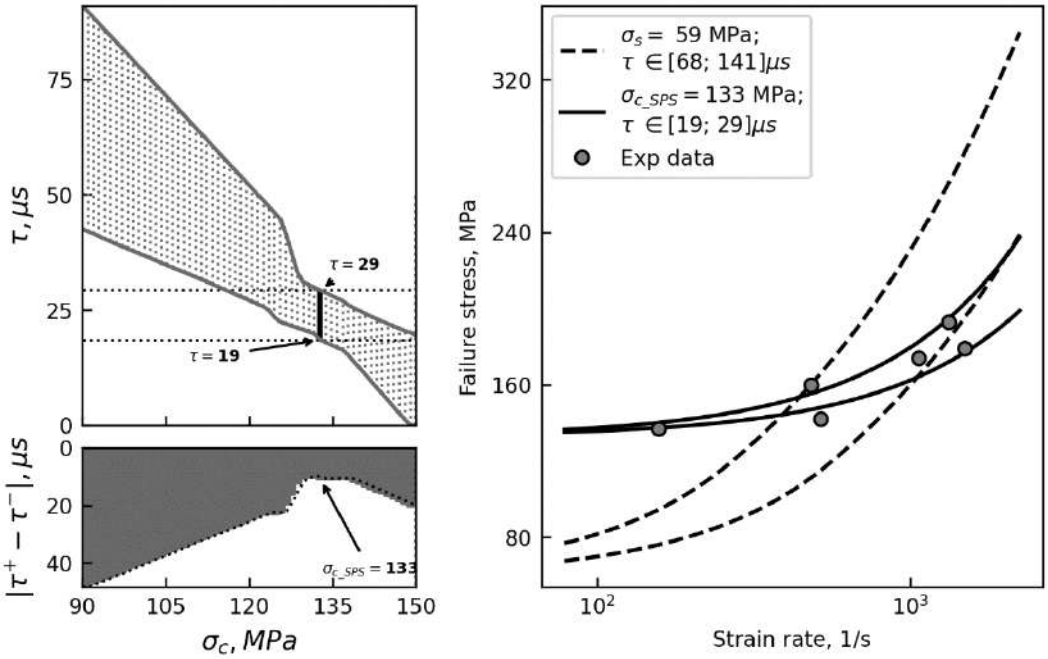

Figure 4.4 Comparison of calculated strain rate dependences of compressive impact strength for meteorite stone MAC88118 with experimental data [5], solid line plotted for parameters $\sigma_c = \sigma_{c\_SPS} = 133\ MPa$, $\tau \in [19; 29]\ \mu s$, dashed line for value $\sigma_c = \sigma_s = 59\ MPa$, $\tau \in [68; 141]\ \mu s$

In certain instances, the distinction is more pronounced when examining alternative materials. To illustrate, the impact compression test data of meteorite stone MAC88118 from [5] may be considered. As illustrated in Figure 4.4, the plotted confidence region exhibits a distinctive narrowing, suggesting the existence of a superior critical stress value that surpasses the experimentally determined

value under slow loading. Moreover, even when plotted on a logarithmic scale, the model curves constructed for the optimal value of $\sigma_c = \sigma_{c\_SPS}$ demonstrate a superior fit to the experimental data.

To emphasize the better agreement of the predicted values of dynamic strength at $\sigma_c = \sigma_{c\_SPS}$ relative to those at $\sigma_c = \sigma_s$, the calculated strain rate dependences are plotted in Figure 4.5 on a linear scale. It is evident that the model curves (solid lines), derived from the analysis of the dynamic test data, align precisely with the trend indicated by the experimental points. It is obvious that the model curves (dashed lines), calculated at values $\sigma_c = \sigma_s$, establish a relatively expansive range of dynamic strength values for the material, offering a markedly approximate estimation of the ultimate stress level.

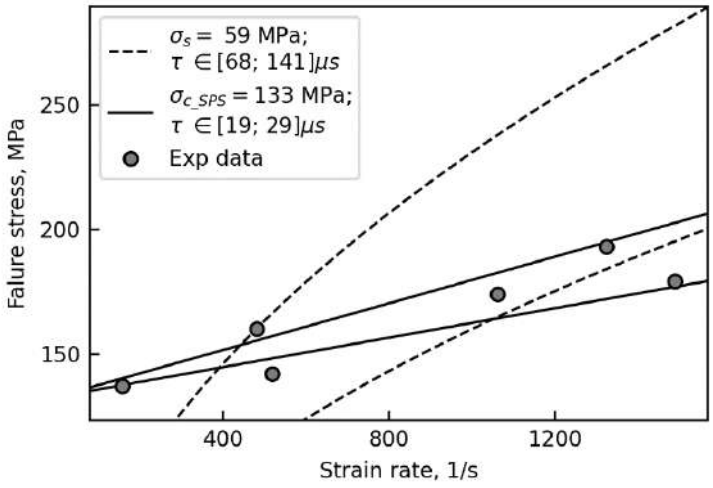

Figure 4.5 Comparison of calculated strain rate dependences of compressive impact strength for meteorite stone MAC88118 with experimental data [5]; solid line is plotted for $\sigma_c = \sigma_{c\_SPS} = 133\ MPa, \tau \in [19; 29]\ \mu s$, dashed line – for $\sigma_c = \sigma_s = 59\ MPa, \tau \in [68; 141]\ \mu s$

Reliability check of the method of estimating the parameter σ_c

To ascertain whether the values of the incubation time and critical stress parameters obtained by the proposed method can more accurately predict the ultimate stress level under high-speed loading, a verification test can be conducted to assess the robustness of the obtained results:

1) split the experimental data:

$$\sigma_{*i} = \sigma_{*i}(\dot{\varepsilon}_i), \qquad i = 1 \dots N$$

Into two sets:

$$\sigma_{*i} = \sigma_{*i}(\dot{\varepsilon}_i), \qquad i = 1 \dots N_1$$

and

$$\sigma_{*i} = \sigma_{*i}(\dot{\varepsilon}_i), \qquad i = N_1 + 1 \dots N.$$

2) For the first data set, estimate the optimal values of the parameters $\sigma_{c\_SPS}^{(1)}$ and $\tau \in \mathrm{T}_{SPS}^{(1)}$ according to the proposed algorithm based on the SPS method for the two-dimensional case.
3) For the first data set, estimate the incubation time $\tau \in \mathrm{T}_1$ using the SPS method described in Section 0, with $\sigma_c = \sigma_s$.
4) Construct curves of strain rate dependence of strength for the obtained values of model parameters:

$$\sigma_c = \sigma_s,\ \tau \in \mathrm{T}_1 \text{ и } \sigma_c = \sigma_{c\_SPS}^{(1)},\ \tau \in \mathrm{T}_{SPS}^{(1)}.$$

5) Compare the obtained model curves with the experimental data from the second set of data.

Repeat steps (2)-(5) for the second data set, to then compare the model curves with the experimental data from the first set.

The results of the algorithm robustness verification for the previously discussed MAC88118 meteorite stone are presented in Figure 4.6. As can be observed in Figure 4.6(a), the strength prediction results for $\sigma_c = \sigma_{c\_SPS}$ exhibit a slight decrease in absolute value when compared to the stress level corresponding to the verification set of experimental points, in comparison to the results for $\sigma_c = \sigma_s$.

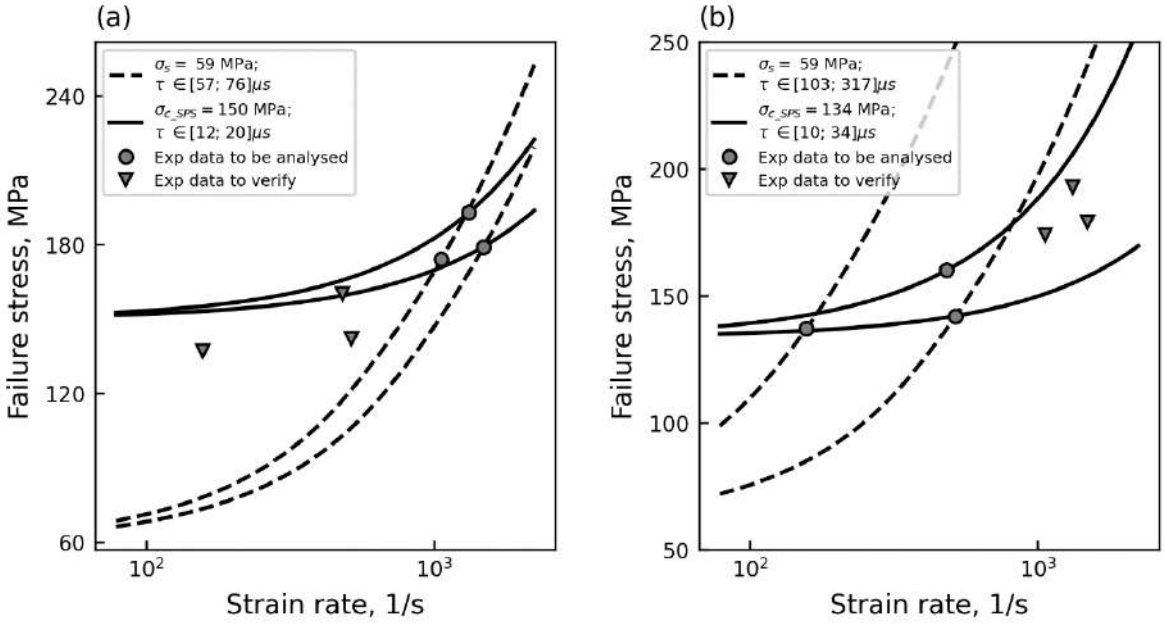

Figure 4.6 The results of testing the stability of the proposed method, on the example of data processing for meteorite stone MAC88118. The circles indicate the experimental data for which the model parameters were estimated. The data used for comparison with the model curves are indicated by triangles.

Figure 4.6.(b) illustrates this peculiarity with greater clarity, as all points in the test set are situated entirely within the predicted interval for $\sigma_c = \sigma_{c\_SPS}$, whereas for $\sigma_c = \sigma_s$ the predicted ultimate stress level is considerably higher than the experimental values. It is also noteworthy that the parameters were estimated using only three experimental points.

The results of the obtained parameter values are also summarized in Table 4.1.

Table 4.1 Results of incubation time estimation for meteorite MAC88118 by SPS method. The confidence level is 90%.

Observation dataset for processing	$\{\boldsymbol{\sigma}_{*i}, \dot{\boldsymbol{\varepsilon}}_{\boldsymbol{i}}\}_{\boldsymbol{i=1}}^{\boldsymbol{N_1}}$	$\{\boldsymbol{\sigma}_{*i}, \dot{\boldsymbol{\varepsilon}}_{\boldsymbol{i}}\}_{\boldsymbol{i=N_1+1}}^{\boldsymbol{N}}$	$\{\boldsymbol{\sigma}_{*i}, \dot{\boldsymbol{\varepsilon}}_{\boldsymbol{i}}\}_{\boldsymbol{i=1}}^{\boldsymbol{N}}$
$\sigma_c = \sigma_s, MPa$	59	59	59
$T, \mu s$	$[57; 76]$	$[103; 317]$	$[68; 141]$
$\sigma_c = \sigma_{c\_SPS}, MPa$	150	134	133
$T_{SPS}, \mu s$	$[12; 20]$	$[10; 34]$	$[19; 29]$

Note that when $\sigma_c = \sigma_s$, a considerably wide range of values is observed for the incubation time. Furthermore, the confidence intervals obtained from processing the initial and subsequent experimental data sets, namely $T_1 = [57; 76]\mu s$ and $T_2 = [103; 317]\ \mu s$, do not even overlap. Concurrently, the limits of the interval $T = [68; 141]\ \mu s$ yielded upon processing the comprehensive data set are approximately equivalent to the mean values of the limits of the intervals T_1 and T_2. It can thus be concluded that, under the assumption that the value of the critical stress is determined by the static strength of the material, $\sigma_c = \sigma_s$, the model curves are guaranteed to predict only a certain average level of ultimate stresses within the range of loading rates that were realized in the experiment. In certain instances, a satisfactory degree of quantitative agreement can be attained, as previously demonstrated in the case of sandstone (see Figure 4.3).

In instances where the critical stress is derived exclusively from the outcomes of dynamic tests, σ_c is equivalent to σ_{c_SPS}. This approach results in a significantly reduced scatter of incubation time values and overlapping confidence intervals for the two SPS trials, namely $T_{SPS}^{(1)} = [12; 20]\ \mu s$ and $T_{SPS}^{(2)} = [10; 34]\ \mu s$. Additionally, the identified values of critical stress, $\sigma_{c\_SPS}^{(1)} =$

$150\,MPa$ and $\sigma_{c\_SPS}^{(2)} = 134\,MPa$, are also relatively similar. Furthermore, the parameter estimates derived from the complete data set were found to be nearly identical to those obtained from the second set: $\sigma_{c\_SPS} \approx \sigma_{c\_SPS}^{(2)}$ and $\mathrm{T}_{SPS} \subset \mathrm{T}_{SPS}^{(2)}$. This indicates that the proposed modification of the SPS method is more resilient to the selection of data for processing and enables not only qualitative but also quantitative modelling of the curve of strain rate dependence of strength under dynamic loading.

Thus, it appears that, on the one hand, according to the incubation time criterion, the critical stress parameter σ_{c} should correspond to the limit stress level at slow loading σ_s. On the other hand, it should also quantitatively match the modeled and experimental strain rate dependence of strength. In some cases, however, another value $\sigma_{\mathrm{c}} = \sigma_{c\_SPS}$ should be chosen. This gives rise to a pertinent query regarding the interpretation of this second value of the critical stress, which will be addressed in the subsequent section of this chapter.

4.2 Strain rate sensitivity of concrete fracture mode

The modified method of processing dynamic test data discussed in the previous section revealed an alternative way of determining the critical stress parameter, the value of which, σ_{c_SPS}, can differ significantly from the strength of the material under static loading, σ_s. The processing of dynamic test data for different materials has demonstrated that, in certain instances, these values exhibit minimal to no discernible difference from one another, or they are essentially identical. In other instances, the values of these parameters may vary by a factor of ten or more. One of the most plausible explanations for the existence of two different potential values of critical stress is the hypothesis that the process of

material failure occurs differently under rapid and slow loading. This discrepancy may be attributed to the internal structure of the material, as well as the disparate stress states that arise within the material under static and dynamic loading.

To ascertain whether the loading rate affects the fracture mode of the material, the dynamic test data of different types of concrete were subjected to processing. The selection of these materials was based on the following considerations. On the one hand, experimental studies of concretes in the dynamic range demonstrate that for the majority of grades, there is a notable correlation between strength and loading rate. This allows for the estimation of critical stress and incubation time parameters. Conversely, a discrepancy between σ_{c_SPS} and the strength of the material under static loading σ_s is observed for these materials. Concurrently, numerous researchers have observed a transformation in the character of concrete fracture as the loading rate increases. In static slow loading, cracks tend to propagate preferentially through the cement matrix, bypassing the more rigid granite inclusions. This phenomenon has been observed in several studies, including those referenced below [150] [151] [152]. At fast loading, the probability of cracks traversing granite inclusions is larger, which is typically manifested in a notable surge in the quantity of fractured filler particles [153] [154] [155]. The results of numerical modeling corroborate this observation. As demonstrated by various authors in works [156], [157], [158] and [159], an increase in the loading rate results in a corresponding rise in the number of broken bonds within the rigid phase. It is noteworthy that the alteration in the character of fracture with rising impact velocity can be discerned not only in two-component materials such as concrete, but also in metallic polycrystals [160].

Therefore, it can be proposed that the type of concrete fracture observed under slow impact can be classified as intracrystalline, whereby cracks propagate through the cement base or along the bond zone of the granite and cement phases.

Conversely, under high-speed impact, the fracture can be classified as transcrystalline, which is characterized by the passage of cracks through the material of the rigid filler. It can be seen that, despite the fact that under both slow and fast loading the same material, concrete, formally fails, from a fundamental scientific perspective it can be considered that two different materials fail in statics and dynamics. Therefore, the critical stress value for transcrystalline concrete fracture, which is characteristic of high-speed loading, should not necessarily align with the static strength value corresponding to the ultimate stress level at intracrystalline fracture.

The two-dimensional modification of the SPS method proposed in Section 4.1 merely estimates the critical stress from the high-speed test data. Consequently, the resulting value σ_{c_SPS} will correspond to the "static strength" for the predominant type of fracture under impact loading. Concurrently, the value σ_s represents the static strength for the slow loading mode, as it correlates with the critical stress level that has been empirically determined under slow loading conditions.

It has been demonstrated that in the case of concretes, it is conventionally assumed that σ_{c_SPS} and σ_s are responsible for the ultimate stress level under static loading for transcrystalline and intercrystalline fracture modes, respectively. Given that the stress level in the material is the determining factor in slow loading, it can be expected that the value of σ_s should not exceed σ_{c_SPS}. It can thus be assumed that if the values of σ_s and σ_{c_SPS} differ markedly from one another, it can be assumed that the material under consideration exhibits fracture mode sensitivity to strain rate.

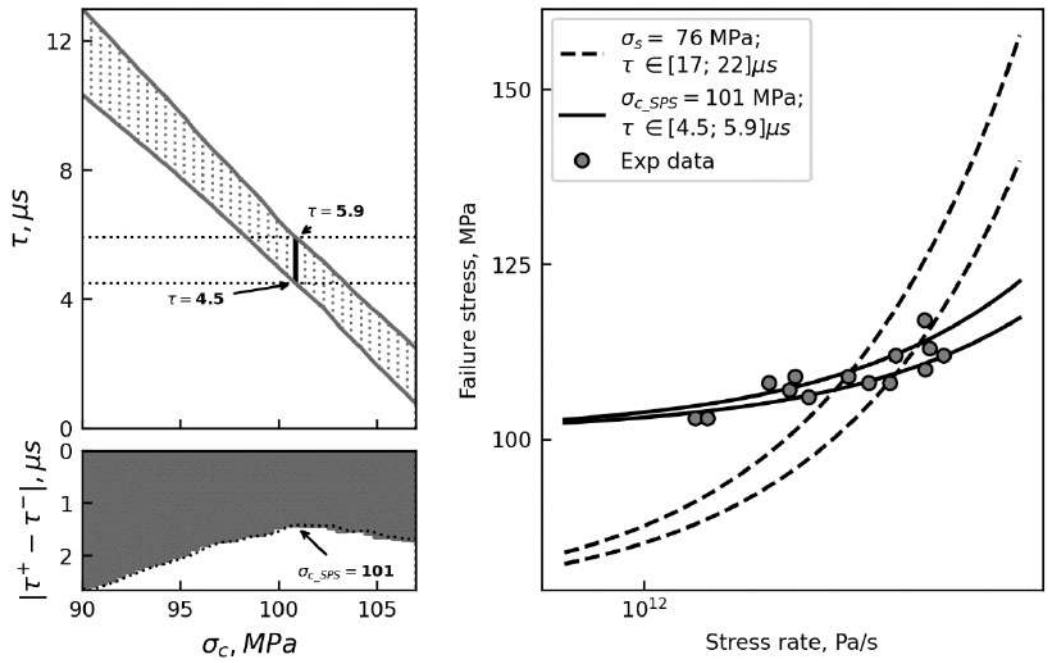

Figure 4.7 Results of the dynamic test data processing of C60 concrete [161]. The left-hand side: confidence region T on the (τ, σ_c) plane. The right-hand side graph: comparison of calculated rate dependences of strength with experimental data, solid line is plotted for $\sigma_c = \sigma_{c\_SPS} = 101\ MPa$, $\tau \in [4.5; 5.9]$ μs; dashed line – for $\sigma_c = \sigma_s = 76\ MPa$ (measured under slow loading), $\tau \in [17; 22]$ μs.

To substantiate the aforementioned assumption, the test data were subjected to processing for a range of concrete grades, besides mortar and granite, which represent the constituent elements of the tested concrete specimens [161, 162,163,164].

Figure 4.7 illustrates the outcomes of processing the dynamic test data of C60 concrete as presented by Guo et al. The resulting value $\sigma_{c\_SPS} = 101\ MPa$ markedly surpassed the ultimate stress level documented in static $\sigma_s = 77\ MPa$. To ensure the accuracy of the derived estimates, a sequential processing of incomplete sets of test data with subsequent comparative analysis was conducted.

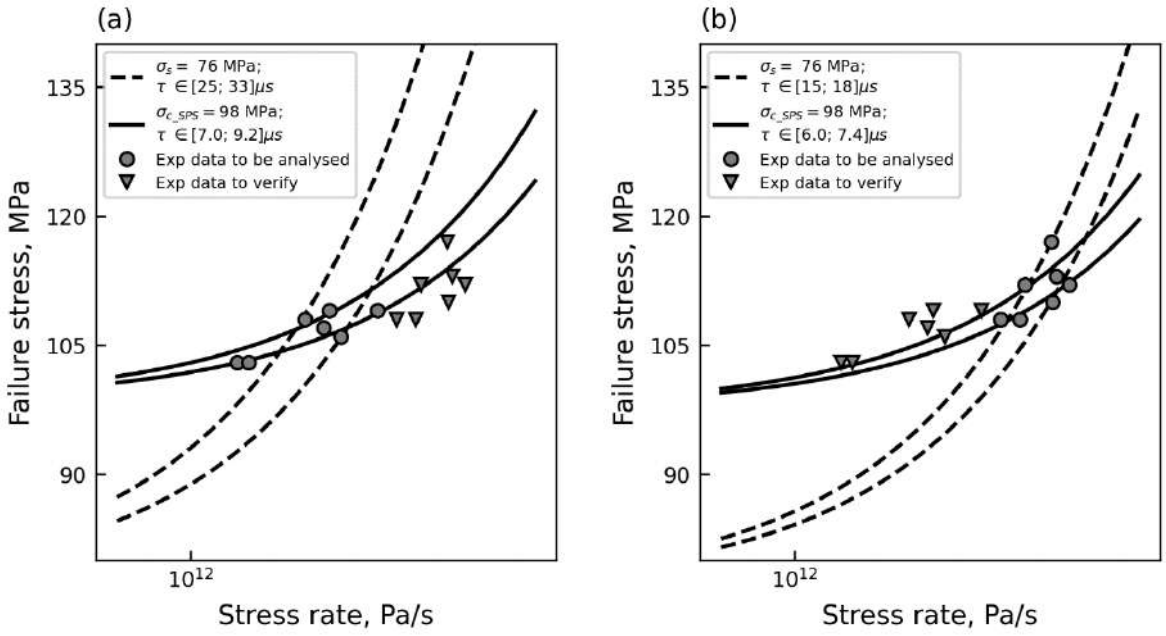

Figure 4.8 Stability test of the method for estimating the parameters τ and σ_c for C60 concrete: (a) – the values were estimated from the first half of the data; (b) – from the second half of the data.

The stability verification of the obtained results demonstrated that even when processing an incomplete volume of experimental points, the value of critical stress σ_{c_SPS}, at which there is the best quantitative agreement with the test data, exceeded the value of static strength σ_s. Furthermore, the investigation revealed a clear trend in the strain rate dependence of the ultimate stress level, which was observed in the test data set. This trend allowed for the estimation of strength parameters for the first and second sets of experimental points, which exhibited near-identical results.

A comparison of the model curves for the obtained values of strength parameters is presented in Figure 4.8, which also includes a comparison with the remaining experimental points. Additionally, as was observed in the previous discussion regarding the MAC88118 meteorite stone, the model curves constructed for values $\sigma_c = \sigma_{c\_SPS}$, tend to correlate more strongly with the complete set of

experimental data than those calculated for the scenario where the critical stress is assumed to be equal to the static strength of the material, $\sigma_c = \sigma_s$. The most illustrative case is shown in Figure 4.8(b). The experimental data points, from which the values of the strength parameters were evaluated, are in quantitative agreement with the model curves constructed for both cases. However, the remaining portion of the test data does not align with the predicted level of critical stresses if we take $\sigma_c = \sigma_s$. Meanwhile, for the case $\sigma_c = \sigma_{c\_SPS}$, there is a notable degree of quantitative agreement.

The conducted verification allows us to conclude that the experimentally obtained strain rate dependence of dynamic strength for the investigated concrete C60, within the framework of the structure-time approach, is much better described when the value σ_{c_SPS} is chosen as the value of critical stress.

The results of the estimation for the parameters σ_c and τ are also presented in Table 4.2. In the case where $\sigma_c = \sigma_s$, the confidence intervals obtained for incomplete datasets, $T_1 = [25; 33]$ μs and $T_2 = [15; 18]$ μs, do not overlap. Concurrently, the confidence interval calculated by processing all experimental points, $T = [17; 22]$ μs, represents a mean value of the T_1 and T_2 intervals.

Table 4.2 Results of estimation of incubation time for C60 concrete by SPS method. The confidence level is 90%.

Observation dataset for processing	$\{\boldsymbol{\sigma}_{*i}, \dot{\boldsymbol{\varepsilon}}_i\}_{i=1}^{N_1}$	$\{\boldsymbol{\sigma}_{*i}, \dot{\boldsymbol{\varepsilon}}_i\}_{i=N_1+1}^{N}$	$\{\boldsymbol{\sigma}_{*i}, \dot{\boldsymbol{\varepsilon}}_i\}_{i=1}^{N}$
$\sigma_c = \sigma_s$, МПа	76	76	76
T, мкс	[25; 33]	[15; 18]	[17; 22]
$\sigma_c = \sigma_{c\_SPS}$, МПа	98	98	101
T_{SPS}, мкс	[7.0; 9.2]	[6.0; 7.4]	[4.5; 5.9]

The outcomes yielded by the two-dimensional adaptation of the SPS methodology appear to be markedly more stable. The confidence intervals obtained

for the partial and full data sets fall within the range of 4.5 to 9.2 μs. Concurrently, a favorable quantitative correlation is evident between the model volume curves. It can thus be concluded that for the range of loading rates achieved in the dynamic tests, the optimal value of the critical stress $\sigma_c = \sigma_{c_{SPS}} = 101\ MPa$ is considerably higher than the static strength value $\sigma_s = 76\ MPa$. This discrepancy may suggest that a shift in the failure mode is probable in C60 concrete when the loading rate is elevated. In other words, the proportion of damaged particles of granite aggregate increases in impact tests, which has a higher value of static strength than the cement base.

The data of dynamic tests for other types of concrete were similarly processed. The data for the main components of these concretes were also analyzed: the corresponding types of mortar and granite aggregate, for which the authors of the experiment conducted separate tests under both high rate and low rate loading [161, 162, 163, 164]. Table 4.3 shows the values of σ_{c_SPS} obtained for these materials, as well as their ratio to the static strength σ_{c_SPS}/σ_s.

Table 4.3 Data processing results for different types of concrete and the corresponding mortars and granite aggregate.

Material name	$\sigma_{c_{SPS}}, MPa$	σ_s, MPa	σ_{c_SPS}/σ_s
C60	101	76	1.33
C80	125	89	1.40
C110	166	122	1.36
M60	72	57	1.26
M80	89	79	1.13
M110	105	84	1.25
granite	236	211	1.12

Note, that for all concretes the ratio σ_{c_SPS}/σ_s varies from 1.33 to 1.40, which indicates the rate sensitivity of the fracture mode. Thus, for the granite aggregate, as for a more homogeneous material, this relation has received essentially less about ~1.12. This means that for such materials, the rate sensitivity of a fracture mode can be neglected.

It should also be noted that the values of σ_{c_SPS}/σ_s for two types of mortars M60 and M110 are about 1.25. This may mean that, there is also a partial change in the fracture mode with increasing loading rate in these materials, where transcrystalline fracture of rather large sand filler particles begins.

4.3 Conclusions to Chapter 4

A novel approach to dynamic test data processing has been devised, allowing for the estimation together two crucial model strength parameters: the incubation time and the critical stress, which determines the stability of the medium in direct correlation with the stress level of the loading action.

The reliability of the results obtained through the proposed method has been validated using data from dynamic tests of brittle materials. It is demonstrated that when incomplete data sets are processed, the discrepancy between the estimated incubation times is significantly reduced in comparison to the traditional estimation approach, where the critical stress is interpreted as the static strength of the specimen under slow loading.

An analytical approach has been developed to determine the dependence of the fracture mechanism in brittle two-component media on the loading rate. The

viability of the proposed method is demonstrated through the processing of test data for concrete, mortar and granite aggregates

Chapter 5 A mechanical interpretation of the incubation time criterion parameters

In the preceding chapters, the efficience of the incubation time criterion in addressing a range of mechanical problems associated with the prediction of critical conditions for various transient processes, including brittle fracture and cavitation in a fluid, has been demonstrated. A notable attribute of the criterion is its relatively limited number of parameters: the incubation time τ, the critical stress σ_c, and the dimensionless parameter α. The mechanical meaning of these parameters was briefly discussed earlier; however, for a more comprehensive analysis, it is essential to contrast the incubation time criterion with other analytical methodologies for examining and predicting the strength of materials under impact loading.

The results shown in Chapter 5 have been reported in the following papers [99, 100].

5.1 A comparative analysis of the failure criteria with the incubation time criterion

The primary characteristic of impact testing is the observation of strain rate dependence of the strength of materials. As the loading rate increases, an increase in the ultimate stress level is observed in the majority of materials under experimental conditions. In the majority of methods employed to ascertain the dynamic strength of materials, the values of model parameters are selected on the basis of the optimal correlation between the predicted strain rate-dependent ultimate stress level and the experimentally determined values. Initially, this property of materials was described by the power dependence of strength on strain

rate, which exponent is a material parameter [13]. However, an analysis of the experimental data revealed that the value of this parameter can vary considerably between different materials, ranging from 0.05 to 0.33. This wide range of values for the exponent suggests that this approach to describing the strain rate dependence of strength is merely a numerical approximation, and that this parameter has no special physical meaning.

Nevertheless, in engineering practice, this approach is the most prevalent. To illustrate, the existing FIB standard posits the existence of two distinct branches of material strength for brittle building materials such as concrete. These branches describe the ultimate stress level in the ranges of slow and fast loading, respectively. In the international standard, these two branches are approximated by a bilinear function in a semi-logarithmic coordinate system. Numerous modifications of this approach have been proposed by various authors, including those presented in [16, 17, 18, 20], yet all of these also represent numerical approximations of the strain rate dependence of strength.

It is noteworthy that in numerical modeling of fracture processes, the most prevalent is the Johnson-Holmquist governing relation [165, 39], in which the influence of strain rate is approximated by a logarithmic dependence.

Among the approaches to the description of dynamic strength, the traditional Tuler-Butcher integral criterion merits particular attention. Its principal difference from the previously mentioned approaches is the assumption that the material fracture process does not occur instantaneously [15]:

$$\int_0^T (\sigma - \sigma_s)^\lambda dt = K,$$

where T and σ represent the pulse duration and amplitude, respectively; σ_s is the threshold stress level under slow loading, while λ and K are material constants. The Tuler-Butcher criterion is predicated on the assumption that a material must be subjected to an overload for a sufficient duration to facilitate fracture. However, this criterion is inherently limited by the inability to empirically ascertain the material constants λ and K. Furthermore, it is not feasible even to think of a direct experimental approach of measuring these values.

Scaling law of Kimberly-Ramish

One of the few conceptual approaches to predicting the stress level under dynamic impact loading is the semi-empirical microstructural model of Paliwal-Ramesh, which considers a brittle elastic medium with microdefects [31]. The results of the numerical simulations, in which the primary parameters of the model were randomly altered within the permissible limits established by the model's developers for most brittle materials, revealed a multitude of potential ultimate stress levels at the moment of fracture σ_f contingent on varying loading rates $\dot{\varepsilon}$. It was discovered that these results can be approximated with a high degree of accuracy by the following relation, referred to by the authors as the scaling law:

$$\frac{\sigma_f}{\sigma_0} = 1 + \left(\frac{\dot{\varepsilon}}{\dot{\varepsilon}_0}\right)^{\frac{2}{3}}, \tag{5.1}$$

where σ_0 and $\dot{\varepsilon}_0$ represent material parameters having the meaning of some characteristic stress level and strain rate, respectively. It is noteworthy that the values of σ_0 and $\dot{\varepsilon}_0$ can be calculated within the framework of the Paliwol-Ramesh microstructural model. Their values are determined by such material parameters as the average size and average density of defects, as well as by the Lamé elastic

constants, density, and fracture toughness. Thus, it can be concluded that at the macro level, these two parameters σ_0 and $\dot{\varepsilon}_0$ provide a comprehensive description of the rate dependence of the material strength. This description is universal for all brittle materials in dimensionless coordinates $\left(\dot{\varepsilon}/\dot{\varepsilon}_0; \sigma_f/\sigma_0\right)$.

A comparative analysis of the results of predicting the strain rate dependence of strength obtained using the incubation time criterion and the Kimberly- Ramesh scaling law is best approached by first establishing the relationship between the material macroparameters σ_c, τ and σ_0, $\dot{\varepsilon}_0$, respectively. It is readily apparent that the limit of the right-hand side of the scaling law (5.1) is 1 when $\dot{\varepsilon} \to 0$. This indicates that the parameter $\sigma_0$can be interpreted as the limit stress level under slow loading or the static strength of the material σ_s. As previously demonstrated in Section 4.2, the critical stress parameter σ_c, as defined in the incubation time criterion, assumes an identical interpretation in the context of material failure occurring in the same way in the entire range of loading rates. It can therefore be posited that for a number of homogeneous materials, the parameters σ_c and σ_0 have an identical meaning.

The mechanical significance of the parameter $\dot{\varepsilon}_0$ can be understood as a specific threshold strain rate, above which there is a notable increase in the stress level at the moment of fracture. Indeed, if the strain rate of the material is equal to the characteristic $\dot{\varepsilon} = \dot{\varepsilon}_0$, then, in accordance with expression (5.1), the dynamic strength of the material will exceed the static strength by a factor of two.

In constructing the strain rate dependence of strength by the incubation time criterion, it is also possible to identify a critical strain rate, thereby dividing the strain rate range into slow and fast values. An examination of the analytical expression for the strain rate dependence (1.7), as given in Section 4.2,

$$\sigma_*(\dot{\varepsilon}) = \begin{cases} \sigma_c + \dfrac{E\dot{\varepsilon}\tau}{2}, & \dot{\varepsilon} \le \dfrac{2\sigma_c}{E\tau}, \\ \sqrt{2\sigma_c\tau E\dot{\varepsilon}}, & \dot{\varepsilon} > \dfrac{2\sigma_c}{E\tau}, \end{cases}$$

it can be observed that the expressions for the static and dynamic branches are selected basing on whether or not the strain rate of the material exceeds a critical value, denoted as $\dot{\varepsilon}_{\text{c}} = \frac{2\sigma_c}{E\tau}$. Similarly, as with the scaling law, if the material strain rate is equal to the critical strain rate $\dot{\varepsilon} = \dot{\varepsilon}_{\text{c}}$), expression (1.7) will predict twice the dynamic strength over the static strength.

To facilitate a comparison of the two approaches, it is expedient to rewrite expression (1.7) in the following form:

$$\frac{\sigma_*}{\sigma_c} = \begin{cases} 1 + \dfrac{\dot{\varepsilon}}{\dot{\varepsilon}_{\text{c}}}, & \dot{\varepsilon} \le \dot{\varepsilon}_{\text{c}}, \\ 2\sqrt{\dfrac{\dot{\varepsilon}}{\dot{\varepsilon}_{\text{c}}}}, & \dot{\varepsilon} > \dot{\varepsilon}_{\text{c}}. \end{cases} \qquad (5.2)$$

Subsequently, on the basis of the aforementioned assumption that the parameters σ_c and σ_0 signify static strength, it is possible to equate the left-hand sides of the resulting expression (5.2) and the scaling law (5.1). Subsequently, after a series of algebraic transformations, we can derive the following relation between the characteristic strain rate $\dot{\varepsilon}_0$ from the Kimberly- Ramesh scaling law and the critical strain rate $\dot{\varepsilon}_{\text{c}}$, which arises from the prediction of the strain rate dependence of strength using the incubation time criterion.

$$\dot{\varepsilon}_0 = \begin{cases} \dot{\varepsilon}_c \sqrt{\dfrac{\dot{\varepsilon}_c}{\dot{\varepsilon}}}, & \dot{\varepsilon} \le \dot{\varepsilon}_c, \\ \dot{\varepsilon} \left(2\sqrt{\dfrac{\dot{\varepsilon}}{\dot{\varepsilon}_c}} - 1 \right)^{-\frac{3}{2}}, & \dot{\varepsilon} > \dot{\varepsilon}_c. \end{cases} \tag{5.3}$$

Form of expression (5.3) demonstrates that the characteristic strain rate $\dot{\varepsilon}_0$, which is a constant in the scaling law, from the perspective of the incubation time criterion is a variable value contingent on the loading rate $\dot{\varepsilon}$. In this instance, it is notable that the characteristic strain rate $\dot{\varepsilon}_0$ is identical to the critical strain rate $\dot{\varepsilon}_c$, when $\dot{\varepsilon} = \dot{\varepsilon}_c$:

$$\dot{\varepsilon}_0|_{\dot{\varepsilon}=\dot{\varepsilon}_c} = \dot{\varepsilon}_c, \qquad \dot{\varepsilon}_c = \frac{2\sigma_c}{E\tau}.$$

It thus emerges that the Kimberly- Ramesh scaling law exhibits a uniform normalization of the strain rate. In contrast, the normalization factor in the incubation time criterion varies in accordance with the strain rate of loading, as expressed in equation (5.3). Accordingly, to conduct a valid comparison in dimensionless form between the strain rate dependence calculated with the incubation time criterion and with the universal scaling law, it is essential to assume that the value of the characteristic strain rate $\dot{\varepsilon}_0$ is equal to $\dot{\varepsilon}_c$.

The results of the comparison, as presented in Figure 5.1(a), demonstrate that at slow loading, when the relative strain rate $\dot{\varepsilon}/\dot{\varepsilon}_c < 1$, as well as at its further increase up to 10^2 (этот кусок я переделал), the rate dependences of DIF predicted within the investigated approaches are in qualitative and quantitative agreement. Nevertheless, as a further increase of the loading rate, the critical stress levels predicted by the scaling law will diverge significantly from the values calculated using the incubation time criterion (see Figure 5.1(b)).

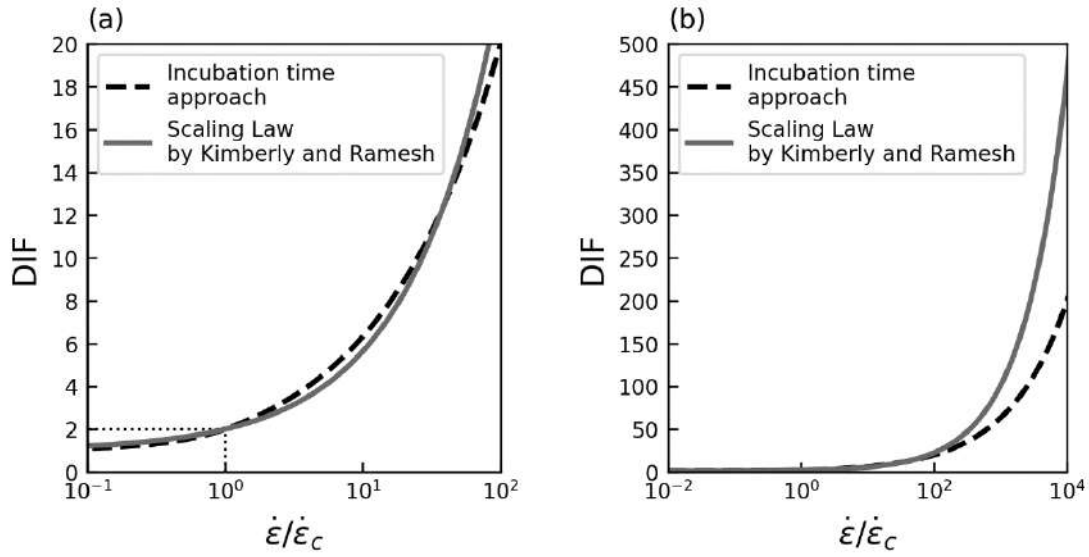

Figure 5.1: A comparison of the strain rate dependences of strength, plotted according to the incubation time criterion and the Kimberley- Ramesh scaling law ($\dot{\varepsilon}_0 = \dot{\varepsilon}_c$).

The comparison of the investigated approaches was also carried out on the example of the description of the strain rate dependence of the strength of meteorite stone MAC88118, which was discussed in detail in Section 4.1. The dynamic strength calculations were performed in accordance with the scaling law for the following parameter values: $\dot{\varepsilon}_0 = 200\ 1/s$ and $\sigma_0 = 50$ MPa. These values were calculated in [5] according to the Paliwal – Ramesh microstructural model. For the structure-time approach, an estimate of the incubation time τ was obtained using a one-dimensional modification of the SPS method, assuming that $\sigma_c = \sigma_0 = 50$ MPa. The estimated incubation time τ is within the range of $[82; 124]$ μs.

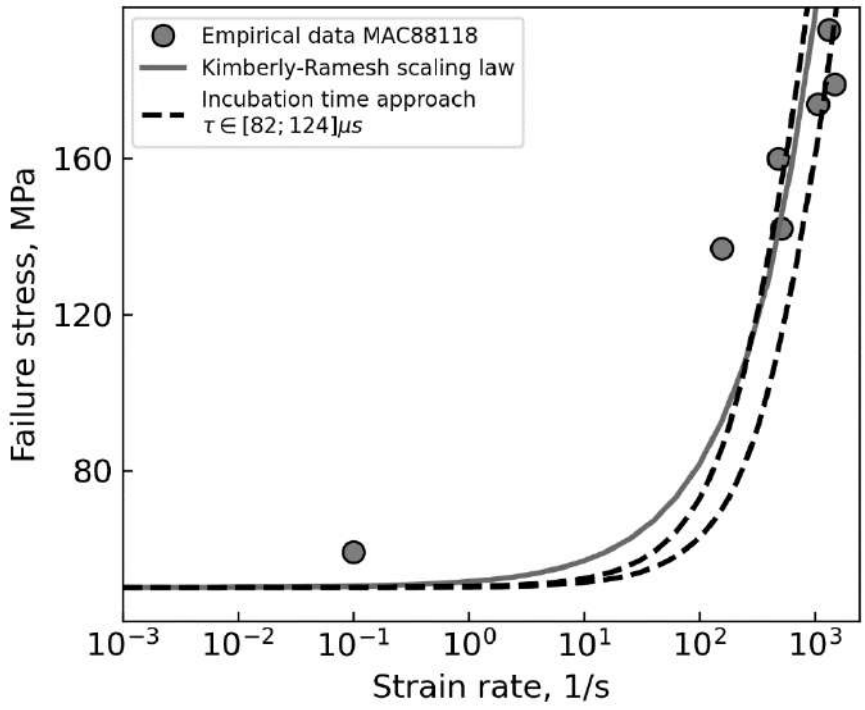

Figure 5.2 Comparison of the strain rate-dependent strength of meteorite stone MAC88118 [5] with the results of dynamic tests. The solid line represents the Kimberly-Ramesh scaling law, while the dashed curves have been calculated in accordance with the incubation time criterion.

As illustrated in Figure 5.2, both approaches demonstrate the capacity to provide a satisfactory representation of the strain rate dependent strength observed in the experiment. Nevertheless, it should be noted that such a high level of agreement is not consistently observed across all cases. For instance, in reference to the processing of test results for silicon carbide SiC-N, the following correction for the Kimberly-Ramesh scaling law was required for better alignment with experimental data, as detailed in work of Holland and McMeeking [166]:

$$\frac{\sigma_f}{\sigma_0} = 1 + 0.1\left(\frac{\dot{\varepsilon}}{\dot{\varepsilon}_0}\right)^{\frac{2}{3}},$$

furthermore, alternative values for the characteristic stress and strain rate parameters were selected: $\sigma_0 = 5200$ MPa and $\dot{\varepsilon}_0 = 131$ 1/s. The initial values were calculated according to the Paliwal- Ramesh microstructural model, resulting in $\sigma_0 = 5400$ MPa and $\dot{\varepsilon}_0 = 5 \times 10^3$ 1/s. In order to construct the strain rate dependence within a structure-time approach, an estimate of the incubation time τ was obtained using a one-dimensional modification of the SPS method. This estimate was found to fall within the range $[5.4; 14.5]$μs, and it was assumed that $\sigma_c = \sigma_0 = 5200$ MPa.

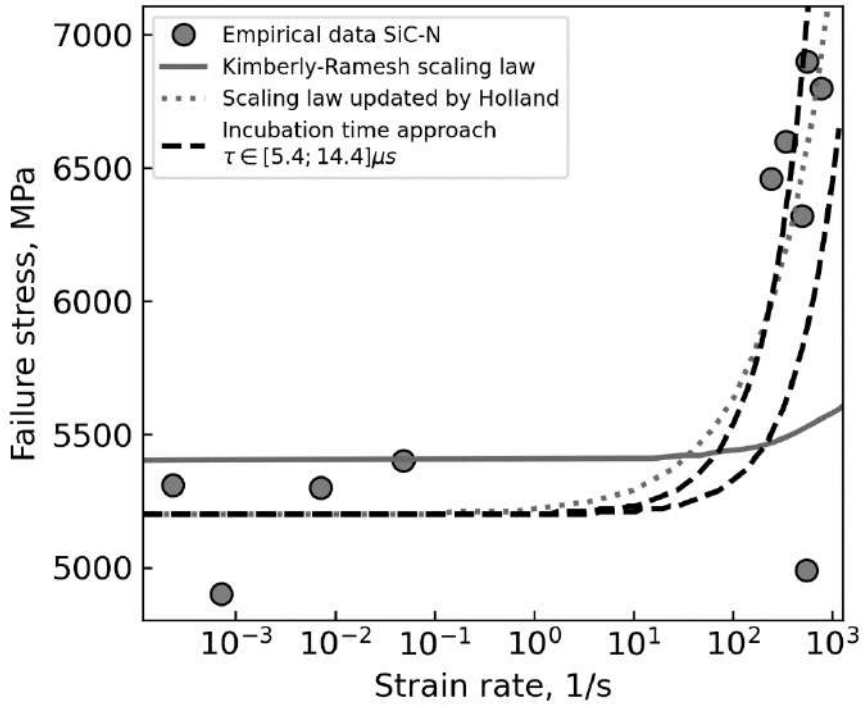

Figure 5.3 Comparison of strain rate dependences of strength with dynamic test data for SiC-N silicon carbide [167].

The results of the calculations are presented in Figure 5.3. Note that the solid curve corresponding to the Kimberly-Ramesh scaling law only qualitatively predicts an increase in the dynamic strength of the material in the range of strain rates of the order of $10^2 - 10^3$ 1/s. Concurrently, the strain rate dependent calculations conducted in accordance with the incubation time criterion and

calculations within the Kimberly-Ramesh relation adjusted by Holland and McMeeking [166] exhibit substantial qualitative and quantitative concordance with the experimentally determined values of dynamic strength.

The comparison of the aforementioned theoretical approaches to the description of the strength of materials under dynamic loading has demonstrated that both methods are capable of qualitatively describing the strain rate dependence. Nevertheless, the conceptual foundation of the incubation time approach confers upon it unquestionable advantages. The introduction of the characteristic fracture time τ as a parameter of material strength, as well as the very principle of fracture process development under conditions of high-speed loading, allows for the calculation of the rate dependence of strength with greater accuracy for any material. Conversely, the Kimberly-Ramesh scaling law does not consistently yield satisfactory quantitative concordance with experimental outcomes, necessitating ungrounded corrections, as evidenced in the case of silicon carbide SiC-N. The relationship (5.3) between the time parameters of the two approaches demonstrates that in the incubation time approach, the normalization of the strain rate is non-uniform, which allows for the achievement of good quantitative agreement with experiments without the introduction of any corrections. Consequently, the concurrence of the normalizing value of the strain rate with the critical value under loading with the identical critical strain rate $\dot{\varepsilon}_0|_{\dot{\varepsilon}=\dot{\varepsilon}_c} = \dot{\varepsilon}_c$, substantiates the assertion that the aforementioned methods are in concordance with each other, albeit only within a specific range of strain rates.

5.2 The strain rate sensitivity of plastic deformation mechanisms

In the aforementioned problems, only two strength parameters, incubation time τ and critical stress σ_c, were typically sufficient to calculate the critical stress level under high-speed loading. However, the introduction of the incubation time criterion in the section 1.1 highlighted the existence of a third dimensionless parameter, α, which is crucial for predicting the dynamic yield strength in certain cases. In this section, one potential interpretation of this parameter is presented, which provides insight into the reasons why it is necessary to introduce it in certain cases.

Application of incubation time criterion for predicting dynamic yield strength

The initial efforts to utilize the incubation time criterion for predicting the strain rate-dependent yield stress exhibited that the inclusion of merely two strength parameters, namely incubation time τ and critical yield stress σ_c^y, is inadequate to achieve a satisfactory agreement between the calculated and experimentally observed values. Accordingly, in [168], a third dimensionless parameter, α, was proposed and the criterion was formulated as follows:

$$\frac{1}{\tau}\int_{t-\tau}^{t}\left(\frac{\sigma(t')}{\sigma_c^y}\right)^{\alpha} dt' \leq 1, \tag{5.4}$$

The critical yield stress, σ_c^y, represents the minimum stress level necessary to initiate plastic deformation mechanisms in the material. As previously demonstrated, the critical yield stress σ_c^y is equal to the static yield stress σ_y, which represents the threshold level of statically applied load that causes

irreversible plastic deformation. This peculiarity necessitates the introduction of a third parameter, α, as there may be a significant discrepancy between the slope of the curve determined by the analytically calculated strain rate dependence of the dynamic yield strength in the case when $\alpha = 1$ and the trend given by the experimentally measured values. This shows that the discrepancy between calculated and experimental values cannot be resolved by simply varying appropriate values of the incubation time τ.

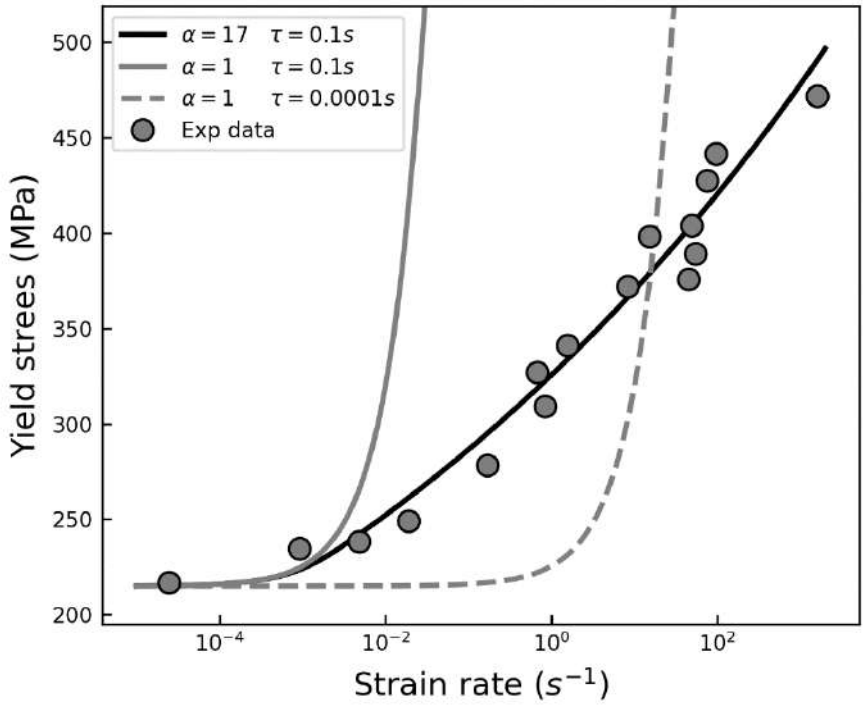

Figure 5.4 The strain rate dependence of yield strength for En3B steel, calculated within the framework of the structure-time approach. The experimental data from [169] are represented by circles, while the calculation from [168] ($\alpha = 17$) is represented by a black solid line. The gray lines correspond to the model curves calculated at $\alpha = 1$

Figure 5.4 shows the results of modeling the strain rate dependence of dynamic yield strength for mild steel En3B from [168]. The black solid line was plotted by A.A. Gruzdkov at the parameter value $\alpha = 17$, which provided a

satisfactory quantitative and qualitative agreement with the Campbell test results [169]. The gray lines indicate the strain rate dependences calculated for $\alpha = 1$. It is noteworthy that by changing the incubation time parameters, the model curve only undergoes a horizontal shift on the graph, while the slope of the dynamic branch remains unaltered.

The introduction of the parameter α is essential for achieving a quantitative correspondence with the measured values of dynamic yield strength across the entire range of deformation velocities. However, in contrast to the other parameters of the criterion, τ and σ_c^y, the parameter α does not have a clear and unambiguous mechanical interpretation. A formal analysis conducted by A.A. Gruzdkov demonstrated that the parameter α can be defined as the sensitivity of the material to the loading action amplitude. Indeed, if the value of α is set to infinity, the amplitude of the loading action becomes the determining factor in the onset of plasticity.

It is important to note, however, that the incubation time criterion assumes that the plastic deformation process occurs in a uniform manner, independent of the loading rate. Consequently, if we abandon the assumption that $\sigma_c^y = \sigma_y$ and assume that alternative microstructural mechanisms become increasingly influential in the evolution of plastic deformation as the loading rate increases, a radically different interpretation of the parameter α emerges.

The strain rate sensitivity of plastic deformation mechanisms

The study of inelastic deformation of metals has revealed that macroscopic plastic deformation can be achieved through a variety of mechanisms at the microlevel. Among these, several principal dislocation mechanisms can be

distinguished, including basic, prismatic, and pyramidal slip, grain boundary slip, and twinning [170, 171]. Moreover, numerous studies have examined the rate sensitivity of plastic deformation micromechanisms [172, 173, 174, 175, 176]. For instance, it has been demonstrated that the intensity of pyramidal and prismatic slip mechanisms is markedly dependent on the loading rate, whereas virtually no rate sensitivity is observed for the twinning process itself [177, 178].

The different levels of strain rate sensitivity exhibited by the various plasticity mechanisms give rise to the formulation of microstructural models, which are mainly used in finite element calculations (e.g. [179, 180, 181]). However, such models are often difficult to use due to the large number of parameters whose values are difficult to determine. Consequently, in cases of high rate loading where only the yield strength level needs to be estimated, the use of macroscopic continuum models that incorporate the average strain rate sensitivity of the plastic deformation microprocesses over a range of levels may prove to be a more convenient approach to calculation.

Considering the incubation time criterion, it can be postulated that the parameter α is the determining factor in the existence of competition between the different plastic deformation microprocesses. As previously demonstrated, there are multiple yielding mechanisms, with the predominant mechanism depending on the strain rate of loading. It follows that the critical yield strength measured under slow loading for the dominant plastic deformation mode in the static case cannot be interpreted as the critical yield strength for the high rate loading mode. Accordingly, the parameter σ_c^y cannot be considered to represent the static yield strength σ_y.

Therefore, it is reasonable to divide the experimental data into different strain rate ranges with the aim of estimating the critical yield strength and incubation time for the prevailing plastic deformation mode in each range. In other

words, in this case, the yield strength of the material is determined by the competition between different plastic deformation mechanisms, each characterized by its unique values of incubation time and critical stress.

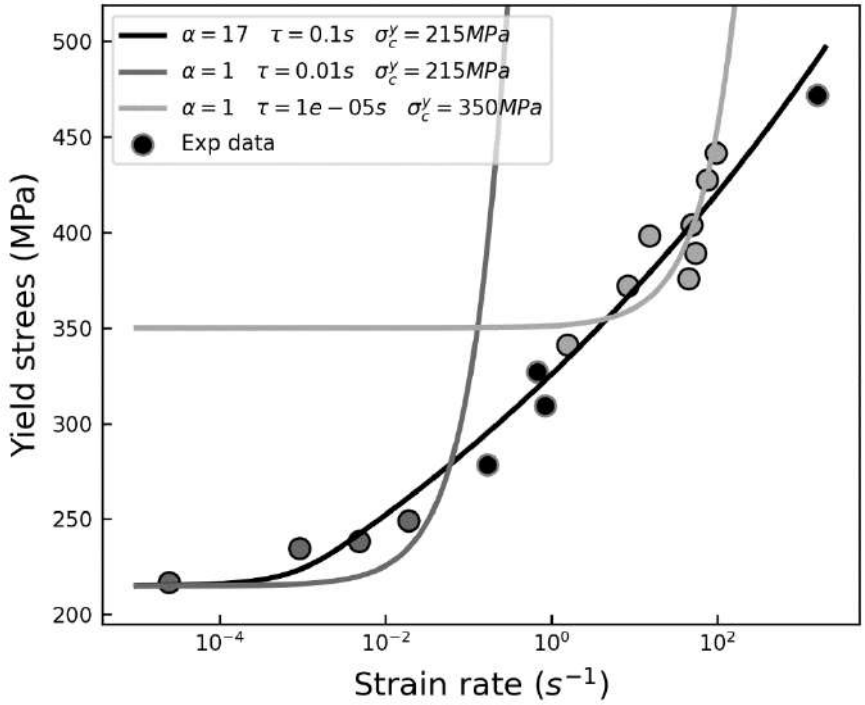

Figure 5.5 Possible scenario of competition between different yield micro-processes, to describe the strain rate sensitivity of the yield strength of En3B steel. The circles are experimental data from [169], the black solid line is the calculation at $\alpha = 17$из from [168], the gray lines correspond to different values of τ and σ_c^y at $\alpha = 1$.

A possible scenario for such a competition is illustrated in Figure 5.5. It is assumed that two different inelastic deformation microprocesses, corresponding to conventional low and high rate loading regimes, compete with each other. The dark and light gray lines illustrate the strain rate sensitivity curves calculated using the incubation time criterion for $\alpha = 1$. The model shows a high degree of agreement with selected experimental data points, indicated by the corresponding gray shading. The initial plastic deformation mode, represented by the dark gray

curve, dominates at low strain rates due to its lower critical yield strength compared to the second mode, represented by the light gray curve. At high strain rates, however, the incubation time parameter becomes the primary factor, and thus the second deformation mode, corresponding to a higher value of τ, becomes the dominant mechanism.

It is evident that the considered yielding processes influence each other and the result of their competitive interaction cannot be modeled by independently calculated strain sensitivity curves. This may be the reason why the intermediate points marked in black are not approximated by any of the gray curves. At the same time, the black curve calculated for $\alpha = 17$ shows a high degree of correlation with the extensive experimental data set. Thus, it can be concluded that the need to introduce the third parameter α is related to the change of the yielding mechanism with increasing loading rate. For this reason, the parameter α was initially proposed in the modeling of the dynamic yield stress, since there are several main mechanisms of inelastic deformation, the competition of which determines the plastic deformation of a continuous medium at the macro level.

A comparative yield strength analysis of ultrafine and coarse grained materials

To test the above hypothesis regarding the competition of different plastic deformation microprocesses, we processed dynamic test data for the same material in different microstructural states: coarse-grained (CG) and ultrafine grained (UFG). Since the ultrafine grain state is typically achieved by intense plastic deformation, it can be postulated that the number of different yield micromechanisms, or at least their relative contribution to the overall deformation process, is significantly reduced. Therefore, further analysis is planned to

demonstrate that the relative difference between $\sigma^{y}_{c\_SPS}$ and σ_y is smaller for the material in the UMZ state than for the coarse-grained state. In other words, it can be postulated that the strain rate sensitivity of the plastic deformation process for the material in the UFM state is significantly reduced compared to that of the same material in its initial coarse-grained state.

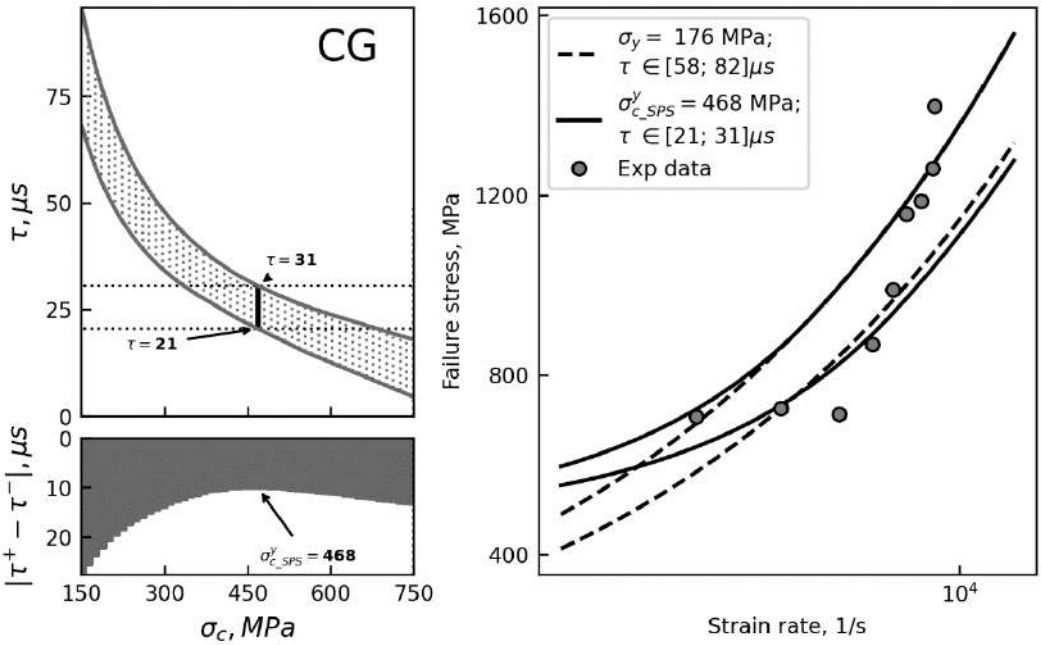

Figure 5.6 Results of dynamic data analysis for coarse-grained AISI 321 steel with 37 μm grain size obtained in [182]. The left graph shows the confidence region and the diagram marking the smallest interval $[\tau^{-};\tau^{+}]$ corresponding to the optimal value of $\sigma^{y}_{c\_SPS}$; the right graph compares the model curves calculated for $\sigma^{y}_{c} = \sigma_y$ and $\sigma^{y}_{c} = \sigma^{y}_{c\_SPS}$.

Test data for AISI 321 stainless steel, which were published in a series of papers [182, 183, 184], were selected as the material for the study. The authors conducted a comprehensive experimental investigation of the material's strength properties under both static and high-speed dynamic loading conditions. It is also noteworthy that the steel was tested under both slow and high rate loading for three

distinct grain sizes: ultrafine grain (UFG) with an average grain size of 0.24 μm, fine grain (FG) of 3 μm, and coarse grain (CG) of 37 μm, respectively.

The same methodology proposed in Section 4.1 for estimating critical stress values for brittle fracture of concrete was used to process the data. The results of the processing for AISI 321 steel in the coarse-grained state are shown in Figure 5.6. Note that the processed experimental data do not show a clear trend for the dynamic branch of the yield stress. Therefore, it is difficult to determine which of the two model curves provides the more accurate quantitative correlation. It is clear that both pairs of curves show a high degree of visual agreement with the dynamic test data points. However, in the plot illustrating the width of the confidence interval for the incubation time, the minimum, although not pronounced, remains evident and allows the determination of the optimum value of $\sigma^{y}_{c\_SPS}$ for the coarse-grained state.

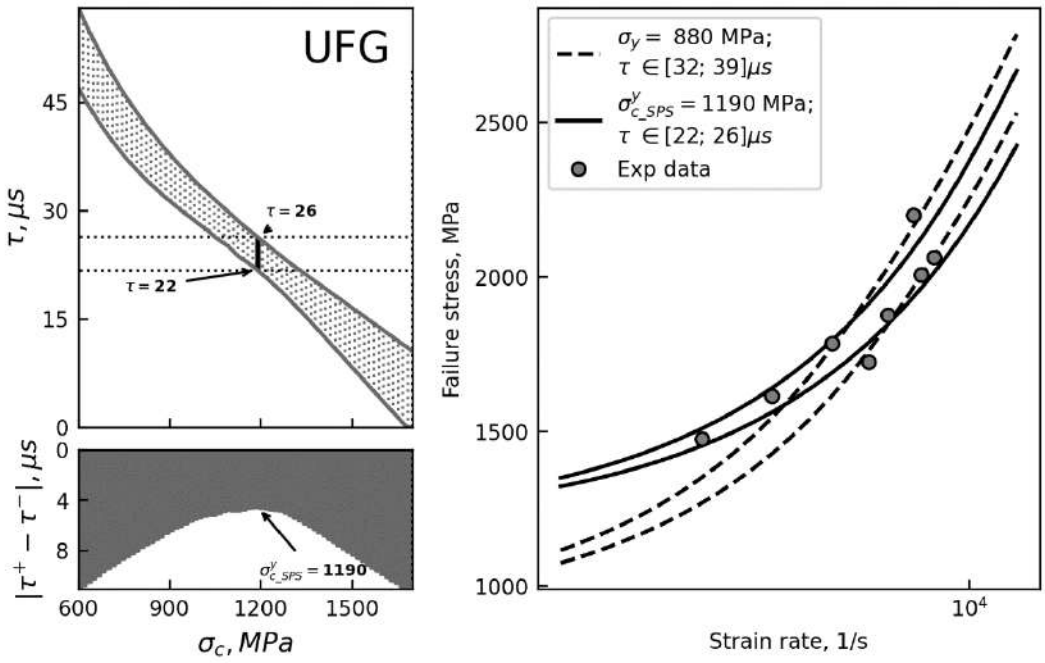

Figure 5.7 Results of analysis of high rate test data for the ultrafine grained state of AISI 321 steel with 0,24 μm grain size obtained by [182].

Figure 5.7 presents a much clearer scenario, illustrating the outcomes of processing the experimental data obtained for the ultrafine-grained state of AISI 321 steel. It can be seen that the model curves (solid lines) obtained by the proposed method align more closely follow the trend indicated by the test data. Furthermore, it is noteworthy that the diagram displaying the width of the confidence interval $[\tau^{-};\tau^{+}]$, exhibits a pronounced minimum, which also indicates the presence of a well-defined dynamic branch of the yield strength derived from the test data.

Table 5.1 Results of estimation of the parameter $\sigma_{c\_SPS}^{y}$ for different states of AISI 321 steel.

	UFG (0.24 мкм)	FG (3 мкм)	CG (37 мкм)
$\sigma_{c\_SPS}^{y}$, МПа	0	620	468
σ_{y}, МПа	880	316	176
$\sigma_{c\_SPS}^{y}/\sigma_{y}$	**1.35**	**1.96**	**2.66**

For clarification, the results obtained by data processing for AISI 321 steel in all states are summarized in Table 5.1. It can be seen that the relative difference between the critical yield strength $\sigma_{c\_SPS}^{y}$ obtained by the SPS method and the static yield strength σ_{y} decreases as the average grain size decreases. This indicates that the relative influence of different plastic deformation mechanisms at the microstructural level is actually less dependent on the loading rate for ultrafine grained materials.

It is important to note that the estimation of the values of the incubation time and the parameter α is of great importance when modeling plastic deformation diagrams under high rate loading according to the relaxation theory of plasticity

[185]. Knowing the exact values of the parameters allows predicting such phenomena as the non-monotonic character of deformation diagrams [186, 187] and thermal softening [188], as well as obtaining good agreement with experimental results.

5.3 Conclusions to Chapter 5

A novel mechanical interpretation of the primary material strength parameters within the structure-time framework was proposed: the incubation time τ and the dimensionless parameter α.

A systematic comparison of the developed methods with existing models, in particular the Kimberly-Ramesh scaling law, was performed. The correlation found with the parameters of the scaling law allowed to reinterpret the incubation time parameter as a parameter that sets the normalization of the strain rate of the sample in a non-uniform way.

An analytical model has been developed to predict the value of the yield strength of polycrystalline materials under high rate loading. This is a result of competition between different mechanisms of plastic flow at the micro level. The viability of the proposed model is demonstrated through a comparative analysis of test data from metals in both coarse and ultrafine grain states.

In the context of the constructed model, a novel interpretation of the dimensionless parameter α was proposed as a parameter indicating the dependence of the dominant plastic deformation mechanism on the loading rate.

Conclusions

1) The new method for estimating the value of incubation time developed in this thesis is based on the randomized sign-perturbed sums (SPS) method. This method allows the estimation of incubation time in the form of a confidence interval as a result of processing experimentally measured time or strain rate dependencies of strength. The advantage of this novel approach is that it allows the estimation of incubation time values with mathematical validity from a limited number of observations, provided that the uncertainty due to interferences is taken into account. The inclusion of a confidence interval makes it possible to calculate the margin of error associated with the estimated incubation time value.
2) The correctness of the method is confirmed by the proved theorem regarding the fulfillment of the conditions for the applicability of the SPS method to the studied problems and regarding the boundedness of the estimation interval. The effectiveness of the method is illustrated by an example of its application to the prediction of the dynamic strength of brittle materials, including various types of rocks and ice at different temperatures.

3) A novel model has been developed to predict the dependence of the acoustic cavitation threshold on the frequency of the ultrasonic wave, as well as the pulse-induced cavitation on the duration of the loading action. The model allows consideration of the effect of temperature and background hydrostatic pressure on the final value of the cavitation threshold. A comparison of the predicted dependencies with the known experimental values of the cavitation threshold demonstrated the effectiveness of the proposed methods.

4) A methodology for estimating the energy intensity of the acoustic cavitation process as a function of the frequency of the initiating ultrasonic wave is

presented. A qualitative agreement between the calculated results and the experimentally observed regularities has been achieved.

5) Based on the results obtained in the study of the cavitation threshold of liquids, an analytical model is constructed to evaluate the influence of the acoustic ultrasonic background field on the phase equilibrium conditions of a continuous medium.

6) The optimal modes of impact contact with a solid medium have been identified. It is shown that the input energy required to generate threshold destructive pulses depends on the duration of these pulses. The calculation of these dependencies for particles of different shapes is performed.

7) The application of the quasi-static Hertz hypothesis to the magnitude of the contact force gives paradoxical results when a cylindrical impactor is considered. The constructed solution to the problem, which considers the supersonic stage of the interaction, has shown that for real bodies, the threshold energy characteristic of a spherical impactor is indeed dependent on.

8) An analytical model of ultrasonically assisted machining of metals has been constructed, which shows that the addition of ultrasonic vibrations leads to a more favorable fracture mode in accordance with the dependencies of the energy consumption on the pulse duration. The calculated dependences of the cutting force on the feed rate are in qualitative and quantitative agreement with the known results of experimental studies.

9) A novel approach to processing dynamic test data has been developed that allows the estimation of both strength parameters: incubation time and critical stress. The stability of the results is demonstrated by processing incomplete sets of experimental data.

10) This study proposes an analytical approach to elucidate the dependence of the fracture mechanism in brittle two-component media on the loading rate. The feasibility of the proposed method is demonstrated by processing test data for concrete, mortar, and granite aggregate.

11) A comparison of the developed methods for the determination of critical fracture conditions with the approaches of other authors, in particular with the Kimberly-Ramesh model, was carried out. The established relationship with the parameters of the scaling law of the Kimberly-Ramesh model allowed to present an alternative, novel interpretation of the incubation time parameter as a parameter determining the non-uniform normalization of the strain rate of the specimen.

12) An analytical model has been developed to predict the value of yield strength of polycrystalline materials under high rate loading. This model takes into account the competition of different micromechanisms of the yielding process. The viability of the proposed model is demonstrated through a comparative analysis of test data from metals in both coarse and ultrafine grain states. In the context of the constructed model, a novel interpretation of the dimensionless parameter α is proposed as a parameter indicating the strain rate sensitivities of inelastic deformation mechanisms governing deformation at the macroscopic level.

Bibliography

[1] D. R. Curran, L. Seaman и D. A. Shockey, «Dynamic failure in solids», Physics Today, т. 30, № 1, pp. 46-55, 1977.

[2] M. A. Meyers, Dynamic behavior of materials, John wiley & sons, 1994.

[3] V. S. Nikiforovskii, S. I. Sabitova и A. E. Strelyaev, «Fracture of solid bodies by dynamic loads», Soviet mining science, т. 6, pp. 517-524, 1970.

[4] K. Ravi-Chandar, Dynamic fracture, Elsevier, 2004.

[5] J. Kimberley и K. T. Ramesh, «The dynamic strength of an ordinary chondrite», Meteoritics & Planetary Science, т. 46, № 11, pp. 1653-1669, 2011.

[6] Q. B. Zhang и J. Zhao, «A review of dynamic experimental techniques and mechanical behaviour of rock materials», Rock mechanics and rock engineering, т. 47, pp. 1411-1478, 2014.

[7] P. Forquin, «Brittle materials at high-loading rates: an open area of research», Philosophical Transactions of the Royal Society A: Mathematical, Physical and Engineering Sciences, т. 375, № 2085, p. 20160436, 2017.

[8] Z. Li, W. Chen и H. Hao, «Mechanical properties of carbon foams under quasi-static and dynamic loading», International Journal of Mechanical Sciences, т. 161, p. 105039, 2019.

[9] Y. Xu, F. Dai и H. Du, «Experimental and numerical studies on compression-shear behaviors of brittle rocks subjected to combined static-dynamic loading», International Journal of Mechanical Sciences, т. 175, № 105520, 2020.

[10] E. Cadoni, D. Forni, E. Bonnet и S. Dobrusky, «Experimental study on direct tensile behaviour of UHPFRC under high strain-rates», Construction and Building Materials, т. 218, pp. 667-680, 2019.

[11] J. Xiao, D. W. Shu и X. J. Wang, «Effect of strain rate and temperature on the mechanical behavior of magnesium nanocomposites», International Journal of Mechanical Sciences, т. 89, pp. 381-390, 2014.

[12] R. J. Thomas и A. D. Sorensen, «Review of strain rate effects for UHPC in tension», Construction and Building Materials, т. 153, pp. 846-856, 2017.

[13] D. E. Grady и J. Lipkin, «Criteria for impulsive rock fracture», Geophysical Research Letters, т. 7, № 4, pp. 255-258, 1980.

[14] J. Lankford, «The role of tensile microfracture in the strain rate dependence of compressive strength of fine-grained limestone-analogy with strong ceramics», International Journal of Rock Mechanics and Mining Science, т. 18, № 2, 1981.

[15] F. R. Tuler и B. M. Butcher, «A criterion for the time dependence of dynamic fracture», International Journal of Fracture Mechanics, т. 4, № 4, pp. 431-437, 1968.

[16] J. W. Tedesco и C. A. Ross, Strain-rate-dependent constitutive equations for concrete, 1998.

[17] D. L. Grote, S. W. Park и M. Zhou, «Dynamic behavior of concrete at high strain rates and pressures: I. experimental characterization», International journal of impact engineering, т. 25, № 9, pp. 869-886, 2001.

[18] Q. M. Li и H. Meng, «About the dynamic strength enhancement of concrete-like materials in a split Hopkinson pressure bar test», International Journal of solids and structures, т. 40, № 2, pp. 343-360, 2003.

[19] H. Meng и Q. M. Li, «Correlation between the accuracy of a SHPB test and the stress uniformity based on numerical experiments», International Journal of Impact Engineering, т. 28, № 5, pp. 537-555, 2003.

[20] X. Q. Zhou и H. Hao, «Modelling of compressive behaviour of concrete-like materials at high strain rate», International Journal of Solids and Structures, т. 45, № 17, pp. 4648-4661, 2008.

[21] Y. Hao и H. Hao, «Dynamic compressive behaviour of spiral steel fibre reinforced concrete in split Hopkinson pressure bar tests», Construction and Building Materials, т. 48, pp. 521-532, 2013.

[22] Y. Hao и H. Hao, «Numerical evaluation of the influence of aggregates on concrete compressive strength at high strain rate», International Journal of Protective Structures, т. 2, № 2, pp. 177-206, 2011.

[23] Y. Hao, H. Hao и X. Zhang, «Numerical analysis of concrete material properties at high strain rate under direct tension», International journal of impact engineering, т. 39, № 1, pp. 51-62, 2012.

[24] R. J. Thomas и A. D. Sorensen, «Review of strain rate effects for UHPC in tension», Construction and Building Materials, т. 153, pp. 846-856, 2017.

[25] D. M. Cotsovos и M. N. Pavlović, «Numerical investigation of concrete subjected to high rates of uniaxial tensile loading», International journal of impact engineering, т. 35, № 5, pp. 319-335, 2008.

[26] M. Pająk и J. Janiszewski, «Influence of aggregate and recycled steel fibres on the strain rate sensitivity of mortar and concrete», Construction and Building Materials, т. 363, p. 129855, 2023.

[27] N. P. Daphalapurkar, K. T. Ramesh, L. Graham-Brady и J.-F. Molinari, «Predicting variability in the dynamic failure strength of brittle materials considering pre-existing flaws», Journal of the Mechanics and Physics of Solids, т. 59, № 2, pp. 297-319, 2011.

[28] J. L. Le, J. Eliáš, A. Gorgogianni, J. Vievering и J. Květoň, «Rate-dependent scaling of dynamic tensile strength of quasibrittle structures», Journal of Applied Mechanics, т. 85, № 2, p. 021003, 2018.

[29] L. Graham-Brady, «Statistical characterization of meso-scale uniaxial compressive strength in brittle materials with randomly occurring flaws», International Journal of Solids and Structures, т. 47, № 18-19, pp. 2398-2413, 2010.

[30] A. L. Tonge и K. T. Ramesh, «Multi-scale defect interactions in high-rate brittle material failure. Part I: Model formulation and application to ALON», Journal of the Mechanics and Physics of Solids, т. 86, pp. 117-149, 2016.

[31] B. Paliwal и K. T. Ramesh, «An interacting micro-crack damage model for failure of brittle materials under compression», Journal of the Mechanics and Physics of Solids, т. 56, № 3, pp. 896-923, 2008.

[32] J. Kimberley, K. T. Ramesh и N. P. Daphalapurkar, «A scaling law for the dynamic strength of brittle solids», Acta Materialia, т. 61, № 9, pp. 3509-3521, 2013.

[33] C. Denoual и F. Hild, «A damage model for the dynamic fragmentation of brittle solids», Computer methods in applied mechanics and engineering, т. 183, № 3-4, pp. 247-258, 2000.

[34] P. Forquin и F. Hild, «A probabilistic damage model of the dynamic fragmentation process in brittle materials», Advances in applied mechanics, т. 44, pp. 1-72, 2010.

[35] B. Erzar, G. Le Blanc, F. Malaise и E. Buzaud, «A micromechanical modeling approach to describe the dynamic spalling of ceramic materials», In AIP Conference Proceedings, т. 1979, № 1, 2018.

[36] P. Forquin и B. Lukić, «On the processing of spalling experiments. Part I: Identification of the dynamic tensile strength of concrete», Journal of Dynamic Behavior of Materials, т. 4, № 1, pp. 34-55, 2018.

[37] B. Erzar, C. Pontiroli и E. Buzaud, «Shock characterization of an ultra-high strength concrete», The European Physical Journal Special Topics, т. 225, № 2, pp. 355-361, 2016.

[38] C. Pontiroli, A. Rouquand и J. Mazars, «Predicting concrete behaviour from quasi-static loading to hypervelocity impact: an overview of the PRM model», European Journal of Environmental and Civil Engineering, т. 14, № 6-7, pp. 703-727, 2010.

[39] G. R. Johnson и T. J. Holmquist, «Response of boron carbide subjected to large strains, high strain rates, and high pressures», Journal of applied physics, т. 85, № 12, pp. 8060-8073, 1999.

[40] T. J. Holmquist, D. W. Templeton и K. D. Bishnoi, «Constitutive modeling of aluminum nitride for large strain, high-strain rate, and high-pressure applications», International Journal of Impact Engineering, т. 25, № 3, pp. 211-231, 2001.

[41] K. Liu, C. Wu, X. Li, Q. Li, J. Fang и J. Liu, «A modified HJC model for improved dynamic response of brittle materials under blasting loads», Computers and Geotechnics, т. 123, p. 103584, 2020.

[42] P. Baranowski, M. Kucewicz, R. Gieleta, M. Stankiewicz, M. Konarzewski, P. Bogusz, M. Pytlik и J. Małachowski, «Fracture and fragmentation of dolomite rock using the JH-2 constitutive model: Parameter determination, experiments and simulations», International Journal of Impact Engineering, т. 140, p. 103543, 2020.

[43] A. F. Fossum и R. M. Brannon, «On a viscoplastic model for rocks with mechanism-dependent characteristic times», Acta Geotechnica, т. 1, pp. 89-106, 2006.

[44] R. M. Brannon и A. F. Fossum, The Sandia GeoModel: theory and user's guide (No. SAND2004-3226), Albuquerque, NM, and Livermore, CA: Sandia National Laboratories (SNL), 2004.

[45] Y. V. Petrov и A. A. Utkin, «Dependence of the dynamic strength on loading rate», Soviet materials science, т. 25, № 2, pp. 153-156, 1989.

[46] Y. V. Petrov и N. F. Morozov, «On the modeling of fracture of brittle solids», Journal of Applied Mechanics, т. 61, № 3, pp. 710-712, 1994.

[47] Y. V. Petrov, A. A. Gruzdkov и V. A. Bratov, «Structural-temporal theory of fracture as a multiscale process», Physical Mesomechanics, т. 15, pp. 232-237, 2012.

[48] Y. V. Petrov, «Incubation Time Criterion and the Pulsed Strength of Continua: Fracture, Cavitation, and Electrical Breakdown», Doklady Physics, т. 49, № 4, p. 246–249, 2004.

[49] G. A. Volkov, A. A. Gruzdkov и Y. V. Petrov, «The incubation time criterion and the acoustic strength of sea water», Acoustical Physics, т. 53, pp. 119-122, 2007.

[50] N. Mikhailova, P. Y. Onawumi, G. Volkov, I. Smirnov, M. Broseghini, A. Roy и Y. S. V. V. Petrov, «Ultrasonically assisted drilling in marble», Journal of Sound and Vibration, т. 460, p. 114880, 2019.

[51] N. A. Kazarinov, Y. V. Petrov и A. V. Cherkasov, «Instability effects of the dynamic crack propagation process», Engineering Fracture Mechanics, т. 242, p. 107438, 2021.

[52] Y. V. Petrov, B. L. Karihaloo, V. V. Bratov и A. M. Bragov, «Multi-scale dynamic fracture model for quasi-brittle materials», International Journal of Engineering Science, т. 61, pp. 3-9, 2012.

[53] A. M. Bragov и A. K. Lomunov, «Methodological aspects of studying dynamic material properties using the Kolsky method», International journal of impact engineering, т. 16, № 2, pp. 321-330, 1995.

[54] D. J. Frew, M. J. Forrestal и W. Chen, «A split Hopkinson pressure bar technique to determine compressive stress-strain data for rock materials», Experimental mechanics, т. 41, pp. 40-46, 2001.

[55] H. Kolsky, «An investigation of the mechanical properties of materials at very high rates of loading», Proceedings of the physical society. Section B, т. 62, № 11, p. 676, 1949.

[56] I. Smirnov и A. Konstantinov, «Evaluation of critical stresses for quasi-brittle materials at various loading rates», Materials Physics & Mechanics, т. 44, № 2, 2020.

[57] I. Smirnov и A. Konstantinov, «Strain rate dependencies and competitive effects of dynamic strength of some engineering materials», Applied Sciences, т. 10, № 9, p. 3293, 2020.

[58] N. Banthia, S. Mindess, A. Bentur и M. Pigeon, «Impact testing of concrete using a drop-weight impact machine», Experimental mechanics, т. 29, pp. 63-69, 1989.

[59] V. Kumar, M. A. Iqbal и A. K. Mittal, «Experimental investigation of prestressed and reinforced concrete plates under falling weight impactor», Thin-Walled Structures, т. 126, pp. 106-116, 2018.

[60] A. Nghiem и T. H. K. Kang, «Drop-Weight Testing on Concrete Beams and ACI Design Equations for Maximum and Residual Deflections under Low-Velocity Impact», ACI Structural Journal, т. 117, № 2, 2020.

[61] N. A. Zlatin, S. M. Mochalov, G. S. Pugachev и A. M. Bragov, «Temporal features of fracture in metals under pulsed intense actions», Fiz. Tverd. Tela, т. 16, № 6, pp. 1752-1755, 1974.

[62] K. B. Broberg, Cracks and fracture, Elsevier, 1999.

[63] D. E. Grady и R. E. Hollenbach, «Dynamic fracture strength of rock», Geophysical Research Letters, т. 6, № 2, pp. 73-76, 1979.

[64] G. I. Kanel', «The development of cleavage fracture», Fiz. Goreniya Vzryva, т. 18, № 4, pp. 84-88, 1982.

[65] S. Kubota, Y. Ogata, Y. Wada, G. Simangunsong, H. Shimada и K. Matsui, «Estimation of dynamic tensile strength of sandstone», International Journal of Rock Mechanics and Mining Sciences, т. 45, № 3, pp. 397-406, 2008.

[66] E. B. Zaretsky и G. I. Kanel, «Impact response and dynamic strength of partially melted aluminum alloy», Journal of Applied Physics, т. 112, № 5, 2012.

[67] A. P. Rybakov, «Spall in non-one-dimensional shock waves», International Journal of Impact Engineering, т. 24, № 10, pp. 1041-1082, 2000.

[68] J. P. Cuq-Lelandais, M. Boustie, L. Berthe, T. De Rességuier, P. Combis, J. P. Colombier, M. Nivard и A. Claverie, «Spallation generated by femtosecond laser driven shocks in thin metallic targets», Journal of Physics D: Applied Physics, т. 42, № 6, p. 065402, 2009.

[69] B. C. Csáji, M. C. Campi и E. Weyer, «Sign-perturbed sums: A new system identification approach for constructing exact non-asymptotic confidence regions in linear regression models», IEEE Transactions on Signal Processing, т. 63, № 1, pp. 169-181, 2014.

[70] S. Kolumbán, I. Vajk и J. Schoukens, «Perturbed datasets methods for hypothesis testing and structure of corresponding confidence sets», Automatica, т. 51, pp. 326-331, 2015.

[71] E. Weyer, M. C. Campi и B. C. Csáji, «Asymptotic properties of SPS confidence regions», Automatica, т. 82, pp. 287-294, 2017.

[72] G. A. Volkov, A. A. Gruzdkov и Y. V. Petrov, «A Randomized Approach to Estimate Acoustic Strength of Water», в Advanced Structured Materials, Cham: Springer International Publishing, 2022, pp. 633-640.

[73] G. A. Volkov, Y. V. Petrov и A. A. Gruzdkov, «Acoustic strength of water and effect of ultrasound on the liquid-vapor phase diagram», Technical Physics, т. 60, pp. 753-756, 2015.

[74] G. A. Volkov, Y. V. Petrov и A. A. Gruzdkov, «Liquid-vapor phase equilibrium conditions in an ultrasonic field», Doklady Physics, т. 60, pp. 229-231, 2015.

[75] N. O. Granichin, G. A. Volkov, A. A. Gruzdkov и Y. V. Petrov, «Instability of the Water Phase Diagram under Short Pulse Loading», Mechanics of Solids, т. 58, № 5, pp. 1599-1605, 2023.

[76] G. Volkov, A. Logachev, N. Granichin, Y.-P. Zhao, Y. Zhang и Y. Petrov, «The influence of background ultrasonic field on the strength of adhesive zones under dynamic impact loads», Materials, т. 14, № 12, p. 3188, 2021.

[77] N. Granichin, G. Volkov и Y. Petrov, «Delamination of the Planar Adhesion Zone under Combined Dynamic Actions», Technical Physics, т. 65, № 1, pp. 68-72, 2020.

[78] N. Gorbushin, N. Granichin, A. Logachev, Y. Petrov и G. Volkov, «Destruction of the adhesion zone by combined pulsed-vibrational impacts», Materials Physics and Mechanics, т. 36, № 1, pp. 114-120, 2018.

[79] Y. Petrov, A. Logachev, N. Granichin и G. Volkov, «Adhesive Joint Fracture Under Combined Pulsed and Vibrational Loading», Structural Integrity, т. 16, pp. 100-105, 2020.

[80] G. Volkov, V. Silberschmidt, A. Mitrofanov, A. Gruzdkov, V. Bratov и Y. Petrov, «Minimization of fracture-pulse energy under contact interaction», Doklady Physics, т. 54, № 7, pp. 332-334, 2009.

[81] G. A. Volkov, N. A. Gorbushin и Y. V. Petrov, «On the dependence of the threshold energy of small erodent particles on their geometry in erosion fracture», Mechanics of Solids, т. 47, pp. 491-497, 2012.

[82] V. Bratov, Y. V. Petrov и G. Volkov, «Existence of Optimal Energy Saving Parameters for Different Industrial Processes», Applied Mechanics and Materials, т. 82, pp. 208-213, 2011.

[83] D. Peck, G. Volkov, G. Mishuris и Y. Petrov, «Resolution of the threshold fracture energy paradox for solid particle erosion», Philosophical Magazine, т. 96, № 36, pp. 3775-3789, 2016.

[84] G. A. Volkov, V. A. Bratov, A. A. Gruzdkov, V. I. Babitsky, Y. V. Petrov и V. V. Silberschmidt, «Energy-Based Analysis of Ultrasonically Assisted Turning», Shock and Vibration, т. 18, № 1-2, pp. 333-341, 2011.

[85] Y. Petrov, V. Bratov, G. Volkov и E. Dolmatov, «Incubation time based fracture mechanics and optimization of energy input in the fracture process of rocks», в Advances in rock dynamics and applications, 2011, pp. 163-183.

[86] Y. Petrov, I. Smirnov, G. Volkov, A. Abramian, A. Bragov и S. Verichev, «Dynamic failure of dry and fully saturated limestone samples based on incubation time concept», Journal of Rock Mechanics and Geotechnical Engineering, т. 9, № 1, pp. 125-134, 2017.

[87] N. Mikhailova, G. Volkov, Y. Petrov, I. Smirnov, P. Onawumi, A. Roy и V. Silberschmidt, «Relations between Parameters of Fracture Processes on Different Scale Levels», Doklady Physics, т. 63, № 11, pp. 459-461, 2018.

[88] G. Volkov и I. Smirnov, «A probabilistic approach to evaluate dynamic and static strength of quasi-brittle materials through high-rate testing», International Journal of Mechanical Sciences, т. 216, p. 106960, 2022.

[89] N. Granichin, G. Volkov, Y. Petrov и M. Volkova, «Randomized approach to determine dynamic strength of ice», Cybernetics and Physics, т. 10, № 3, pp. 122-126, 2021.

[90] M. V. Volkova, O. N. Granichin, G. A. Volkov и Y. V. Petrov, «On the possibility of using the method of sign-perturbed sums for the processing of dynamic test data», Vestnik St. Petersburg University, Mathematics, т. 51, pp. 23-30, 2018.

[91] M. Volkova, G. Volkov, O. Granichin и Y. Petrov, «Sign-perturbed sums approach for data treatment of dynamic fracture tests», в 2017 IEEE 56th Annual Conference on Decision and Control (CDC), 2017.

[92] A. Chevrychkina, A. Evstifeev и G. Volkov, «Analysis of the Strength Characteristics of Acrylonitrile–Butadiene–Styrene Plastic under Dynamic Loading», Technical Physics, т. 63, № 3, pp. 381-384, 2018.

[93] S. Atroshenko, A. Chevrychkina, A. Evstifeev и G. Volkov, «Destruction of ABS Polymer in the Glass State under Dynamic Stressing», Physics of the Solid State, т. 61, № 11, pp. 2075-2082, 2019.

[94] A. D. Evstifeev и G. A. Volkov, «A Variational Approach to the Determination of the Dynamic Strength of a Material», Technical Physics, т. 68, № 2, pp. 139-143, 2023.

[95] A. Evstifeev, G. Volkov, A. Chevrychkina и Y. Petrov, «Dynamic Strength Characteristics of Materials: Influence of the Specimen Size on Strain Rate», Technical Physics, т. 64, № 4, pp. 523-526, 2019.

[96] A. Evstifeev, G. Volkov, A. Chevrychkina и Y. Petrov, «Strength Performance of 1230 Aluminum Alloy under Tension in the Quasi-Static and Dynamic Ranges of Loading Parameters», Technical Physics, т. 64, № 5, pp. 620-624, 2019.

[97] M. V. Volkova, O. N. Granichin, Y. V. Petrov и G. A. Volkov, «Dynamic fracture tests data treatment based on the randomized approach», Advances in Systems Science and Applications, т. 17, № 3, pp. 34-41, 2017.

[98] R. Lukashov и G. Volkov, «An analytical approach to deduce loading rate-sensitivity of fracture mode of concrete and mortar», International Journal of Impact Engineering, т. 187, p. 104915, 2024.

[99] G. A. Volkov и Y. V. Petrov, «On the Analysis of Two Theoretical Approaches to Predict the Material Strength under Dynamic Loading», Mechanics of Solids, т. 57, № 8, pp. 1958-1963, 2022.

[100] G.A. Volkov, Y.V. Petrov, and A.A. Gruzdkov, «Comparative study of features of the process of inelastic deformation of metals under high-rate and low rate loading» in "XIII All-Russian Congress on Theoretical and Applied Mechanics", 2023. [in Russian]

[101] S. H. Cho, Y. Ogata and K. Kaneko, "Strain-rate dependency of the dynamic tensile strength of rock," International Journal of Rock Mechanics and Mining Sciences, vol. 40, no. 5, pp. 763-777, 2003.

[102] X. Wu and V. Prakash, "Dynamic compressive behavior of ice at cryogenic temperatures," Cold Regions Science and Technology, vol. 118, pp. 1-13, 2015.

[103] D. Saletti, D. Georges, V. Gouy, M. Montagnat and P. Forquin, "A study of the mechanical response of polycrystalline ice subjected to dynamic tension loading using the spalling test technique," International Journal of Impact Engineering, vol. 132, p. 103315, 2019.

[104] G. Volkov, Y. Petrov и A. Utkin, «On some principal features of data processing of spall fracture tests», Physics of the Solid State, т. 59, № 2, pp. 310-315, 2017.

[105] N. Mikhailova, G. Volkov, Y. Meshcheryakov, Y. Petrov и A. Utkin, «Failure-delay effect in destruction of steel samples under spalling conditions», Technical Physics, т. 62, № 4, pp. 547-552, 2017.

[106] L. (. Rozenberg, High-intensity ultrasonic fields, Springer Science & Business Media, 2013.

[107] H. G. Flynn, Physics of acoustic cavitation in liquids, in Physical Acoustics, Ed. by W. P. Mason, New York: Academic, 1964.

[108] C. E. Brennen, Cavitation and bubble dynamics, Cambridge university press, 2014.

[109] G. L. Sharipov, A. M. Abdrakhmanov и B. M. Gareev, «Luminescence of Tb 3+ and Gd 3+ ions in sonolysis under the conditions of a single bubble moving in aqueous solutions of TbCl 3 and GdCl 3», Technical Physics, т. 58, pp. 255-258, 2013.

[110] S. K. Bhangu и M. Ashokkumar, «Theory of sonochemistry. Sonochemistry: From Basic Principles to Innovative Applications», 2017, pp. 1-28.

[111] K. J. Pahk, S. Lee, P. Gélat, M. O. de Andrade и N. Saffari, «The interaction of shockwaves with a vapour bubble in boiling histotripsy: The shock scattering effect», Ultrasonics Sonochemistry, т. 70, p. 105312, 2021.

[112] E. Stride, T. Segers, G. Lajoinie, S. Cherkaoui, T. Bettinger, M. Versluis и M. Borden, «Microbubble agents: New directions», Ultrasound in medicine & biology, т. 46, № 6, pp. 1326-1343, 2020.

[113] M. B. Mane, V. M. Bhandari, K. Balapure и V. V. Ranade, «A novel hybrid cavitation process for enhancing and altering rate of disinfection by use of natural oils derived from plants», Ultrasonics sonochemistry, т. 61, p. 104820, 2020.

[114] B. Dollet, P. Marmottant и V. Garbin, «Bubble dynamics in soft and biological matter», Annual Review of Fluid Mechanics, т. 51, № 1, pp. 331-355, 2019.

[115] M. Zupanc, Ž. Pandur, T. S. Perdih, D. Stopar, M. Petkovšek и M. (. Dular, «Effects of cavitation on different microorganisms: The current understanding of the mechanisms taking place behind the phenomenon. A review

and proposals for further research», Ultrasonics sonochemistry, т. 57, pp. 147-165, 2019.

[116] G. B. Lebon, I. Tzanakis, K. Pericleous, D. Eskin и P. S. Grant, «Ultrasonic liquid metal processing: The essential role of cavitation bubbles in controlling acoustic streaming», Ultrasonics sonochemistry, т. 55, pp. 243-255, 2019.

[117] J. Campbell, «Cavitation in liquid and solid metals: role of bifilms», Materials Science and Technology, т. 31, № 5, pp. 565-572, 2015.

[118] V. G. Baidakov и A. M. Kaverin, «Attainable superheatings and stretchings of methane–hydrogen solutions», International Journal of Heat and Mass Transfer, т. 163, p. 120498, 2020.

[119] F. Caupin, «Escaping the no man's land: Recent experiments on metastable liquid water», Journal of Non-Crystalline Solids, т. 407, pp. 441-448, 2015.

[120] Wei, Aibo, L. Yu, L. Qiu и X. Zhang, «Cavitation in cryogenic fluids: A critical research review», Physics of Fluids, т. 34, № 10, 2022.

[121] V. A. Akulichev, «Acoustic cavitation in cryogenic and boiling liquids», Applied Scientific Research, т. 38, № 1, pp. 55-67, 1982.

[122] E. A. Neppiras, «Acoustic cavitation», Physics reports, т. 61, № 3, pp. 159-251, 1980.

[123] V. A. Akulichev и V. I. Il’ichev, «Acoustic cavitation thresholds of sea water in different regions of the world ocean», Acoustical Physics, т. 51, № 2, pp. 128-138, 2005.

[124] A. A. Gruzdkov и Y. V. Petrov, «Cavitation breakup of low-and high-viscosity liquids», Technical Physics, т. 53, pp. 291-295, 2008.

[125] A. S. Besov, V. K. Kedrinskiı, N. F. Morozov, Y. V. Petrov и A. A. Utkin, «On the Similarity of the Initial Stage of Failure of Solids and Liquids under Impulse Loading», Doklady Physics, т. 46, № 5, pp. 363-365, 2001.

[126] K. B. Bader, J. L. Raymond, J. Mobley, C. C. Church и D. Felipe Gaitan, «The effect of static pressure on the inertial cavitation threshold», The Journal of the Acoustical Society of America, т. 132, № 2, pp. 728-737, 2012.

[127] M. Dular, B. Stoffel и B. Širok, «Development of a cavitation erosion model», Wear, т. 261, № 5-6, pp. 642-655, 2006.

[128] B. Vyas и C. M. Preece, «Stress produced in a solid by cavitation», Journal of Applied Physics, т. 47, № 12, pp. 5133-5138, 1976.

[129] M. G. Sirotiuk, “Experimental studies of ultrasonic cavitation,” in Powerful ultrasonic fields, M, Nauka, 1968, pp. 167-220. [in Russian]

[130] K. L. Johnson, Contact mechanics, Cambridge university press., 1987.

[131] I. Argatov, G. Mishuris и Y. Petrov, «Threshold fracture energy in solid particle erosion», Philosophical Magazine, т. 93, № 19, p. 2485–2496, 2013.

[132] I. V. Simonov, «The dynamical problem of the impression of an axisymmetric punch into an elastic half-space», Inzh. Zh. Mekh. Tverd. Tela, т. 2, p. 163–165, 1967.

[133] J. C. Thompson and A. R. Robinson, "An Exact Solution for the Superseismic Stage of Dynamic Contact Between a Punch and an Elastic Body," Journal of Applied Mechanics, vol. 44, pp. 583-586, 1977.

[134] F. M. Borodich, «Some contact problems of anisotropic elastodynamics: integral characteristics and exact solutions», International journal of solids and structures, т. 37, № 24, pp. 3345-3373, 2000.

[135] R. Skalak и D. Feit, Impact on the surface of a compressible fluid, 1966.

[136] R. J. Bedding и J. R. Willis, «High speed indentation of an elastic half-space by conical or wedge-shaped indentors», Journal of Elasticity, т. 6, № 2, pp. 195-207, 1976.

[137] A. G. Gorshkov and D. V. Tarlakovsky, Dynamical contact problems with moving boundaries, Moscow: Nauka, 1995. [in Russian]

[138] V. I. Babitsky, V. K. Astashev и A. Meadows, «Vibration excitation and energy transfer during ultrasonically assisted drilling», Journal of sound and vibration, т. 308, № 3-5, pp. 805-814, 2007.

[139] D. Kumabe, Vibratory cutting: Per. from Japan / Edited by I.I. Portnov, V.V. Belov. Belov, Moscow: Mashinostroenie, 1985. [in Russian]

[140] V. K. Astashev, V. I. Babitsky и K. Khusnutdinova, «Ultrasonically assisted machining», в Ultrasonic Processes and Machines: Dynamics, Control and Applications, 2007, pp. 249-314.

[141] A. Roy и V. V. Silberschmidt, «Ultrasonically assisted machining of titanium alloys», в Machining of titanium alloys, Berlin, Heidelberg, Springer Berlin Heidelberg, 2014, pp. 131-147.

[142] E. Ceretti, M. Lucchi и T. Altan, «FEM simulation of orthogonal cutting: serrated chip formation», Journal of materials processing technology, т. 95, № 1-3, pp. 17-26, 1999.

[143] O. Pantalé, J. L. Bacaria, O. Dalverny, R. Rakotomalala и S. Caperaa, «2D and 3D numerical models of metal cutting with damage effects», Computer methods in applied mechanics and engineering, т. 193, № 39-41, pp. 4383-4399, 2004.

[144] M. V. Ramesh, K. N. Seetharamu, N. Ganesan и G. Kuppuswamy, «Finite element modelling of heat transfer analysis in machining of isotropic materials», International journal of heat and mass transfer, т. 42, № 9, pp. 1569-1583, 1999.

[145] V. K. Astashev и V. I. Babitsky, «Ultrasonic cutting as a nonlinear (vibro-impact) process», Ultrasonics, т. 36, № 1-5, pp. 89-96, 1998.

[146] A. V. Mitrofanov, V. A. Babitsky и V. V. Silberschmidt, «Finite element simulations of ultrasonically assisted turning», Computational materials science, т. 28, № 3-4, pp. 645-653, 2003.

[147] A. V. Mitrofanov, V. I. Babitsky и V. V. Silberschmidt, «Finite element analysis of ultrasonically assisted turning of Inconel 718», Journal of materials processing technology, т. 153, pp. 233-239, 2004.

[148] N. Ahmed, A. V. Mitrofanov, V. A. Babitsky и V. V. Silberschmidt, «3D finite element analysis of ultrasonically assisted turning», Computational materials science, т. 39, № 1, pp. 149-154, 2007.

[149] V. Bratov и Y. Petrov, «Optimizing energy input for fracture by analysis of the energy required to initiate dynamic mode I crack growth», International Journal of Solids and Structures, т. 44, № 7-8, pp. 2371-2380, 2007.

[150] A. Brara и J. R. Klepaczko, «Fracture energy of concrete at high loading rates in tension», International Journal of Impact Engineering, т. 34, № 3, pp. 424-435., 2007.

[151] H. Wu, Q. Zhang, F. Huang и Q. Jin, «International Journal of Impact Engineering», Experimental and numerical investigation on the dynamic tensile strength of concrete, т. 32, № 1-4, pp. 605-617, 2005.

[152] X. Chen, S. Wu и J. Zhou, «Experimental and modeling study of dynamic mechanical properties of cement paste, mortar and concrete», Construction and Building Materials, т. 47, pp. 419-430, 2013.

[153] D. Yan и G. Lin, «Dynamic properties of concrete in direct tension», Cement and concrete research, т. 36, № 7, pp. 1371-1378, 2006.

[154] D. Yan и G. Lin, «Influence of initial static stress on the dynamic properties of concrete», Cement and Concrete Composites, т. 30, № 4, pp. 327-333, 2008.

[155] J. Xiao, L. Li, L. Shen и C. S. Poon, «Cement and Concrete Research», Compressive behaviour of recycled aggregate concrete under impact loading, т. 71, pp. 46-55, 2015.

[156] X. F. Li, X. Li, H. B. Li, Q. B. Zhang и J. Zhao, «International Journal of Impact Engineering», Dynamic tensile behaviours of heterogeneous rocks: the grain scale fracturing characteristics on strength and fragmentation, т. 118, pp. 98-118, 2018.

[157] R. Zhou, Z. Song и Y. Lu, «3D mesoscale finite element modelling of concrete», Computers & Structures, т. 192, pp. 96-113, 2017.

[158] J. Cui, H. Hao и Y. Shi, «Numerical study of the influences of pressure confinement on high-speed impact tests of dynamic material properties of concrete», Construction and Building Materials, т. 171, pp. 839-849, 2018.

[159] M. Li, H. Hao и J. Cui, «Numerical investigation of the failure mechanism of concrete specimens under tri-axial dynamic loads» Engineering Fracture Mechanics, т. 266, p. 1084252022, 2022.

[160] A. M. Lennon и K. T. Ramesh, «The thermoviscoplastic response of polycrystalline tungsten in compression» Materials Science and Engineering: A, т. 276, № 1-2, pp. 9-21, 2000.

[161] Y. B. Guo, G. F. Gao, L. Jing и V. P. W. Shim, «Response of high-strength concrete to dynamic compressive loading» International Journal of Impact Engineering, т. 108, pp. 114-135, 2017.

[162] Y. B. Guo, G. F. Gao, L. Jing и V. P. W. Shim, «Quasi-static and dynamic splitting of high-strength concretes–tensile stress–strain response and effects of strain rate» International Journal of Impact Engineering, т. 125, pp. 188-211, 2019.

[163] Y. B. Guo, G. F. Gao, L. Jing и V. P. W. Shim, «Dynamic properties of granite rock employed as coarse aggregate in high-strength concrete», International Journal of Impact Engineering, т. 156, p. 103955, 2021.

[164] Y. B. Guo, G. F. Gao, L. Jing и V. P. W. Shim, «Dynamic properties of mortar in high-strength concrete», International Journal of Impact Engineering, p. 104216, 2022.

[165] G. R. Johnson и T. J. Holmquist, «An improved computational constitutive model for brittle materials», In AIP conference proceedings, т. 309, № 1, pp. 981-984, 1994.

[166] C. C. Holland и R. M. McMeeking, «The influence of mechanical and microstructural properties on the rate-dependent fracture strength of ceramics in uniaxial compression», International Journal of Impact Engineering, т. 81, pp. 34-49, 2015.

[167] H. Wang и K. T. Ramesh, «Dynamic strength and fragmentation of hot-pressed silicon carbide under uniaxial compression», Acta Materialia, т. 52, № 2, pp. 355-367, 2004.

[168] A. Gruzdkov, Y. V. Petrov и V. I. Smirnov, «An invariant form of the dynamic criterion for yield of metals», Physics of the Solid State, т. 44, pp. 2080-2082, 2002.

[169] J. D. Campbell и W. G. Ferguson, «The temperature and strain-rate dependence of the shear strength of mild steel», Philosophical Magazine, т. 21, № 169, pp. 63-82, 1970.

[170] S. R. Agnew и Ö. Duygulu, «Plastic anisotropy and the role of non-basal slip in magnesium alloy AZ31B», International Journal of plasticity, т. 21, № 6, pp. 1161-1193, 2005.

[171] H. Wang, B. Raeisinia, P. D. Wu, S. R. Agnew и C. N. Tomé, «Evaluation of self-consistent polycrystal plasticity models for magnesium alloy AZ31B sheet», International Journal of Solids and Structures, т. 47, № 21, pp. 2905-2917, 2010.

[172] I. Ulacia, N. V. Dudamell, F. Gálvez, S. Yi, M. T. Pérez-Prado и I. Hurtado, «Mechanical behavior and microstructural evolution of a Mg AZ31 sheet at dynamic strain rates», Acta materialia, т. 58, № 8, pp. 2988-2998, 2010.

[173] W. Tang, K. L. Halm, D. R. Trinkle, M. K. Koker, U. Lienert, P. Kenesei и A. J. Beaudoin, «A study of stress relaxation in AZ31 using high-energy X-ray diffraction», Acta Materialia, т. 101, pp. 71-79, 2015.

[174] A. G. Beer и M. R. Barnett, «Influence of initial microstructure on the hot working flow stress of Mg–3Al–1Zn», Materials Science and Engineering: A, т. 423, № 1-2, pp. 292-299, 2006.

[175] B. Bhattacharya и M. Niewczas, «Work-hardening behaviour of Mg single crystals oriented for basal slip», Philosophical Magazine, т. 91, № 17, pp. 2227-2247, 2011.

[176] R. Korla и A. H. Chokshi, «Strain-rate sensitivity and microstructural evolution in a Mg–Al–Zn alloy», Scripta Materialia, т. 63, № 9, pp. 913-916, 2010.

[177] H. Wang, P. Wu, S. Kurukuri, M. J. Worswick, Y. Peng, D. Tang и D. Li, «Strain rate sensitivities of deformation mechanisms in magnesium alloys», International Journal of Plasticity, т. 107, pp. 207-222, 2018.

[178] Y. B. Chun и C. H. J. Davies, «Twinning-induced negative strain rate sensitivity in wrought Mg alloy AZ31», Materials Science and Engineering: A, т. 528, № 18, pp. 5713-5722, 2011.

[179] J. A. García-Grajales, A. Fernández, D. Leary и A. Jérusalem, «A new strain rate dependent continuum framework for Mg alloys», Computational Materials Science, т. 115, pp. 41-50, 2016.

[180] C. A. Bronkhorst, B. L. Hansen, E. K. Cerreta и J. F. Bingert, «Modeling the microstructural evolution of metallic polycrystalline materials under localization conditions», Journal of the Mechanics and Physics of Solids, т. 55, № 11, pp. 2351-2383, 2007.

[181] R. A. Lebensohn, A. K. Kanjarla и P. Eisenlohr, «An elasto-viscoplastic formulation based on fast Fourier transforms for the prediction of micromechanical fields in polycrystalline materials», International Journal of Plasticity, т. 32, pp. 59-69, 2012.

[182] A. A. Tiamiyu, U. Eduok, J. A. Szpunar и A. G. Odeshi, «Corrosion behavior of metastable AISI 321 austenitic stainless steel: Investigating the effect of grain size and prior plastic deformation on its degradation pattern in saline media», Scientific reports, т. 9, № 1, p. 12116, 2019.

[183] A. A. Tiamiyu, A. G. Odeshi и J. A. Szpunar, «Characterization of coarse and ultrafine-grained austenitic stainless steel subjected to dynamic impact load: XRD, SEM, TEM and EBSD analyses», Materialia, т. 4, pp. 81-98, 2018.

[184] A. A. Tiamiyu, A. G. Odeshi и J. A. Szpunar, «Multiple strengthening sources and adiabatic shear banding during high strain-rate deformation of AISI 321 austenitic stainless steel: Effects of grain size and strain rate», Materials Science and Engineering: A, т. 711, pp. 233-249, 2018.

[185] N. Selyutina, E. N. Borodin, Y. Petrov и A. E. Mayer, «The definition of characteristic times of plastic relaxation by dislocation slip and grain boundary sliding in copper and nickel», International Journal of Plasticity, т. 82, pp. 97-111, 2016.

[186] S. Zhao, Y. Petrov и G. Volkov, «Modeling the Nonmonotonic Behavior Flow Curves under Dynamic Loads», Physical Mesomechanics, т. 25, № 3, pp. 221-226, 2022.

[187] S. Zhao, Y. Petrov и G. Volkov, «The modified relaxation plasticity model and the non-monotonic stress–strain diagram», International Journal of Mechanical Sciences, т. 240, p. 107919, 2023.

[188] S. Zhao, Y. Petrov, Y. Zhang, G. Volkov, Z. Xu и F. Huang, «Modeling of the thermal softening of metals under impact loads and their temperature–time correspondence», International Journal of Engineering Science, т. 194, p. 103969, 2024.